

MEASUREMENT AND PREDICTION OF CHEMICAL
FLOCCULATION FOR SEDIMENT CONTROL IN
FLOWING WATER

By

NEHA BHADBHADE

Bachelor of Engineering in Instrumentation and Controls
University of Pune
Pune, Maharashtra, India
2004

Master of Science in Environmental Engineering
Oklahoma State University
Stillwater, Oklahoma
2009

Submitted to the Faculty of the
Graduate College of the
Oklahoma State University
in partial fulfillment of
the requirements for
the Degree of
DOCTOR OF PHILOSOPHY
July, 2014

MEASUREMENT AND PREDICTION OF CHEMICAL
FLOCCULATION FOR SEDIMENT CONTROL IN
FLOWING WATER

Dissertation Approved:

Dr. Jason. R. Vogel

Dissertation Adviser

Dr. Daniel Storm

Dr. Glenn Brown

Dr. Gregory Wilber

ACKNOWLEDGEMENTS

This dissertation is dedicated to my father who was my friend, my strength and without whom this journey would have never happened. I would like to thank Oklahoma Department of Transportation, Oklahoma Transportation Center and Woolpert Inc. for funding our research study. I would like to take this opportunity to express all my gratitude to my advisors Dr. Jason Vogel and Dr. Daniel Storm and Dr. Brown for their encouragement and support throughout my research work. I would like to extend a very special thanks to Dr. Billy Barfield for his expertise in the subject and his unending guidance and patience and to Sam Harp for his programming efforts. I would like to thank the BAE shop floor members Mr. Wayne Kiner, Mr. Jason Walker, Mr. Nick Semtner and Mr. Mike Veldmen for their help in constructing and troubleshooting the experiment apparatus. I would like to thank all the graduate and the undergraduate students who helped me with the project work. I really appreciate everything you have done for me. I would like to also thank the entire faculty and staff of the Biosystems and Agricultural Engineering Department for giving me the opportunity to be a part of this wonderful family. This journey has been truly amazing. Lastly, I would like to thank all my wonderful friends and family for their support. A very special thanks to my parents Rupa and Mangesh Bhadbhade. Your efforts in nurturing my dreams cannot be put into words. Thank you for everything.

Disclaimer: Acknowledgements reflect the views of the author and are not endorsed by committee members or Oklahoma State University

Name: NEHA BHADBHADE

Date of Degree: JULY, 2014

Title of Study: MEASUREMENT AND PREDICTION OF CHEMICAL FLOCCULATION FOR SEDIMENT CONTROL IN FLOWING WATER SEDIMENT REDUCTION

Major Field: BIOSYSTEMS AND AGRICULTURAL ENGINEERING

Abstract: Land disturbance activities on construction sites can increase the rate of soil erosion at alarming rates, especially during intense storm events. Freshwater streams receiving the sediment laden runoff can experience adverse ecological effects due to depleting oxygen levels caused by deposition of excessive sediment in them. Most conventional sediment control techniques like silt fence, sedimentation basin and check dams can remove sand and large aggregates, however they are ineffective in removal of clay particles, which remain in suspension for longer duration and are the primary source of turbidity. Therefore, flocculation can be used to increase the settling rate of the clay particles. Currently, flocculant treatment is often applied on a trial and error basis on construction sites. The goal of this research is to develop a process-based approach to measure and predict the flocculation of sediment in stormwater runoff. The specific research objectives were: (1) To conduct flume experiments on five soils from Oklahoma to measure the flocculation efficiency; (2) To use a mathematical modeling to predict the flocculation efficiency for those five soils using polymer flocculant and perform a sensitivity analysis on the mathematical model; and, (3). To characterize the turbulence within a jar test apparatus through similitude studies. The flume investigations were utilized to characterize flocculation both spatially and temporally for different soil types. The uniqueness of the apparatus and the experiment procedures allowed the control of the input variables, yet allowed for the simulation of suspended sediment distributions in the flow similar to those observed in construction site runoff. A flocculation model was developed to predict flocculation efficiency for different soil types using chemical flocculant. The calibrated model predicted flocculation removal efficiency for the flume runs for four of the five soils investigated. Spatial and temporal turbulence measurements were used to characterize the floc distribution within a jar-test apparatus, which has the potential to improve the laboratory estimation of flocculation efficiency for many applications. The flocculation measurement methods and model developed by this research are useful tools for predicting sediment removal from stormwater runoff and for optimizing the design of sediment control systems that utilize flocculation.

TABLE OF CONTENTS

Chapter	Page
I. INTRODUCTION	1
Particle Settling	2
Flocculation for Control of Sediment in Stormwater Runoff.....	4
<i>Flocculation and Coagulation</i>	4
<i>Types of Flocculants</i>	5
Need for Research	6
<i>Research Objectives</i>	7
II. REVIEW OF LITERATURE.....	9
Introduction	9
Factor Affecting Floc Formation.....	9
<i>Number Concentration of the Particles</i>	10
<i>Flocculation Efficiency Factor ‘α’</i>	11
<i>Collision Frequency Factor ‘K’</i>	11
Physical Characteristics of Floccs.....	14
<i>Size and Shape of Floccs</i>	15
<i>Effective Density</i>	15
<i>Floc Strength</i>	16
<i>Settling Velocity of Floccs</i>	17
Mathematical Modeling of Flocculation	19
Summary	21
III. FLUME EXPERIMENT METHODOLOGY AND FLOCCULATION MODEL DESCRIPTION.....	22
Introduction	22
Flume Experiment Description and Methodology	23
Flume Apparatus	23
<i>Soil Separator</i>	23
<i>Soil Injection System</i>	24
<i>Constant Head Tank</i>	27
<i>Flocculant Injection System</i>	28
<i>Oscillating Grid Assembly</i>	30
<i>Flume</i>	31
<i>Acoustic Doppler Velocimeter</i>	32

Chapter	Page
Description of the Experiment Runs	32
Description of the Soils.....	33
Flocculation Model Approach.....	36
Conclusions.....	42
IV. FLUME INVESTIGATION OF POLYMER FLOCCULATION EFFECTIVENESS IN STORMWATER RUNOFF	43
Abstract	43
Introduction	44
Methodology	45
<i>Experimental Flume Setup</i>	45
<i>Description of Experiment Runs</i>	49
Background Information on Selected Soils from Oklahoma.....	50
Results and Discussion.....	52
<i>Sediment Removal</i>	52
<i>Turbidity Removal</i>	57
Conclusions	62
V. MODELING OF CHEMICAL FLOCCULATION FOR SEDIMENT RUNOFF FROM CONSTRUCTION SITES	63
Abstract	63
Review of Flocculation Models	65
Flocculation Model Description	69
<i>Determination of b and c</i>	70
<i>Population balance equation to determine the rate of flocculation</i>	72
Determination of Stickiness Coefficient using the Flocculation Model.....	74
Results and Discussion.....	76
Estimation of Stickiness Coefficient.....	76
Sensitivity Analysis.....	79
<i>Model Response to Change in Stickiness Coefficient ‘α’</i>	80
<i>Model Response to change in turbulent energy dissipation rate ‘ϵ’</i>	81
Conclusions	82
VI. SPATIAL AND TEMPORAL HYDRODYNAMICS OF A CIRCULAR JAR TEST: IMPACTS ON FLOCCULATION ESTIMATION.....	84
Abstract	84
Introduction	85
Methodology	89
Analysis and Discussion.....	91
<i>Mixing Condition Analysis</i>	91
<i>Settling Condition Analysis</i>	95
Geometric Scaling of Turbulence Parameters	98

Conclusions	101
VII. CONCLUSIONS AND FUTURE RESEARCH RECOMMENDATIONS	103
Conclusions	103
Recommendations for Future Work	105
REFERENCES	108
APPENDICES	115
Appendix I: Sediment Port Diagram	115
Appendix II: Turbidity measurements for Port A soil	116
Appendix III: Turbidity measurements for Port B soil.....	118
Appendix IV: Turbidity measurement for Kamie B soil.....	120
Appendix V: Turbidity measurement for Norge B soil.....	122
Appendix VI: Turbidity measurement for Stephenville B soil	124
Appendix VII: Sediment removal efficiencies for all the soils	126
Appendix VIII: Matlab Codes for Flocculation Model.....	129
Appendix IX: Matlab Code for jar test studies.....	140

LIST OF TABLES

Table	Page
1.1. Comparison of the settling velocities for unaggregated clay, silt and sand particles.....	3
2.1. Models for effective density of flocs	16
3.1. Summary of the type of flume experiments conducted	33
3.2. Particle and floc size distribution methodology used by Krishnappan and Marsalek	37
4.1. Description of the experimental apparatus.....	48
4.2. Average upstream and downstream turbidity measured	58
5.1. Collision frequency functions	69
5.2. Average turbulent energy dissipation rates ' ϵ ' with distance downstream.....	75
5.3. NSE and R^2 values for predicted and measured sediment removal efficiencies for all the soils	76
5.4. Stickiness coefficient values and total error for low and high mixing intensity runs for all soils.....	79
6.1. Dimensions of the model and the upscale prototype jar test apparatus	89
6.2. Average turbulence properties:	94
6.3: Reynolds number in the actual and the prototype jar test	99
6.4: Comparison of rotational speeds in prototype with the scaled rotational speeds needed in actual jar test apparatus for constant turbulent energy dissipation rates	100

LIST OF FIGURES

Figure	Page
3.1. Soil separator used to remove sand particles and large aggregates	24
3.2. Diagrammatic representation of flow of sediment during normal flow operation.....	25
3.3. Diagrammatic representation of flow of sediment during back flow operation	26
3.4. Sediment and water tank.....	26
3.5. Diagram of the constant head tank used to regulate flow into the flume.....	27
3.6. Constant head tank as constructed for regulating flow into the flume.....	28
3.7. Flocculant injection system used for constant flocculant dosage into the flume	29
3.8. Oscillating grid assembly used to mix sediment and flocculant uniformly	30
3.9. Flume apparatus used for determination of flocculation efficiency.....	31
3.10. Sontek YSI, 16 MHz ADV used for velocity measurement	32
3.11. Distribution of Port, Kamie, Norge and Stephenville soil series in Oklahoma	34
3.12. Undispersed sediment particle size distribution for all soils for parent and separated Soil slurry measured from pipette tests.....	35
3.13. Dispersed sediment particle size distribution for all soils for parent and separated soil slurry measured from pipette tests	36
3.14: Schematic of the method used for partitioning of flocculated particles	38
4.1: Schematic flow diagram of the experimental setup for flume experiments.....	47
4.2. Undispersed sediment particle size distribution for all soils for parent and separated Soil slurry measured from pipette tests.....	51
4.3. Dispersed sediment particle size distribution for all soils for parent and separated soil slurry measured from pipette tests	52

Figure	Page
4.4. Suspended sediment concentration for low mixing intensity control run A) Top port and tailgate B) Bottom port	55
4.5. Suspended sediment concentration for low mixing intensity flocculation run A) Top port and tailgate B) Bottom port	56
4.6. Range and the average percent sediment removal efficiency for all soil.....	57
4.7. Upstream and downstream turbidity measurement results for port b soil for control runs A) Low mixing intensity run B) High mixing intensity run.....	59
4.8. Upstream and downstream turbidity measurement results for port b soil for flocculation runs A) Low mixing intensity run B) High mixing intensity run	60
4.9. Range and average upstream and downstream turbidity measured for all the soils.....	61
5.1. Settling velocities of flocs for three different relationships: i) Lau and Krishnappan (1997); ii) Tambo and Watanabe (1979) iii) Our model	72
5.2. Measured vs modeled cumulative distribution of flocculated sediment for all the soils.....	77
5.3. Change in flocculation efficiency with change in stickiness coefficient ' α '	81
5.4. Change in flocculation efficiency with change in turbulent energy dissipation rate	82
6.1. Schematic diagram showing the different length scales of turbulence	87
6.2. Frontal view of the prototype jar test apparatus showing velocity measurement locations. z1: 0.03 m; z2: 0.05 m; z3: 0.08 m; z4: 0.1 m above from the blade	91
6.3. Root mean square turbulent velocity profiles A) Radial; B) Axial; C) Tangential.....	92
6.4: Profile of Total Kinetic Energy (TKE) at different vertical distance above the blade at different speeds.....	93
6.5. Profile of turbulent energy dissipation rate as distance above the blade at different speeds.....	95
6.6. Kinetic energy profile across the entire measurement duration.....	96
6.7. Temporal profiles of the turbulent energy dissipation rate at different distances above from the blade at different speeds in prototype jar test apparatus a) 0.1 m b) 0.08 m c) 0.05 m d) 0.03m.....	97
6.8. Floc size distribution at various rotational speeds for change in ' ϵ ' with time and vertical distance from blade for the model jar test apparatus A) 53 rpm B) 105 rpm C) 158 rpm	101

CHAPTER I

INTRODUCTION

Soil erosion is a naturally occurring process on landforms. However, with land disturbance activities like urban development, tillage, highway construction, mining and agriculture, the rate of soil erosion can increase at alarming rates, especially during intense storm events. Freshwater streams receiving the sediment laden runoff can experience adverse ecological effects due to depleting oxygen levels caused by deposition of excessive sediment in them. Turbidity is an indicator of the presence of suspended sediment in water and therefore turbidity measurements are important as they can help in design appropriate erosion sediment control systems. The focus of this dissertation was on sediment control in stormwater runoff from construction sites. Sediment is a primary pollutant in stormwater runoff from construction sites. When land is excavated and bare, more than 90% of the surface soil can erode (Canning, 1988). Forested lands undergo erosion at rate of 1 ton/acre/year (USEPA, 2005). However, construction sites can erode at a rate in the range anywhere between 7.2 to 500 tons/acre/year, which is significantly high compared to erosion rates of predevelopment (USEPA, 2005). Turbidity of a stormwater runoff from construction sites is typically greater than 2000 NTU. The sediment runoff is mainly composed of sand, silt and clay and their small and large aggregates (Patil et al., 2011).

Finer clays and colloidal sized sediment particles are the most difficult to trap due their low settling rates and are the primary source of turbidity. Excessive suspended sediment in the fresh water streams can have adverse impacts on the aquatic ecosystem as mentioned below:

- It causes siltation reducing the water carrying capacity of the streams. (Trent et al., 1976)
- It can have various lethal and sublethal effects on aquatic organisms. (Wood and Armitage, 1997; Newcombe and MacDonald, 1991; Rier and King, 1996; Sedell et al., 1990)

In order to maintain the water quality and a healthy ecosystem it is necessary to control excessive sediment from getting washed off into the water bodies. Before discussing the best available sediment control techniques, it is important to understand the fundamentals of particle settling.

Particle Settling

Suspended sediments are ultimately removed from the stormwater runoff by gravity which is termed as 'sedimentation'. There are four types of ways in which particle settling occurs: (Reynolds and Richards, 1996):

- ***Discrete Particle Settling (Type I):*** Settling of those particles whose physical characteristics like size, shape, mass and density do not change over the settling time and depth. Particle settling occurs individually.
- ***Flocculant Settling (Type II):*** Settling of particles whose size, shape and specific gravity change over the settling time and depth. Particles interact with each other naturally or chemically to form larger particles that can settle out quickly.
- ***Hindered Settling and Compressed Settling (Type III & IV):*** In hindered settling concentrated suspended sediments form a blanket and then settle out as one mass. And in compressed settling, the weight of the particles above cause particles to settle out and

form a compact layer. Type III and IV settling are controlled processes and do not occur typically in the stormwater runoffs.

A comparison of the settling velocities of single, unaggregated, sand silt and clay particles calculated using the Stokes Law equation is shown in Table 1.1. The shape of the particles is assumed to be spherical and the density of the individual particles is 2.65 kg/m^3 . The temperature of the water was assumed to be 15°C . Sand and coarser silt particles settle out quickly. Fine silt particles and clay particles have very low settling velocities. Clay particles in the size range of $2\mu\text{m}$ and lower could take more than two and half years to settle a depth of one foot. Therefore it is evident that it is important to remove the finer silt and clay particles from the stormwater runoff to prevent sediment pollution in the receiving streams.

Table 1.1. Comparison of the settling velocities for unaggregated clay, silt and sand particles.

Particle Class	Size Range (mm)	Settling Velocity (m/s)	Settling Time (settle 1 foot)
Clay	<0.002	3.6E-9 (maximum)	>2.5 years
Silt	0.002- 0.05	3.6E-9 to 2.24E-6	1 day to 2.5 years
Sand	0.05- 2.00	2.7E-6 to 0.003	1.5 minutes to 1 day

The most conventional sediment control techniques used on construction sites are:

- Silt fences
- Sedimentation basin
- Check dams and Wattles

Previous research has shown that conventional techniques are not efficient in removal of fine silt and clay sized particles less than $12 \mu\text{m}$ (Barrett et al., 1995; Faucette et al., 2008; Millen et al., 1997; Bhardwaj et al., 2008; Kang et al., 2013). Therefore, it is necessary to enhance the settling rates of the particles fine silt and clay particles. Particle settling rates can be increased by using

flocculation. The following section discusses the theory and the advantages of using flocculation treatment for the control of sediments in stormwater runoffs.

Flocculation for Control of Sediment in Stormwater Runoff

Flocculation and Coagulation

Flocculation is a well-established treatment process in water and wastewater treatment industry. Its application in control of sediment in stormwater runoffs from construction sites is very recent. Clay particles are negatively charged particles that tend to repel the neighboring clay particles causing them to form a stable solution of suspended sediment (Jury and Horton, 2004). Flocculation is a physicochemical process where the addition of the flocculant causes the clay particles to destabilize, allowing them to bind to each other and form a larger “floc” particle that is capable of settling quickly. It is often considered to be the same as coagulation. Though both are similar, the destabilization mechanisms of flocculation and coagulation are different. Coagulation is an electrostatic process where the destabilization of the particles occurs due the double layer diffusion or charge neutralization. The chemicals causing particle coagulation are called as coagulants. Factors affecting the process of coagulation are particle size, surface charge and water chemistry. The higher the surface charge, the higher the required coagulant concentration for coagulation. Ions like Mg^{++} , Ca^{++} and Fe^{++} help to neutralize some of the surface charge during coagulation, so the degree of hardness of water can help in lowering the coagulant demand. Most of the coagulants are either aluminum salts or iron salts. Aluminum sulfate ($Al_2SO_4, 14H_2O$) (commonly referred to as alum), ferrous sulfate ($FeSO_4, 7H_2O$), ferric sulphate ($Fe_2(SO_4)_3, 9 H_2O$), ferric chloride ($FeCl_3, 6 H_2O$), lime ($Ca(OH)_2$), quick lime (CaO) and sodium aluminate ($Na_2Al_2O_4$) are the most commonly used coagulants (Reynolds and Richard, 1996). Flocs formed by coagulation are generally small in size. They have low settling velocities and can be broken easily under high shear. Flocculation, on the other hand, destabilizes

the particles by interparticle bridging. The flocculant is a long chained, linear polymer having a high molecular weight. Clay particles attach to one or more branches of the flocculant and the branches coil up to form flocs. Flocs formed because of flocculation have higher settling velocities and are more porous in nature than floc formed by coagulation. In general, flocculation is a physic-chemical process which depends upon type of flocculant, clay mineralogy, flocculant dosage, and sediment concentration and shear rate due to turbulent or laminar flow or inertia of the particles in turbulent flow.

Types of Flocculants

Flocculants are both natural and synthetic in nature (Brostow et al., 2009). Some examples of natural flocculants are gums, glues, alginates and starch. Synthetic flocculants are polyacrylamide monomer (PAM) derived complex compounds that are either cationic (cPAMs) or anionic (aPAMs) in nature. PAMs are water soluble and can be manufactured in both solid and liquid forms. cPAMs, which carry a positive charge, are formed by the copolymerization of acrylamide with quaternary ammonium derivatives (Barvenik, 1994). cPAMs have lower molecular weight compared to the aPAMs. cPAMs are toxic in nature and therefore are less preferred compared to the aPAMS (Barvenik, 1994). On the other hand, aPAMS are formed by the copolymerization of acrylic acid with polyacrylamide. They carry a negative charge and have high molecular weights. The advantages of aPAMS is that they are both less toxic and expensive compared to the cPAMS (Stephens, 1991, Barvenik, 1994; Green et al., 1999).

Solid flocculants (aPAMs or cPAMS) come in the form of powders or blocks. Blocks of flocculant are commonly called 'floc logs'. They dissolve as they come in contact with water slowly releasing the flocculant. Disadvantages of solid flocculants include: they do not mix uniformly with sediment runoff requiring more amount of flocculant to treat the same runoff; if the floc logs are left in the stagnant pool, they continue to dissolve releasing flocculant causing

overdosing; and, sediment can cover floc logs and dry, making the floc logs ineffective for the upcoming storm events.

Liquid flocculants are made of long polymer chains. Liquid flocculants are highly viscous in nature and need to be mixed with water before the application for an optimum period of 60 to 120 minutes (TramFloc.Inc, 2013). If mixed at high intensities, there is a chance of breaking the polymer chains, reducing their effectiveness. Liquid flocculants uniformly mix with the sediment runoff allowing more particles to bind together and therefore have higher efficiency compared to solid flocculants. However, the flocculant chains tend to loosen up at temperatures greater than 40°C, thus reducing the effectiveness of the flocculant. Therefore, liquid flocculants need to be stored at or below room temperatures to keep their effectiveness intact (TramFloc.Inc, 2013)

Need for Research

A number of factors affect the performance of a flocculation system on construction sites and each application will have unique soils, climate, contributing area, and reduction goals. Currently, flocculant treatment is often applied on a trial and error basis by construction site operators and engineers (Harper, 2007). There is a need for a predictable and scientific approach based on the physical processes that predict the flocculation of sediment in stormwater runoff. Physical processes defining the formation and the breakage of the flocs, mass transport of the sediment through the stormwater channel and sedimentation can be converted into mathematical routines. These mathematical routines can help to better understand the sediment flow dynamics and predict the amount of sediment trapped by the flocculation system. Algorithms defining the physical processes can be developed into software programs. These software programs can be used as a design tool for sizing flocculation systems on individual construction sites for sediment and turbidity control.

Research Objectives

The research objectives of this research study are as follow:

1. Conduct flume investigations to measure the flocculation efficiency and the parameters affecting the effectiveness of chemical flocculants in stormwater runoff for selected soils.
2. Use mathematical modeling to predict the flocculation efficiency and determine the stickiness coefficient for the soils on which the flume experiments were conducted. Perform a sensitivity analysis on the flocculation model to examine the model response the change in the various input parameters.
3. Determine the hydrodynamics of the jar test apparatus through similitude studies which affects the formation of the flocs. This study is the first step towards understanding the relationship between field operation, laboratory flume studies, and jar tests.

Chapter II will present the comprehensive literature review on previous flocculation studies to provide a fundamental basis and motivation for further research in this field. In Chapter III the flocculation model approach used to determine the stickiness coefficients is discussed in depth. Chapter III also gives a detailed description of the experimental work done for the collection of the data to support the model. Chapter IV, Chapter V and Chapter VI are presented in form of manuscripts to be submitted to scientific journals. In Chapter IV the flume experiments conducted to measure the flocculation efficiency and turbidity reduction are discussed in detail and the results of the flocculation studies conducted on five soils from Oklahoma are presented. The focus of Chapter V is on the mathematical modeling of the flocculation to predict the stickiness coefficient for the selected five soils and then perform a sensitivity analysis to see which flocculation parameter has a greater effect on the flocculation rate. Chapter VI discusses the similitude studies done to characterize the hydrodynamics of a laboratory jar test apparatus in order to determine the turbulent energy dissipation rate which is an important parameter that

affects flocculation. Chapter VII briefly highlights the scientific contributions of the research work presented and the need for future research. This research was completed as part of grants from Oklahoma Department of Transportation (ODOT), Oklahoma Transportation Center (OkTC) and Woolpert Inc, to conduct research on use of liquid flocculant for turbidity and sediment control in stormwater runoff.

CHAPTER II

REVIEW OF LITERATURE

Introduction

The preceding chapter gave an insight into the importance of modeling suspended sediment transport in stormwater runoff from construction sites. Also, since colloids and clays cannot be trapped effectively with conventional techniques, flocculation treatment is a reasonable treatment option for the removal of these fine particles. Modeling the process of flocculation is a complex process as it involves the understanding of all the physical and chemical factors involved. The process of flocculation has been researched for decades and many theories have been proposed on the formation of the flocs and their physical characteristics. The review of the literature presented in this chapter will be based mainly on three themes: factors affecting the formation of the flocs, physical characteristics of the flocs and mathematical modeling of flocculation. The following sections give an overview on the factors involved in the formation of the flocs.

Factors Affecting Flocculation

Flocculation is a physicochemical process that can occur naturally due to the interaction between the particles having opposite charges or can be induced by adding a flocculant to enhance the rate of particle growth. Particle interactions take place depending on the nature of the motion of the particle.

When the particles interact randomly in quiescent flow, the flocculation is said to be ‘perikinetic’ and when particles are allowed to interact by inducing mixing the flocculation is said to be ‘orthokinetic’ (Thomas et al., 1999; Yusa 1997; Gregory & O’Melia, 1989). The nature of flocculation in a stormwater channel is generally orthokinetic owing to the mixing induced due to the turbulent flow patterns of the stormwater runoff. The three most important factors that are necessary for the formation of flocs are:

- Collision rates of the particles that cause particle interactions
- Probability that the interacting particles will stick together
- Number concentration of the sediment particles undergoing flocculation

In the most simplistic way, the mathematical representation for the rate of flocculation is given by (Thomas et al., 1999):

$$\frac{dn}{dt} = \alpha K(i, j) n_i n_j \quad (2.1)$$

where, $\frac{dn}{dt}$ = Rate of floc formation,

$K(i, j)$ = Collision frequency,

α = Flocculation efficiency,

n_i and n_j = Number of particles, and

i, j = Size classes of the particles.

Number Concentration of the Particles

The number concentration of the particles is an important factor for flocculation to occur. Equation 2.1 demonstrates that the rate of flocculation increases with an increase in the number concentration of the particles (Thomas et al., 1999), due to increase in the particle interactions.

Flocculation Efficiency Factor ' α '

Thomas et al., (1999) defined ' α ' as the degree of destabilization of the particles. The greater the value of ' α ', the greater is the degree of destabilization and the better the efficiency of flocculation (Thomas et al., 1999; Amirtharajah et al., 2007). Theoretically ' α ' can take any value between 0 and 1 depending upon the soil, water and flocculant chemistry (Amirtharajah et al., 2007). However, the calibration of the coefficient is very difficult experimentally and therefore in mathematical modeling ' α ' could also be used as correction, or calibration, factor, which no longer confines its values between 0 and 1 (Thomas et al., 1999).

Collision Frequency Factor ' K '

The collision frequency factor ' K ', is governed by the transport phenomenon and in mathematical models is applied as fixed function that defines the particle interactions (Thomas et al., 1999). Smoluchowski (1916) developed the collision frequency function for perikinetic flocculation as represented by:

$$K_{i,j} = \frac{2kT}{3\mu} \left(\frac{1}{d_i} + \frac{1}{d_j} \right) (d_i + d_j) \quad (2.2)$$

where, k = Boltzmann's constant (J/K),

T = Temperature (K),

μ = dynamic viscosity (Ns/m²), and

d_i, d_j = diameter of the particles in size class i, j .

Camp and Stein (1943) extended Smoluchowski's work to show that for orthokinetic flocculation, the rate of flocculation was a function of the velocity gradient ' G ' and defined the collision frequency function as given by:

$$K_{i,j} = \frac{G}{6} (d_i + d_j)^3 \quad (2.3)$$

where G = velocity gradient (s⁻¹).

O'Melia (1980), McAnally and Mehta (2000) and Krishnappan and Marsalek (2002), have shown that particle collisions mainly occur due the following four mechanisms,

- Brownian motion
- Laminar or turbulent shear,
- Inertia of turbulent flow, and
- Differential Settling.

O'Melia (1980) concluded that for clay and colloidal particles, Brownian motion was the dominant process for particle interaction. Winterwerp (1988) concluded that the effects of Brownian motion were negligible for modeling estuarial sediment flocculation and therefore took into account the particle interactions caused only due to turbulent flow. Lick and Lick (1988) and Tsai et al. (1987) modeled the flocculation of sediment under uniform stress conditions and considered the effects due to Brownian motion negligible. However, McAnally and Mehta (2000) and Krishnappan and Marsalek (2002) modeled flocculation of sediment in natural systems and incorporated the collision frequency factor taking into account all the mechanisms. Krishnappan and Marsalek (2002) used an effective collision frequency function that was a weighted sum of collision frequencies due to four collision mechanisms. The equation for the effective collision frequency was:

$$K_{i,j}^{eff} = K_{i,j}^{BR} + \sqrt{(K_{i,j}^{SH})^2 + (K_{i,j}^{IN})^2 + (K_{i,j}^{DS})^2} \quad (2.4)$$

where $K_{i,j}^{eff}$ = Effective collision frequency (m³/s), and

$K_{i,j}^{BR}, K_{i,j}^{SH}, K_{i,j}^{SH}, K_{i,j}^{DS}$ = Collision frequencies for Brownian motion, laminar or turbulent shear, inertia of turbulent flow and differential settling (m³/s)

Camp and Stein (1943), Saffman and Turner (1956), Kusters et al., (1997), Parker et al., (1972), Argaman and Kaufman (1971) and Tambo and Watanabe (1979) modeled the flocculation of sediment in agitated vessels. The change in the number of particles, described by Parker et al. (1972), is a function of velocity gradient G (s⁻¹) and is given by:

$$G = \sqrt{\frac{\varepsilon}{\nu}} \quad (2.5)$$

where, ε = Turbulent energy dissipation rate (m^2s^{-3}), and

ν = Kinematic viscosity (m^2s^{-1}).

Irrespective of whether the flow pattern is turbulent in natural or agitated systems, the particle interactions in turbulent flow are a function of the turbulent energy dissipation rate. Tapp et al., (1981) showed that the size of the particles was controlled by the velocity gradient ‘ G ’, which is the function of the turbulent energy dissipation rate, as shown in equation 2.5. Therefore, it is important to know the turbulent energy dissipation rate to predict the size of the flocs. In laboratory, the turbulent energy dissipation rate can be controlled with the help of mixing devices. The commonly used mixing devices are paddle mixers, static grids, oscillating grids and Couette mixers. Paddle mixers have spatially varying shear rates and the maximum shear rates are observed at the center near the blades of the impeller. Static grids, generate freely decaying, isotropic turbulence (Roach, 1986), however they cannot provide high initial mixing intensities that are needed to maximize the number particle interactions. Oscillating grids, provide more homogenous turbulence at various intensities depending upon the speed the motor. Serra et al., (2008) evaluated the efficiency of three different mixing devices: paddle mixer, oscillating grids and Couette mixers. They concluded that the Couette mixing device produced large flocs compared to the other two devices. However, it is difficult to predict the local turbulence within the Couette mixers. Liem et al.,(1999) showed that the kinetic energy dissipated by the oscillating grids is dependent on the drag force and the relative mean velocity between the grids and the fluid. Thus the turbulent energy dissipation rate for oscillating grids was expressed as:

$$\varepsilon = \frac{U_R F_d}{\rho V} \quad (2.6)$$

where, U_R = Relative mean velocity between the oscillating grid and fluid (m/s),

F_d = Drag force (kg-m/s²),

ρ = Density of the fluid (kg/m³), and

V = Volume of the fluid (m³).

The drag force depends upon the relative mean velocity of the area of the grid, and is given by (Liem et al., 1999):

$$F_d = \frac{1}{2} U_R^2 C_d A_s \rho \quad (2.7)$$

where, C_d = Drag coefficient, and

A_s = Grid area (m²)

C_d It is determined based on the grid geometry and the rod Reynolds number R_d is given by (Colomer et al., 2005):

$$C_d = 1 + 10R_d^{-2/3} \quad (2.8)$$

$$R_d = \frac{U_R d}{\nu} \quad (2.9)$$

where, d = Rod diameter (m).

Physical Characteristics of Floccs

After the floccs are formed, their settling rate depends upon their physical characteristics. Floccs are generally characterized by their size, shape, density and strength. These physical characteristics constantly change with time and space and affect the settling velocity of the floccs (Khelifa and Hill, 2007).

Size and Shape of Flocs

Floc size and the structure depend mainly on the flocculant and the sediment mineralogy (Thomas et al., 1999). As particles start interacting with each other, they start growing rapidly. As the size of the flocs increases their porosity increases and the structural starts becoming loose and open. Those larger flocs become more susceptible to breakage (Spicer and Pratsinis, 1995). Floc structure is important because it mainly affects the density. Therefore, flocs reach an equilibrium size which balances the aggregation and fragmentation processes. (Spicer and Pratsinis, 1995; Parker et al., 1972; Tambo and Watanabe, 1979). Additionally, increased shear reduces the average equilibrium size of the flocs (Spicer and Pratsinis, 1995). A number of attempts have been made to model the size of the flocs based on the structures. Many of the models have been derived from fractal theory, which assumes that the flocs formed are self-similar in structure and are independent of the scale of the parameter that is selected for the fractal relationship (Khelifa and Hill, 2007; Dryer and Manning; 1997; Krone, 1978; Kranenburg, 1994). The fractal dimension of the flocs can be measured either as the observed diameter, perimeter or the area of the flocs (Chen and Eisma, 1995). Flocs do not have a self-similar structure (Khelifa and Hill, 2007). This can lead to the over prediction of the density (Khelifa and Hill, 2007). Krishnappan and Marsalek (2002) modeled flocs assuming that they had spherical shape and grew in geometric progression. The disadvantage of such an assumption is that it introduces empiricism in the mathematical model for the density of the flocs along with a number of fitting parameters.

Effective Density

The density of flocs reduces and the porosity increases as the size of the flocs increases. Larger flocs especially formed using polymer flocculant have long chained open structure and therefore are less dense. Table 2.1 summarizes some of the methods used to model the effective density of the flocs. The effective density of the flocs is considered as the difference between the

density of the floc and that of water. All the density models have some kind of empiricism associated with them owing to the differences in the experimental conditions.

Table 2.1. Models for effective density of flocs (Khelifa and Hill, 2007).

Reference	Effective floc density expression	Description
Tambo and Watanabe (1979)	$\rho_a - \rho_w = \frac{a}{(d_f/1)^K}$	Empirical model based on dimensionless floc diameter ' d_f '. a and K are constants
Mc Cave (1984)	$\rho_a - \rho_w = \begin{cases} 1 & \text{for } D_a \leq 1\mu m \\ \alpha D_a^{-0.42} & \text{for } 1 \leq D_a \leq 50\mu m \\ \alpha D_a^{-1.3} & \text{for } 1 \leq D_a \leq 1200\mu m \\ 0.003 & \text{for } D_a \geq 1200\mu m \end{cases}$	Empirical model where density is in g/cm ³
Kranenburg (1994)	$\rho_a - \rho_w \propto (\rho_s - \rho_w) \left(\frac{R_p}{R_a}\right)^{3-D}$	Based on fractal theory assuming self-similar structure
Lau and Krishnappan (1997)	$\rho_a - \rho_w = (\rho_s) \exp(-0.02D_a)^{-1.85}$	Empirical equation where floc diameter ' D_a ' is microns and density is in g/cm ³

Floc Strength

Once a floc is formed, its strength depends on the number and strength of the individual bonds within the floc (Jarvis et al., 2005). If the strength of the individual bonds is less than the stress applied at its surface, the floc will breakup. Generally, floc strength is measured either macroscopically (measures energy required in the system for floc breakage) or microscopically (measures the inter-particle forces within individual flocs) (Jarvis et al., 2005). To measure floc strength macroscopically, increased shear rate can be applied to the formed floc and related to the energy dissipation applied to the maximum or average floc size remaining (Jarvis et al., 2005). One example used to measure floc strength macroscopically are impeller-based systems. This is accomplished by applying a known shear rate to a grown floc suspension within a vessel. Other methods use image analysis to measure floc size. For the micromechanical approach, floc strength is measured by the tensile force required to break single flocs (Yeung et al. 1997). Zhang et al. (1999) used a micromechanical method, where they measured the compression force

required to break flocs between a glass slide and a fiber optic probe. When the shear rate increases beyond the critical point, flocs break up until equilibrium is restored. Once flocs breakup, some of the broken fragments will not be able to reform (Jarvis, et al., 2005). Thomas (1964) concluded that under turbulent conditions the rupture of flocs is predominantly due to the pressure differences on opposite sides of the floc. Matsuo and Unno (1981) found that floc breakup results predominantly from the surface shear brought about by the difference in deformability between the surrounding fluid and the floc (Jarvis et al., 2005).

Settling Velocity of Flocs

Particle settling velocity is dependent on a large number of parameters such as the particle's shape, size, and density and is influenced by the temperature and viscosity of the water (Kang et al., 2007). With emergence of better imaging techniques, settling velocity measurement are done without disturbing the flocs. Stoke's law is used to calculate the velocity of spherical particles settling under laminar and steady-state conditions; however. This equation cannot be used when the flocculating particles are continually changing in size and shape (Davis and Cornwell, 1998). However, since the settling velocity is ultimately a function of the size and density of the flocs and the viscosity of the fluid, many researchers prefer to use the Stoke's law and modify it to represent the settling velocity of the flocs as a function of the variable density and size of the flocs (Khelifa and Hill, 2007; Lau and Krishnappan, 1997; McCave 1975). Ha and Maa (2010) estimated the relation between the suspended sediment concentration (SSC), turbulence, and settling velocity in a laboratory tank by using a 5-MHz acoustic Doppler velocity meter (ADV). The objectives were to examine the dependence of settling velocity on the SSC and turbulence, to evaluate the confidence of ADV-derived settling velocity by comparing it with other approaches such as Owen tube (OT), and to elucidate the limitation and possible improvement of ADV's analytical approach for estimating the settling velocity. They found that settling velocity increased non-linearly with SSC in the range of 300-700 mg L⁻¹, and the

turbulence can increase the settling velocity up to one order of magnitude higher than the settling velocity for non-turbulent conditions. This turbulence effect can explain why the settling velocity derived by the ADV is 1 to 3 orders of magnitude higher than settling velocity estimated by Owen tube (OT), where the ambient turbulence was totally blocked, and OT itself caused breaking of the flocs while trapping samples into the tube. Besides, the collected sediment particles (flocs) may stick to the inner wall of the tube during the settling, which leads to retarding the settling velocity. The settling velocity in this study was expressed as a function of SSC, given by:

$$W_s = mC^{n-1} \quad (2.1)$$

where, W_s = Settling velocity (m/s),

C = Sediment concentration (mg/L), and

m and n are empirical constants.

Khelifa and Hill (2007) use a modified Stoke's law to develop an equation to express the settling velocity of flocs, given by:

$$V_f = \left(\frac{4}{3} \theta g C_d^{-1} \frac{\Delta\rho}{\rho_w} D_f \right)^{0.5} \quad (2.2)$$

where, V_f = Settling velocity (m/s),

θ = Dimensionless particle-shape factor,

g = Acceleration due to gravity (m/s^2),

C_d = Dimensionless drag coefficient,

$\Delta\rho$ = Effective density of the floc (kg/m^3), and

ρ_w = Density of water (kg/m^3).

Mathematical Modeling of Flocculation

Mathematical modeling of particle aggregation due to flocculation began in the year 1916, with the classical population balance theory proposed by Smoluchowski (1916) and is given by:

$$\frac{\partial n(x_i, t)}{\partial t} = \frac{1}{2} \sum_{j=1}^{i-1} A(x_i - x_j, x_j) n(x_i - x_j, t) n(x_j, t) - \sum_{j=1}^{\infty} A(x_i, x_j) n(x_i, t) n(x_j, t) \quad (2.1)$$

where, A = Coagulation kernel, and

x_i, x_j = Particles in size class i and j respectively.

Smoluchowski (1916) mathematical representation for particle growth is applicable only for perikinetic flocculation. Smoluchowski (1916) flocculation model is based on the assumption that only two particles can collide any given time. In equation 2.12, the second term on the right hand side represents the number of particles lost due to flocculation and the first term on the right hand shows the number of particles gained in higher size classes due to flocculation with particles in lower size class. In general there are two types of flocculation models namely; size class based model and distribution-based model (Maerz et al., 2011). Research work done by Krishnappan (1991), Krishnappan and Marsalek, (2002) McAnally and Mehta (2002), and Somsundaran and Runkana (2003) and Maggi et al., (2007), has utilized size class based model for modeling flocculation of suspended sediment. The distribution-based model approach was developed by Wirtz and Eckhardt (1996). They used the distribution-based model to model the growth of phytoplankton in natural ecosystem. This approach was used by Maerz et al., (2011) to model suspended sediments. Basically, the model takes into account two factors to account for the variability in the size of the flocs; the change in the total mass concentration and the change in the average radius of the particles. Size class based models are useful in understanding the time evolution of the flocs which is not possible with distribution-based models. However, size class based models are complex to model due to limited knowledge on change in the floc sizes

depending on shape and density. Parameterization of floc density and size is based on empirical or semi empirical relationships and these models are computationally intensive especially when used in conjunction with 2D and 3D transport models (Maerz et al., 2011). On the other hand, distribution based models are less complex. Many researchers like Winterwerp (1998), Maggi et al., (2007) and Son and Hsu (2009) used size class based model in conjunction with fractal theory. However, again these models are also semi-empirical in nature and require complex experimental measurements to predict time evolution of flocs. Models presented by both Son and Hsu (2009) and Winterwerp (1998) did not produce good satisfactory results for the floc size distribution in mixing tanks (Son and Hsu, 2009). Argaman and Kaufman (1970) proposed that rate of floc formation is directly proportional to the mean square turbulent velocity, given by

$$H_{1F} = -4\pi K_s \alpha R_f^3 n_1 n_f [u'^2]_a \quad (2.2)$$

where, H_{1F} = Rate of floc formation,

K_s = Parameter that relates the effectiveness of floc formation ,

$[u'^2]_a$ = Mean square turbulent velocity (m/s),

R_f = Radius of the floc (mm),

n_1 = Number of primary particles, and

n_f = Number concentration of flocs.

Their proposed rate of floc breakup is given by

$$B_{1T} = B \frac{R_f^2}{R_1^2} n_f [u'^2]_a \quad (2.3)$$

where, B_{1T} = Rate of floc breakup,

B = Floc breakup constant, and

R_1 = Radius of the primary particle (mm).

The Argaman and Kaufman (1970) model is suitable for mixed reactor based processes where the rate of flocculation can be based on the ratio of the number concentration of the primary particles in the influent and effluent. It also does not represent the time evolution of the flocs. An algorithm to calibrate the parameters of the model was developed by Ayesa et al., (1991).

Summary

From the previous research on flocculation, there is a consensus that the process of flocculation is highly dynamic and depends upon a number of physical and chemical factors including the mineralogy of the clays, type of flocculant and the physical processes responsible for particle interaction. The shape, size and the density of the flocs is highly dependent on the way the flocs are formed. Flocs are geometrically irregular and change with space and time. Therefore, though it is possible to determine the shape and measure the size of the flocs using certain techniques such as imaging, it is very difficult to model floc sizes and density without some empiricism. Finally, flocculation models are either distribution based or size-class based. Size-class based models can predict the time evolution of the flocs and therefore have an advantage over the distribution-based models for non-batch processes

CHAPTER III

FLUME EXPERIMENT METHODOLOGY AND FLOCCULATION MODEL DESCRIPTION

Introduction

For this research, a laboratory research flume and a computer model were used. The flume allowed us to control the input variables important for flocculation to occur, while the model allowed us to predict flocculation efficiency at remote field locations. Five soils from across Oklahoma were utilized in the flume to measure the flocculation efficiency at different turbulence levels and with or without flocculant. The results from the flume were used to calibrate the model. In this chapter, the flocculation modeling approach will be discussed and the detailed description of the flume experimental methodology will be presented.

Flume Experiment Description and Methodology

Flume Apparatus

The main components of the experimental apparatus were

- Soil separator to separate sand and large aggregates from small aggregates, and silt and clay particles from the bulk soil,
- Sediment injection system,
- Constant head tank to provide constant flow into the flume,
Flocculant injection system
- Oscillating grid assembly to produce isotropic turbulence and mix the sediment and the flocculant, and
- Flume with the sampling ports to measure the suspended sediment's concentration, and trays to measure the total deposited sediment.

Soil Separator

Sand and large aggregates do not typically flocculate, and have higher settling velocities compared to silt and clays. In a field application the forebay will likely trap most, if not all of these sand and large aggregates. Thus, a soil separator was designed based on Stoke's Law to remove sand and the large aggregates from the bulk soil used in our laboratory experiments. Each particle size class had a different settling velocity. The particles in the size class of sand and greater had settling times less than, or equal to 13 s. The weir had a flow depth of 0.03m, and the length of the soil separator was 3m, which was calculated based on the settling velocity of a small sand particle (0.05 mm diameter). Dry soil was mixed with water having an approximate flow of 87 liter per minute. Slurry consisting of all particles having a size less than sand was discharged over a rectangular weir. Figure 3.1 shows the soil separator.



Figure 3.1. Soil separator used to remove sand particles and large aggregates.

Soil Injection System

The slurry, which primarily consisted of silt, clay and small aggregates, was pumped into a conical tank for uniform mixing and storage. When the sediments in the slurry settle in the tank they form a thick bed at the bottom of the tank. The sediment slurry required mixing well before it was injected into the flume to obtain a uniform concentration distribution. Thus, the sediment injection system was designed to operate in two modes: normal flow mode, and back flush mode. Under the normal flow mode the sediment coming from the bottom the tank was re-circulated back into the tank from the inlet at the top of the tank. The back flow mode was used when the sediment had settled for a long time in the tank and needed to be mixed. Once the initial mixing was done, the back flow mode was reverted to normal flow mode. An impeller was also mounted on top of the tank and ran during the experiments to ensure that the slurry was well mixed.

Figure 3.2 and Figure 3.3 show the schematic diagram of the sediment injection system in normal and back flow operating modes, and Figure 3.4 shows the sediment injection system.

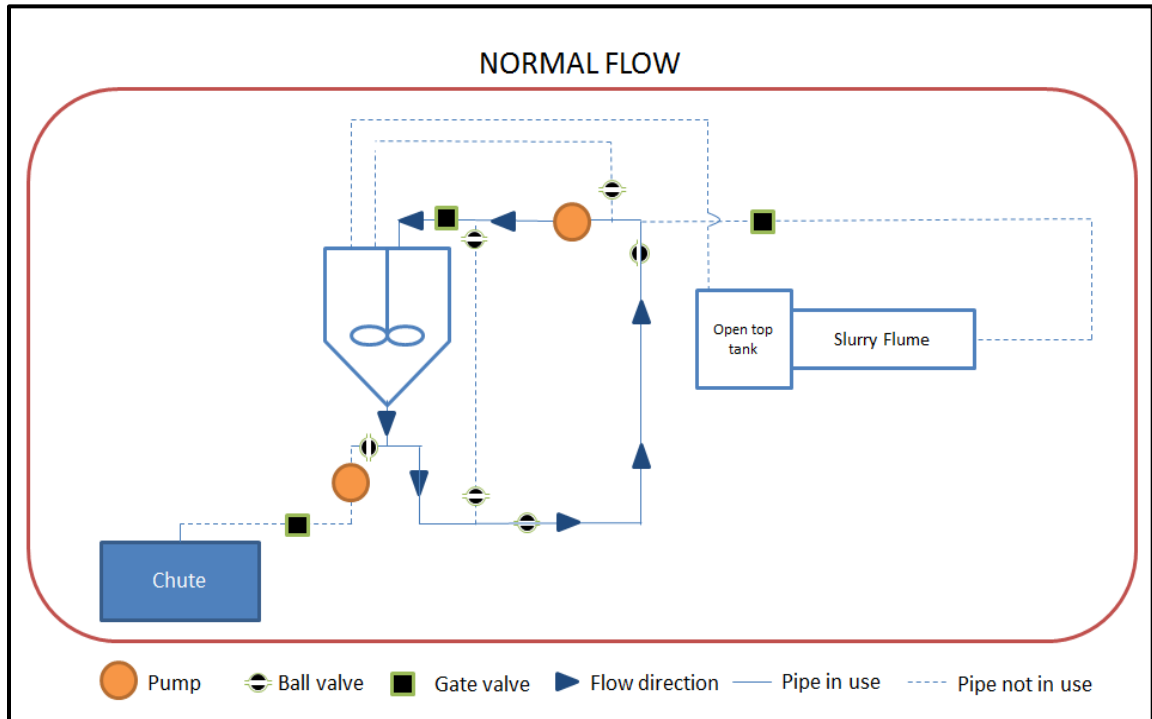


Figure 3.2. Diagrammatic representation of flow of sediment during normal flow operation.

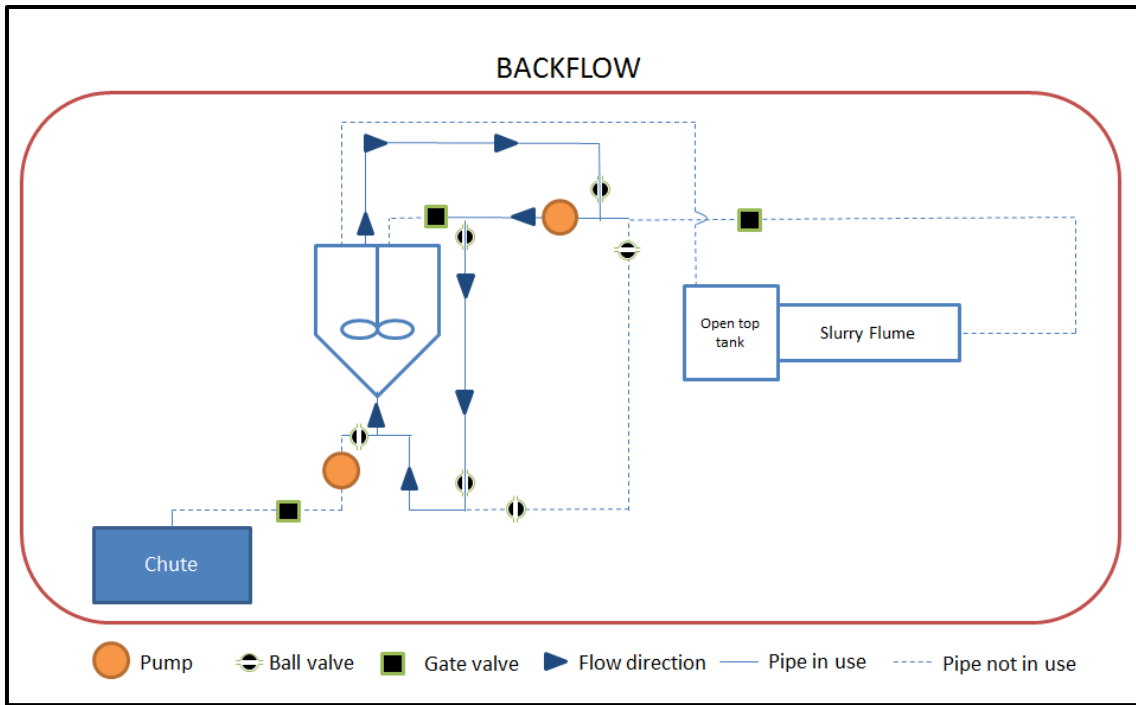


Figure 3.3. Diagrammatic representation of flow of sediment during back flow operation.

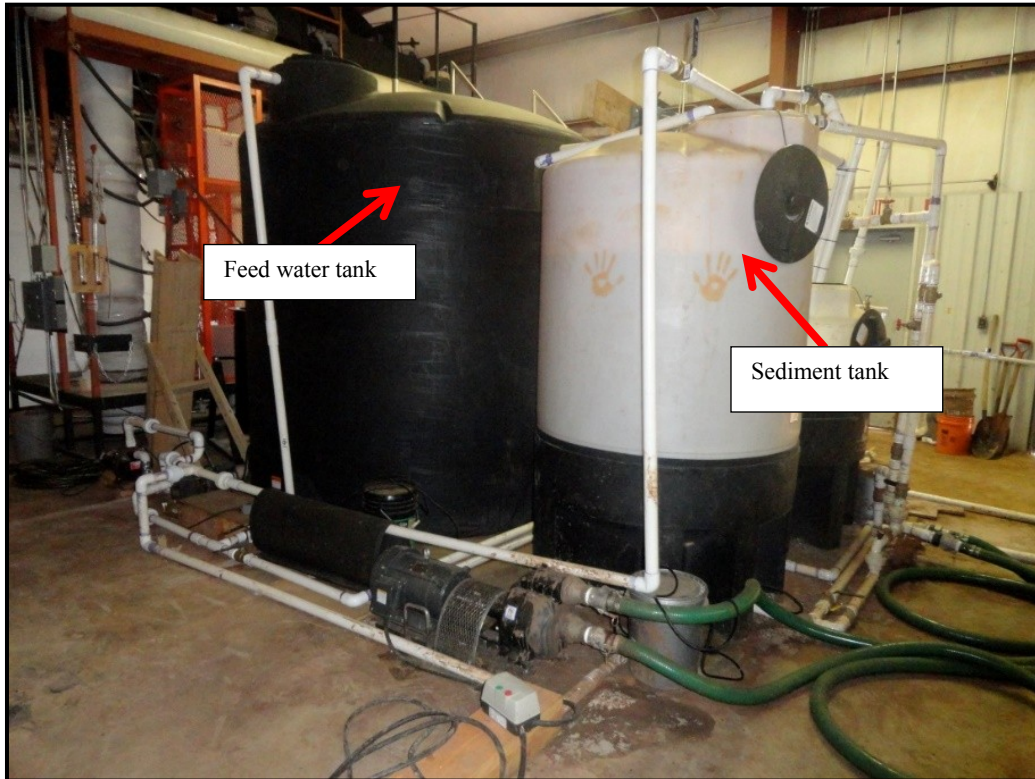


Figure 3.4. Sediment and water tank.

Constant Head Tank

A uniform flow rate of 170 liter per minute was maintained in the flume by use of a constant head tank. Figure 3.5 shows a diagram of the constant head tank, and Figure 3.6 shows a picture of the constant head tank. The tank has dimension of 3m x 1.5m x 1m (L x W x H). Flow straighteners were installed in the tank as shown in the diagram. The constant head tank has a V-notch weir at one end, and a tailgate at the other end. A water level of 0.2m over the V-notch weir corresponded to a flow of 170 liter per minute. The water flowing from the backside of the constant head tank into the overflow tank was recirculated back into the feed water tank.

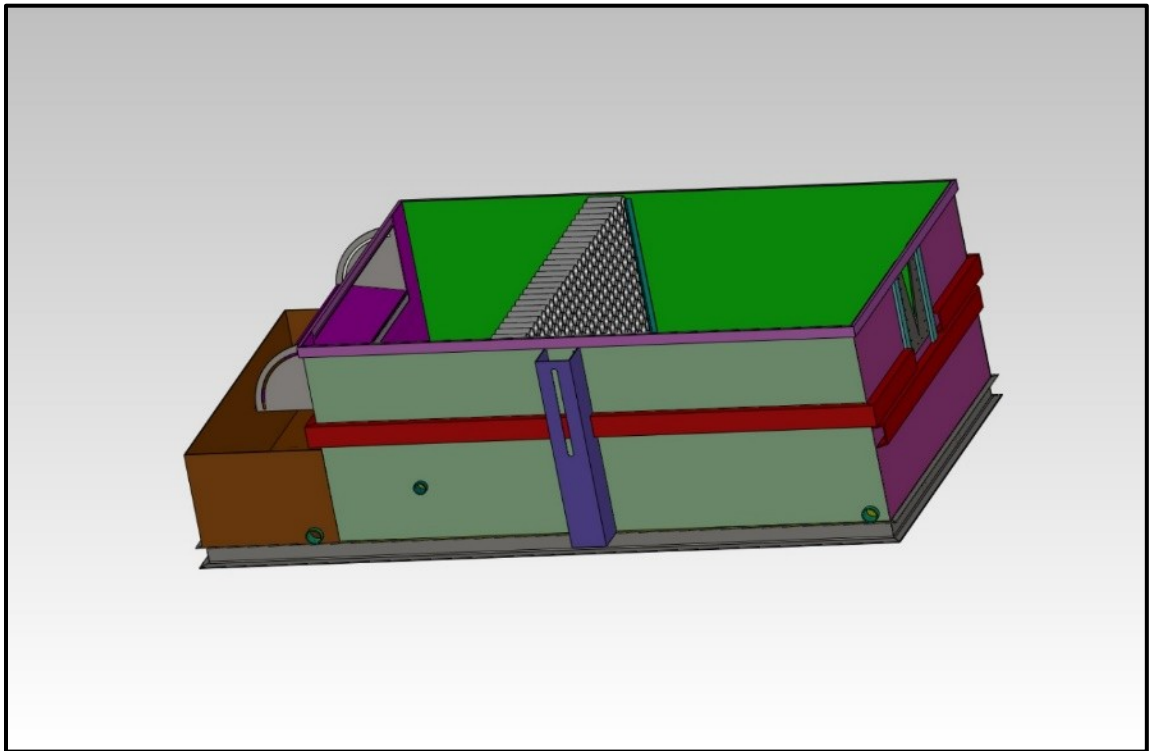


Figure 3.5. Diagram of the constant head tank used to regulate flow into the flume. (Drawn in Solid works by Mr. Wayne Kiner)



Figure 3.6. Constant head tank as constructed for regulating flow into the flume.

Flocculant Injection System

Hydrofloc 445L™, an anionic polyacrylamide (aPAM) based flocculant manufactured by Aqua Ben Corporation, California was used to test all the soils. The flocculant was mixed with water to a concentration of 30g/L in the tank as shown in Figure 3.7. The flocculant flow rate using the peristaltic pump was calibrated such that the flocculant concentration in the sediment flow in the flume was 0.15g/L.

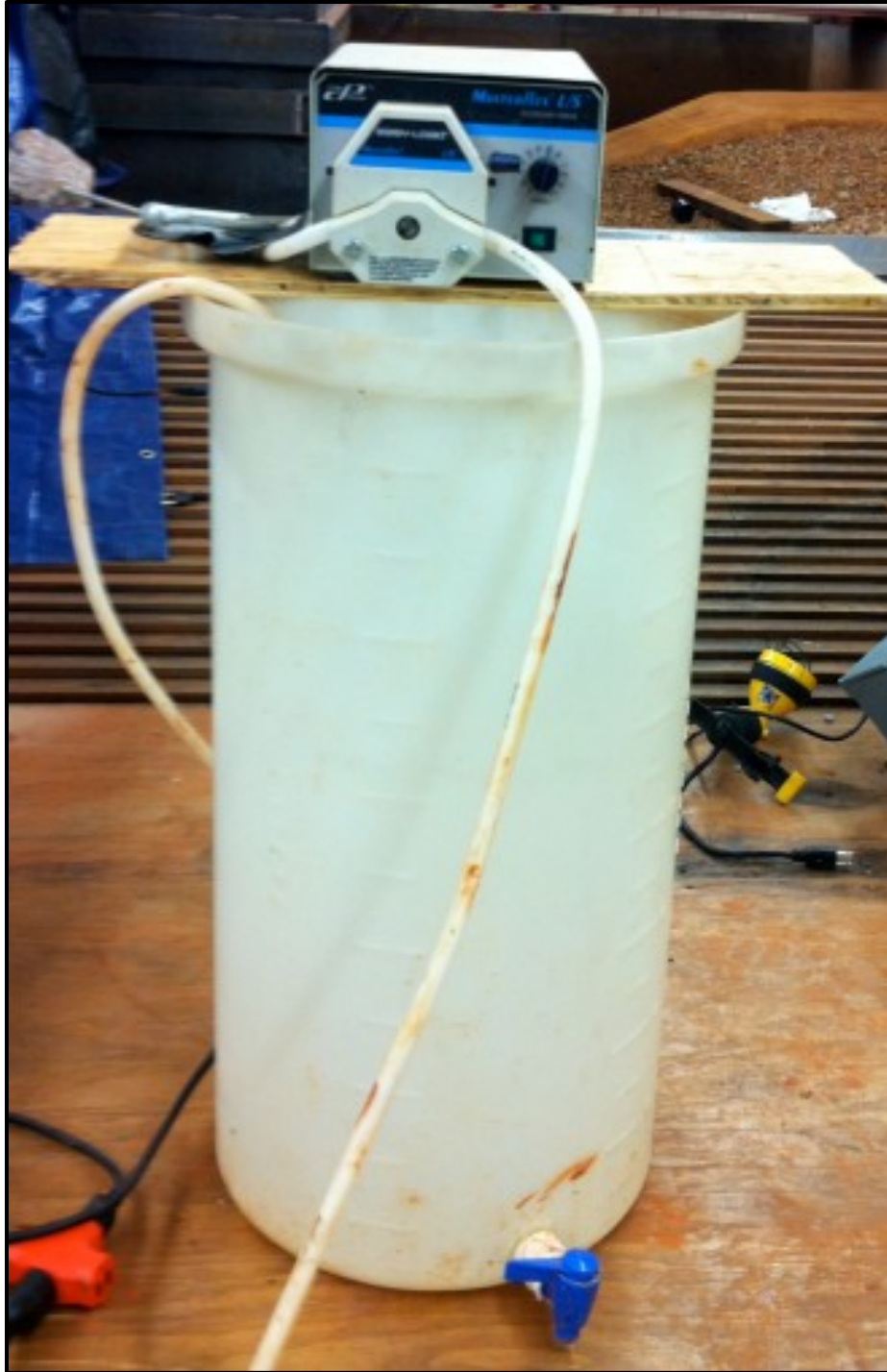


Figure 3.7. Flocculant injection system used for constant flocculant dosage into the flume.

Oscillating Grid Assembly

An oscillating grid-type mixing device was used to induce uniform mixing. By controlling the mixing intensity, using variable speeds, the drag force was controlled. By controlling the drag force the velocity gradient can be controlled, and thus the floc sizes can be estimated for different combinations of grid geometry and grid speeds. The oscillating grid apparatus consisted of a DC motor with speed controller, chain and sprocket drive, cams, linear guides for the grids to move up and down smoothly, and the grid. The oscillating grid assembly had nine individual grids. The mesh size of each grid was 0.01 inch, and the rod diameter was 5mm. The individual grid assembly consisted of three grids each as shown in Figure 3.8. The grids were oscillated at two different speeds of 99 rpm and 148 rpm each.

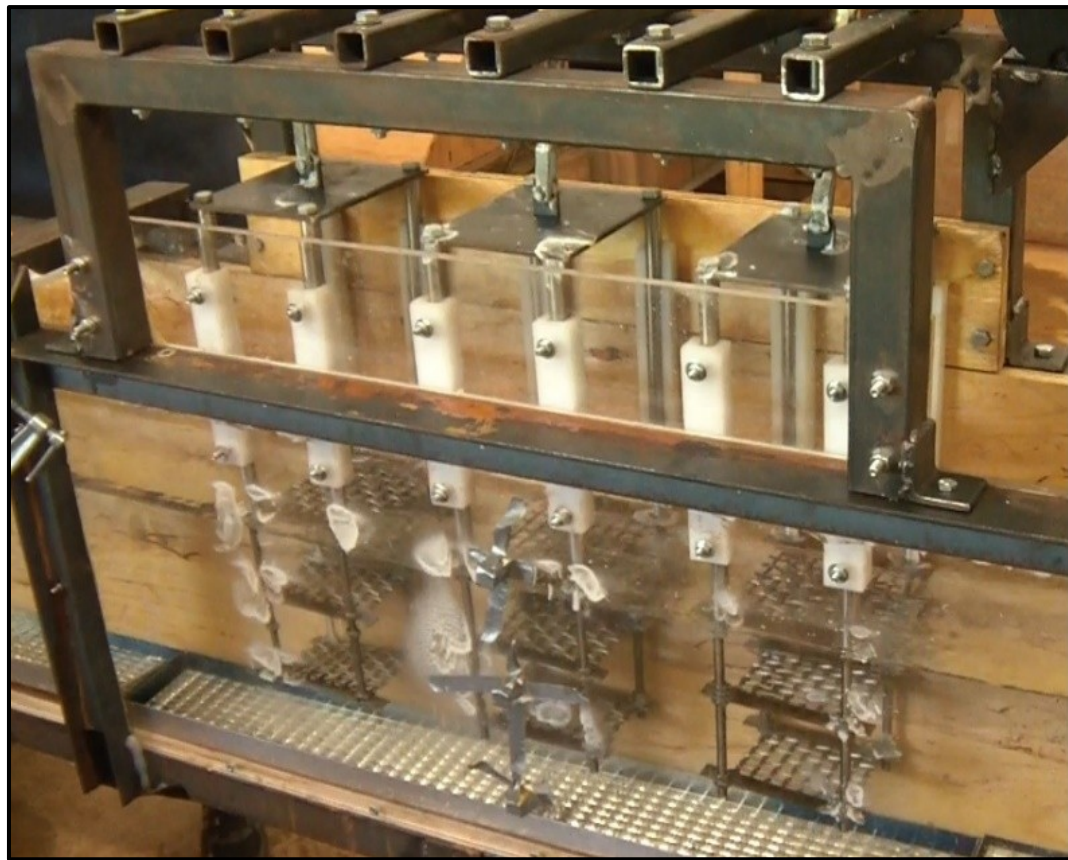


Figure 3.8. Oscillating grid assembly used to mix sediment and flocculant uniformly.

Flume

Flume dimensions are 9m x 0.2m x 0.5m. The flume had sampling ports on one side as shown in Figure 3.9. The sampling ports are placed at a distance of 0.07m and 0.3m from the bottom of the flume. The stations, numbered from 1 to 6, were located a distance of 0.7m, 1.6m, 3.5m, 5.3m, 7.2m and 9m from the start of the flume. Pitot tubes were fixed at each sampling ports facing upstream in the center of the flume.



Figure 3.9. Flume apparatus used for determination of flocculation efficiency.

Acoustic Doppler Velocimeter

A Sontek Inc. (San Diego, CA) 16 MHz Acoustic Doppler Velocimeter (ADV) as shown in Figure 3.10 was used to measure the instantaneous velocity of flow. The instantaneous velocity data was used to determine the turbulent energy dissipation rate and the total turbulent kinetic energy. This information was used to predict the floc sizes.

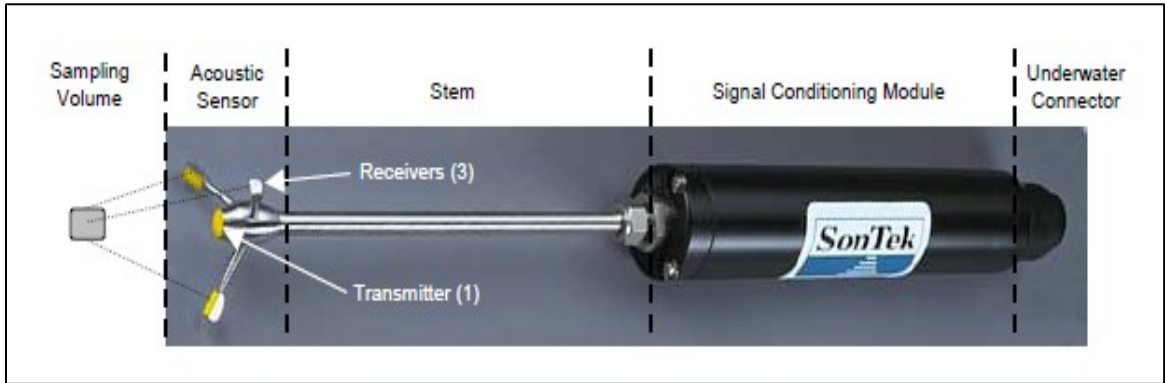


Figure 3.10. Sontek Inc. (San Diego, CA), 16 MHz ADV used for velocity measurement .

Description of the Experimental Runs

Each experiment had duration of approximately 10 minutes. Due to the slope on the flume, the tailgate height was fixed to ensure that the top port at Station 1 remained immersed in water throughout the experiment. During the experiment, the depth of the water at every station was measured. A sample of the sediment was collected at the injection port to determine the suspended sediments introduced into the system. Turbidity meters were installed at the upstream, and the downstream end of the flume. The sediment flow was controlled based on the upstream turbidity such that it was maintained in the range of 1500-2000 NTU, and it was continuously monitored throughout the experiment. Samples were collected at 1-minute interval in 250 ml bottles from the six stations, and the tailgate from the top and the bottom port simultaneously. Samples were collected from odd numbered station at time intervals of 1, 3, 5...etc. minutes and even samples were collected from the even numbered station at 2, 4, 6..etc. minutes. The first

sample was collected from all stations and the tailgate at 0 minute. The ADV was used to measure the turbulent velocity at a location of 3m from the start of the flume. Table 3.1 summarizes the types of the flume experiments conducted.

Table 3.1: Summary of the type of flume experiments conducted (NA: Not Applicable).

Type of Run	Mixing Intensity		
	No Mixing	Low Mixing Intensity	High Mixing Intensity
Control (No flocculant added)	2 runs	2 runs. Oscillating grid speed = 99 rpm	2 runs. Oscillating grid speed = 148 rpm
Flocculation Run	NA	3 runs. Oscillating grid speed = 99 rpm	3 runs. Oscillating grid speed = 148 rpm

The control runs were conducted to determine the mass of the sediment that settled out without the addition of the flocculant. Low and high velocity gradient flocculation runs were performed in triplicates in order to compare these data, check for the repeatability, and get a better estimate of the stickiness coefficient. The control runs were conducted in duplicates to compare and check for similarity in the trend of the data.

Description of the Soils

The soil series that were used for the experiments were Port (A & B horizon), Kamie (B horizon), Stephenville (B horizon) and Norge (B horizon). ‘A horizon’ is referred as the top soil or the surface soil. B horizon is referred as the subsurface soil that lies below the A horizon. The difference between the two horizons is due to the organic and the clay mineral content. The A horizon generally has more organic and lesser mineral content compared to the B horizon. Figure 3.11 shows a map of the distribution of the soils in Oklahoma and the approximate location from where they were collected for the experimental work. As described previously, the parent soil

material was passed through a soil separator to remove sand and large aggregates. A pipette test was conducted on both the parent soil and the separated soil slurry to determine the particle size distribution. The undispersed and the dispersed sediment particle size distribution for the parent and the separated soil slurry are shown in Figure 3.12 and 3.13 respectively.

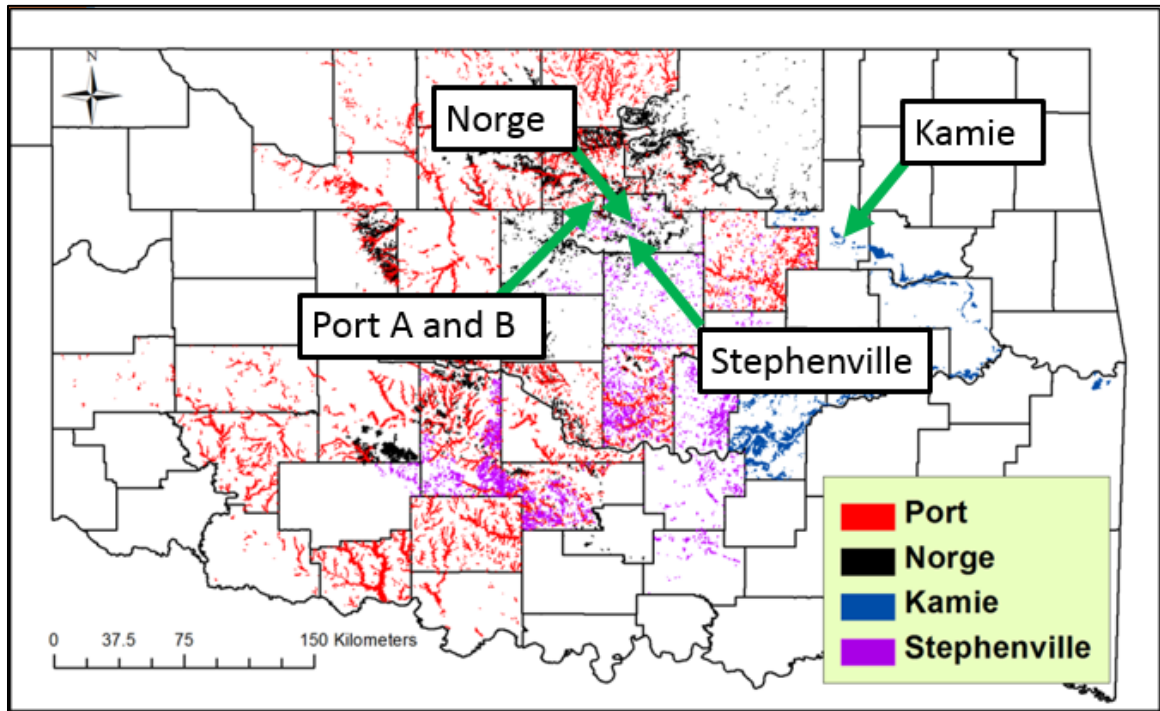


Figure 3.11. Distribution of Port, Kamie, Norge and Stephenville soil series in Oklahoma.

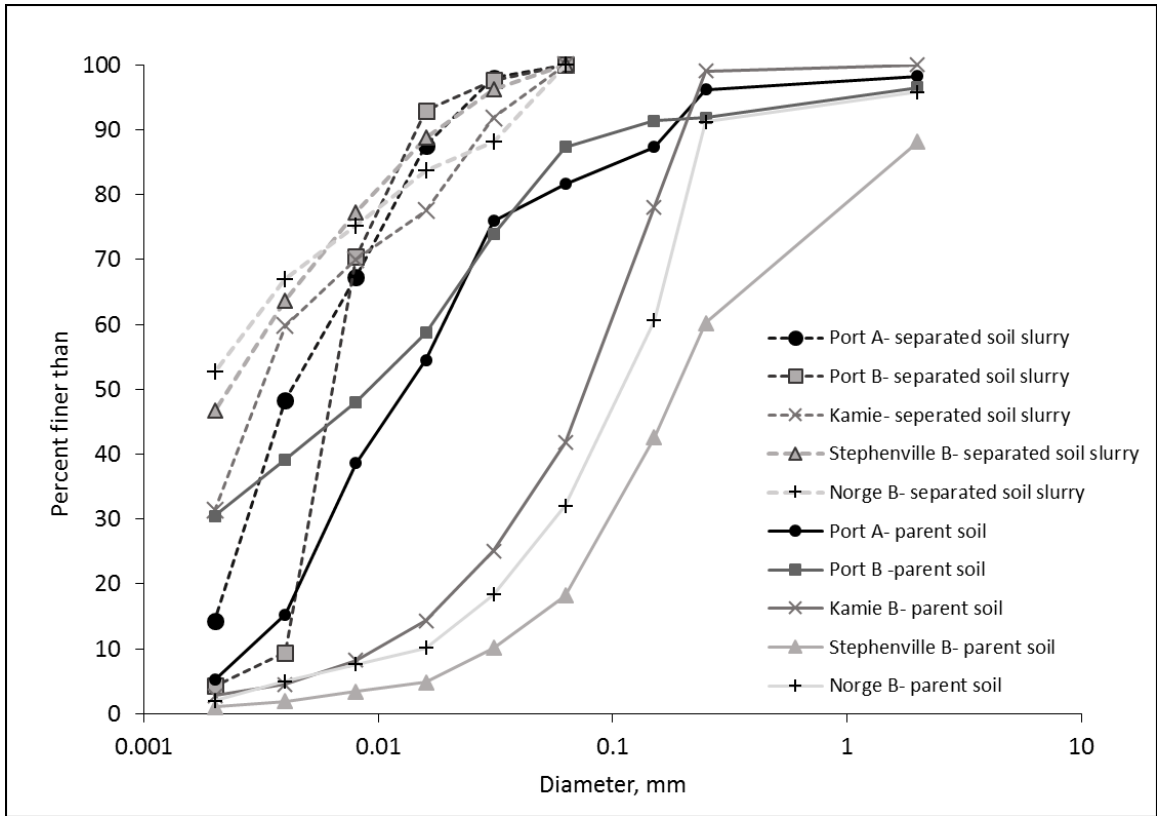


Figure 3.12. Undispersed sediment particle size distribution for all soils for parent and separated soil slurry measured from pipette tests

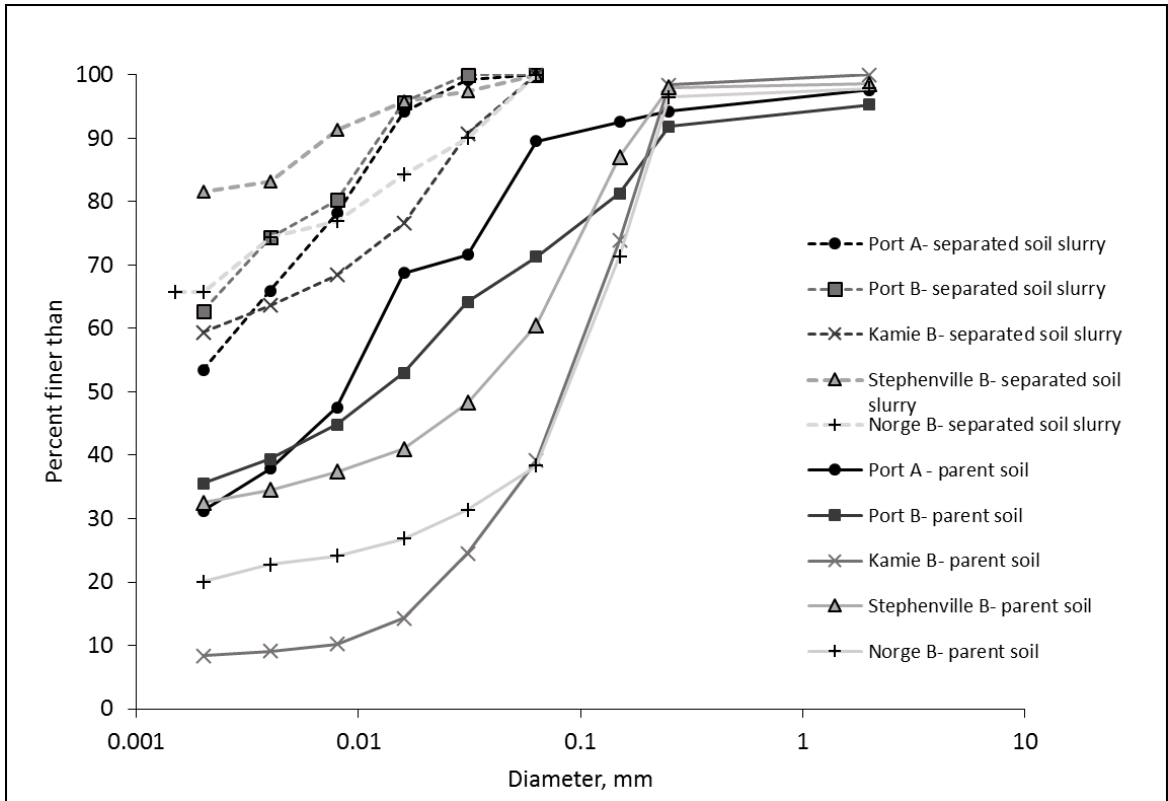


Figure 3.13. Dispersed sediment particle size distribution for all the soil for parent and separated soil slurry measured from pipette tests

The flume apparatus allowed direct measurement of the flocculation efficiency in controlled experiments. However, to predict flocculation a flocculation model was developed that can predict the flocculation efficiency using a polymer flocculant. This model was derived of a flocculation model developed by Krishnappan and Marsalek (2002). The following section describes the flocculation model approach in detail.

Flocculation Model Approach

Krishnappan and Marsalek (2002) modeled flocculation for a stormwater detention pond. The model uses a geometric progression for particle volumes, with resulting particle sizes, particle volumes, and particle volume ranges given in Table 3.2.

Table 3 2. Particle and floc size distribution methodology used by Krishnappan and Marsalek (2002).

Bin Number	1	2	3	4	M
Particle Diameter	d_1	$1.26d_1$	$1.59d_1$	$2d_1$	$\left[\frac{2^{M-1}}{3}\right]d_1$
Mean Particle Volume	v_1	$2v_1$	$4v_1$	$8v_1$	$2^{M-1}v_1$
Particle Volume Range	$\frac{2}{3}v_1$ to $\frac{4}{3}v_1$	$\frac{4}{3}v_1$ to $\frac{8}{3}v_1$	$\frac{8}{3}v_1$ to $\frac{16}{3}v_1$	$\frac{16}{3}v_1$ to $\frac{32}{3}v_1$	$\frac{2^M}{3}v_1$ to $\frac{2^{M+1}}{3}v_1$

This progression of particle sizes is such that all particle interactions for bin i for particle classes $j = 1$ to $i-1$ will form flocs that will go to either in bin i or bin $i+1$ as shown in Figure 3.14. The primary clay particles are assumed to be in bin 1. The other particles in the size range greater than bin 1 are distributed as flocs having 2^{i-1} primary particles. The number of collisions between particle from bin j (the source) with those from bin i depends on the two particle sizes and turbulence characteristics. If i is the bin number for the target particle and j is the bin number for the source particle, the number of collisions per unit time for the two particle sizes is equal to a loss of particles from bin j and a gain for bin i . The rate at which particle interactions are occurring between particles in bin i and bin j , is given by:

$$N_{ij,t} = n_{i,t}K_{ij}^{eff}n_{j,t} \quad (3.1)$$

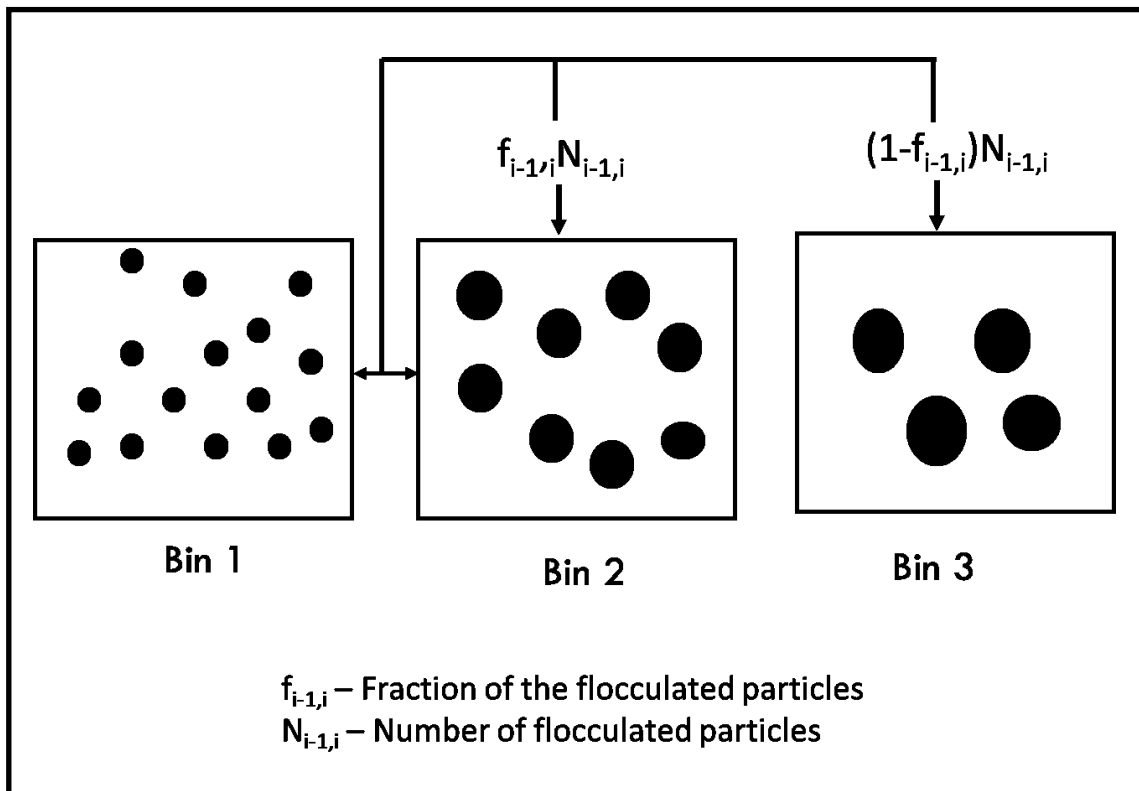


Figure 3.14. Schematic of method used for partitioning flocculated particles (Krishnappan and Marsalek, 2002).

where $N_{ij,t}$ is the rate of particle interaction $n_{i,t}$ and $n_{j,t}$ are the number concentrations of flocs in bins i and j and K_{ij}^{eff} ($m^3 s^{-1}$) is the resultant collision frequency calculated as the weighted sum of the collision frequencies due to the four mechanisms: Brownian motion, turbulent shear, inertia of turbulent flow, and differential settling. The collision frequency functions are described mathematically through Equations 3.2 to 3.6.

Brownian motion is described by

$$K_{i,j}^B = \frac{2 B_z T (r_i + r_j)^2}{3 \rho \nu r_i r_j} \quad (3.2)$$

B_z = Boltzmann constant (J/K),

T = Temperature (K),

ρ = Density of water (kgm^{-3}),

ν = Kinematic viscosity of water (m^2s^{-1}) of water, and

r_i, r_j = Radii of the particles in i, j size class (m).

The laminar or turbulent shear is given by

$$K_{i,j}^{SH} = \frac{4}{3} \left(\frac{\varepsilon}{\nu} \right)^{0.5} (r_i + r_j)^3 \quad (3.3)$$

ε = Turbulent energy dissipation rate (m^2s^{-3})

Inertia of turbulent flow is given by

$$K_{i,j}^{IN} = 1.21 \frac{\rho_s}{\rho_j} \left(\frac{\varepsilon^3}{\nu^5} \right)^{0.25} (r_i + r_j)^2 \text{abs}(r_i^2 - r_j^2) \quad (3.4)$$

ρ_s = Density of flocs (kgm^{-3}), and

ρ_j = Density of primary particles (kgm^{-3}).

Differential settling is given by:

$$K_{i,j}^{DS} = \frac{2\pi g \rho_s - \rho_w}{9\nu \rho_w} (r_i + r_j)^2 \text{abs}(r_i^2 - r_j^2) \quad (3.5)$$

ρ_w = Density of water (kgm^{-3}), and

g = Acceleration due to gravity (ms^{-2}),

Finally the, effective collision frequency is given by

$$K_{i,j}^{eff} = K_{i,j}^{BR} + \sqrt{(K_{i,j}^{SH})^2 + (K_{i,j}^{IN})^2 + (K_{i,j}^{DS})^2} \quad (3.6)$$

Based on the distribution of particle sizes shown in Table 3.1, when a particle of size j interacts with particle i , such that $j < i$, and flocculates, there are two options for its destination. It either goes to particle bin i or $i+1$. The fraction of particles going into bin i or $i+1$, based on a mass balance, and is given by

$$\rho_{si}n_i v_i + \rho_{sj}n_j v_j = \rho_{si}n_{PSi}v_i + \rho_{s,i+1}n_{PS,i+1}v_{i+1} \quad (3.7)$$

ρ_{si} and ρ_{sj} = Densities of the floc sizes i and j respectively, and

n_{PSi} and $n_{PS,i+1}$ = The number of flocs going to bins i and $i+1$.

Equation 3.7 can be solved for the fraction of particles $f_{i,j}$ going to each bins i and $i+1$, and is given by

$$f_{i,j} = \frac{\rho_{si}v_i + \rho_{sj}v_j - \rho_{s,i+1}v_{i+1}}{\rho_{si}v_i - \rho_{s,i+1}v_{i+1}} \quad (3.8)$$

The rate of change of floc numbers, n_i in a given bin i is determined by subdividing the process into three components. The rate of loss of particles in bin i due to effective collisions with larger flocs in bins j which is given by:

$$\text{Rate of loss to larger sizes} = - \sum_{j=i}^{N_{max}} \beta_i K_{ij}^{eff} n_i n_j \quad (3.9)$$

where, $\beta_{i,j}$ is called coagulation factor and is given by:

$$\beta_{i/j} = \alpha_0 \left(1 - \frac{R_{i/j}}{S_{Nmax} + 1} \right)^n \quad (3.10)$$

where, N_{max} is the total number of flocculation bins for the given simulation, α_0 is the true stickiness coefficient that must be determined for each soil and flocculant, n is an empirical constant Krishnappan suggests a value of 6), $R_{i/j}$ is the number of primary particles in bin i/j , and

S_{Nmax} is the maximum number of primary particles that can exist in a largest floc. The rate of gain of the particles to bin i due to effective collisions with smaller particles is given by:

$$\text{Rate of gain from small floc sizes} = \sum_{j=1}^i \beta_{i/j} f_{ij} K_{ij}^{eff} n_i n_j \quad (3.11)$$

Rate of gain from floc formation in bin $i-1$ resulting in flocs that are larger than those in bin $i-1$ and are transferred to bin i . is given by:

$$\text{Rate of gain to higher bin sizes} = \sum_{j=1}^{i-1} (1 - f_{i-1,j}) \beta_{i-1} K_{i-1,j}^{eff} n_{i-1} n_j \quad (3.12)$$

In order to do a mass balance such that the total rate of change of primary particles (clay particles) summed over all bins, it is necessary to convert equations to rates of change of primary particles. For this we multiply the rate of losses and gain by 2^{ij-1} . Therefore to find out the total rate of the particles have undergone interaction and growth, we add the loss and gain equations which is as given by:

$$\begin{aligned} \frac{dn_{pp,i}}{dt} = & - \sum_{j=i}^{Nmax} 2^{i-1} \beta_i K_{ij}^{eff} n_i n_j + \sum_{j=1}^i 2^{j-1} \beta_i f_{ij} K_{ij}^{eff} n_i n_j \\ & + \sum_{j=1}^{i-1} 2^{j-1} (1 - f_{i-1,j}) \beta_{i-1} K_{i-1,j}^{eff} n_{i-1} n_j \end{aligned} \quad (3.13)$$

The above equation represents the population balance equation for the flocculation process. However, coming back to the issue of particle density, Krishnappan and Marsalek (2002) developed the following empirical relationship for particle density

$$\rho_{s,i} - \rho_w = (\rho_{s,1} - \rho_w) \exp(-bd_i^c) \quad (3.14)$$

where, $\rho_{s,i}$, ρ_w , and $\rho_{s,1}$ are the densities of floc of size i , water, and the primary clay particle, of diameter $d_{s,1}$, and b , and c are empirical constants. Dividing both sides of the Eq.3.14 by ρ_w ,

converts to a relationship for specific gravity, SG_i or:

$$\frac{SG_i - 1}{SG_1 - 1} = \exp(-bd_i^c) \quad (3.15)$$

where d_i is the diameter of the particle in bin ‘ i ’ and is in micrometer. Krishnappan and Marsalek (2002) suggest values of 0.02 and 1.45 for b and c when using floc diameter in micrometers. However, their model has been applied for flocculation of cohesive sediment with no polymer flocculant treatment. The density of the flocs formed using liquid polymer flocculant are very different from those formed due to natural flocculation and therefore, the values of the empirical constants b and c , which are important in predicting the floc densities, will be different. In order to determine the values of b and c using polymer flocculant, a jar test was performed in conjunction with a pipette test to determine the settling velocities of the sediment particles. A MATLAB code was written to optimize the b and c values, such that the predicted settled velocity of the flocs would be as close as possible to the measured settling velocity. 41

Conclusions

Flume apparatus allowed us to understand flocculation and measure the flocculation efficiency for five soils from Oklahoma. In addition to the flume experiments, a flocculation model was developed, which can be used to predict the flocculation efficiency for different soils using polymer flocculant in laboratory or in the field.

CHAPTER IV

FLUME INVESTIGATION OF POLYMER FLOCCULATION EFFECTIVENESS IN STORMWATER RUNOFF

Abstract

The turbidity of construction site runoff may impact surface water quality and aquatic habitat. Because traditional sediment control techniques are not effective in removing clay-size particles that contribute the most to increased turbidity in construction site runoff, flocculants may be utilized to remove these particles and decrease turbidity levels. The objective of this study was to determine the flocculation efficiency and the overall turbidity reduction for simulated runoff containing suspended sediment from five soils in Oklahoma, USA, using a polymer flocculant. These experiments were conducted in a rectangular flume with monitoring stations at the beginning, end, and several locations along its length. The average turbidity reduction for these soils when using the polymer flocculant ranged from 71 to 80 percent and the average reduction in the suspended sediment concentration ranged from 55 to 60 percent. Turbidity reduction efficiency was greater than the sediment removal efficiency during the flocculation experiments because of greater removal of finer particles, such as clay and fine silts, that have a greater impact on turbidity than suspended sediment concentrations. The selected low- and high-mixing intensities did not significantly affect the flocculation efficiency. Therefore, for polymer flocculant either mixing intensity is acceptable to uniformly mix the flocculant and sediment particles and can be used to achieve similar flocculation efficiencies.

Keywords: stormwater, flocculation, settling, turbidity

Introduction

Turbidity of construction site runoff is of concern because of the potential impact on water quality and aquatic habitats because many contaminants are often associated with sediment. Stormwater runoff from construction sites have large amounts of sediments which are composed of sand, silts, clays, colloidal particles and their small and large aggregates. Clay and colloidal particles in the size range of 4 μm and lower often do not naturally aggregate quickly and remain in suspension for prolonged periods (Patil et al., 2011). The commonly used techniques for sediment control on construction sites include silt fences, rock ditch checks, sediment detention ponds, fiber rolls, and vegetated filter strips primarily rely on settling due to gravity for sediment removal (Barfield et al., 2011). Sand, large aggregates and small aggregates with high settling velocities can be trapped easily in a reasonably sized settling basin. Clay and colloidal particles in the size range of up to 4 microns have very small settling velocities and can take weeks to months to settle, and therefore generally require some form of enhanced settling for removal from stormwater runoff (Haan et al., 1994). Research by Barrett et al., 1995, Millen et al., 1997 have shown that conventional sediment techniques can trap larger particles but cannot remove finer particles that are the primary source of turbidity. Flocculation is a method that can improve the settling characteristics of the clay particles; the addition of flocculant to the stormwater runoff will cause multiple particles to bind together, by either charge neutralization or by chemisorption; thereby increasing their effective size and ultimately their ability to settle quickly (Droppo et al., 2008; Jarvis et al., 2005). The factors affecting the performance of the flocculation system are: drainage area characteristics that impact sediment concentration such as area, slope, rainfall intensity; soil type characterized by the amount and dispersivity of clay; type of flocculant; and flocculant dosage. Due to the uniqueness of each construction site and huge variability in the soil type, there is currently limited information available on the effectiveness of flocculation on

suspended sediment removal and turbidity reduction (McLaughlin and Bartholomew, 2007). The objective of this study was to conduct flume experiments to determine the overall flocculation efficiency and turbidity reduction for five soils from Oklahoma: Port A horizon (Port A), Port B horizon (Port B), Kamie B horizon (Kamie B), Stephenville B horizon (Stephenville B), and Norge B horizon (Norge B) using a polyacrylamide (PAM) chemical flocculant.

Methodology:

Experimental Flume Setup

The experimental flume setup consisted of a constant head tank, a rectangular flume with sampling ports, flocculant injection, soil separating flume, slurry tank, and oscillating grids. A schematic flow diagram of the entire system is shown in Figure 4.1 and the detailed description of various components of the experimental apparatus are shown in Table 4.1. Sand and large aggregates do not flocculate well, and often inhibit flocculation (McLaughlin and Bartholomew, 2007). Therefore, a soil separator was designed and utilized prior to the flume experiments to remove the sand-sized particles and large aggregates by adding parent soil into the soil separator, leaving only clay, silt and small aggregates in the resulting soil slurry. To remove the sand-sized and larger particles a constant flow rate of 87 liter per minute was maintained at the inlet of the soil separator, which allowed enough time for the larger particles to settle down eventually separating silt-sized and smaller particles from the sand-sized particles. The soil slurry from the separator was pumped into a tank and kept well mixed by circulation and an impeller type mixer. A constant head tank fed water to a flume at a uniform flow rate. Flow straighteners incorporated inside the tank smoothed the flow before it entered the flume. The rectangular flume was 9.1 m long, 0.15 m wide and 0.46 m deep. Eleven trays having dimensions of 0.762m x 0.15m x 0.025m were placed at the bottom of the flume to collect the settling sediments and the flocculated mass. A variable speed oscillating grid assembly consisting of three sets of vertically

moving grids was used to provide mixing. Samples to measure the suspended sediment concentration were collected at six stations located downstream and an additional sample was collected at the tailgate. In addition, an acoustic A Sontek Inc. (San Diego, CA), 16 MHz Acoustic Doppler Velocimeter (ADV) was used to measure the turbulent velocities. The particle size class distribution of the input slurry was measured separately using pipette analysis, as described in the USDA Kellogg Soil Survey Laboratory Manual (Method 3A).

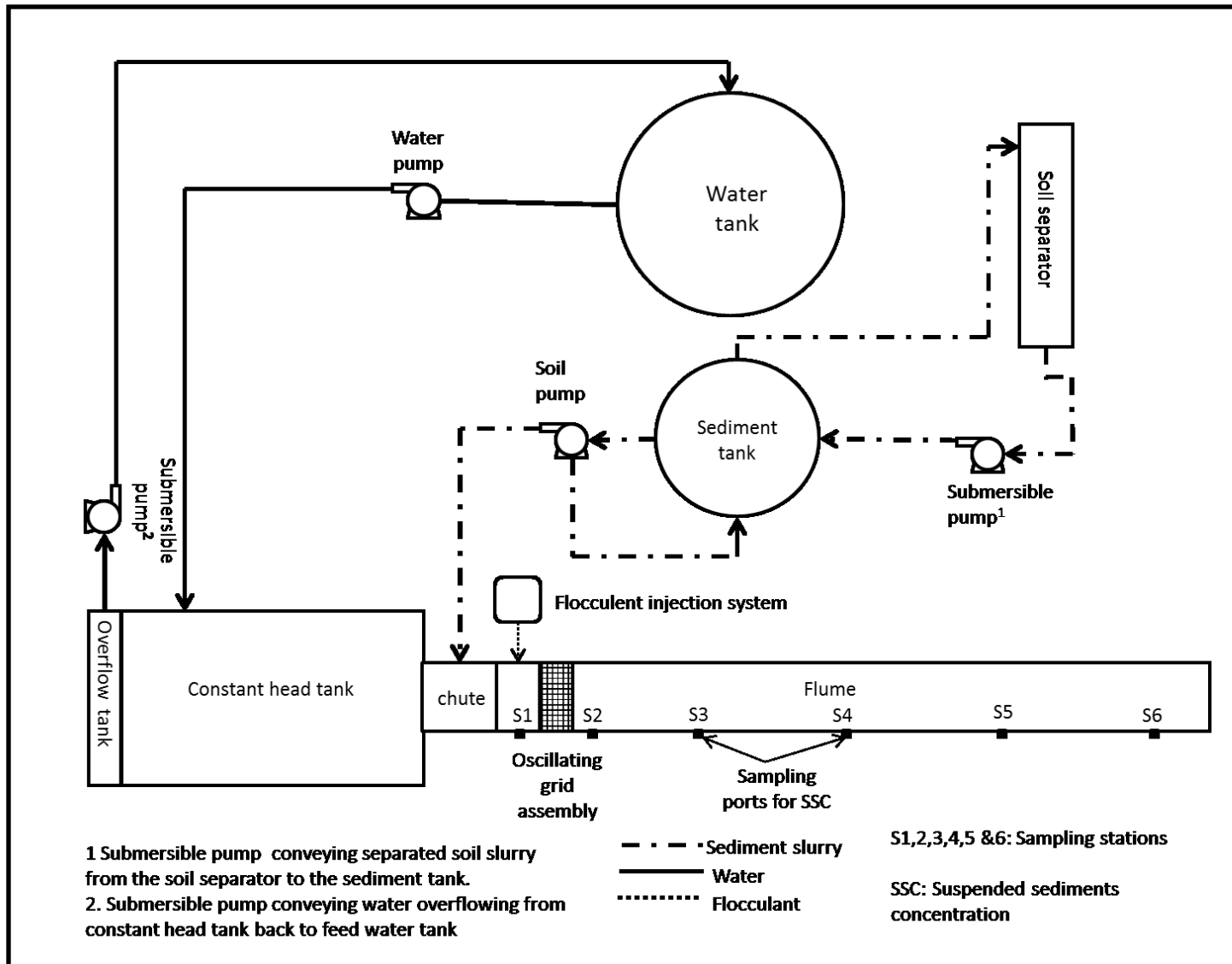


Figure 4.1. Schematic flow diagram of the experimental setup for flume experiments

Table 4.1. Description of the experimental apparatus.

Component	Description	Dimension/ Capacity
Soil Separator	Rectangular flume with overflow weir plate at the outlet	Flume :3.0 m x 0.2 m x 0.6 m (L x W x H) Weir Plate: 0.3 m x 0.2 m Weir depth= 0.03 m
Sediment injection system	Conical tank with backflow and normal flow systems and impeller for mixing	Capacity: 1700 Liters
Flocculant injection system	Peristaltic pump system mounted on a tank containing the flocculent mixture.	Capacity of Flocculant Tank: 50 Liters
Oscillating grid Assembly	Three sets of oscillating grids each having three individual grids.	Rod diameter: 0.0004 m Grid dimension: 0.15 m x 0.15 m Individual grid spacing: 0.076 m Distance between each set of grids: 0.15 m
Constant head tank	Rectangular metallic tank with flow straighteners and V-notch weir at the outlet.	3 m x 1.5 m x 0.9 m (L x W x H)
Flume	Rectangular metallic flume with sampling ports along the flume	9.1 m x 0.15 m x 0.46 m (L x W x H) Distance of Top port from bottom of the flume: 9 inches Distance of Bottom port from the bottom of the flume : 3 inches Location of the sampling stations downstream from start of the flume Station 1: 0.7 m Station 2: 1.6 m Station 3: 3.5 m Station 4: 5.3 m Station 5: 7.2 m Station 6: 8.9 m Tailgate: 9.1 m

Description of the Experimental Runs

During the flume experiment, the flow rate of water flowing from the constant head tank into the flume was maintained at 170 liter per minute. The separated soil slurry consisting of the finer particles was added to water entering the flume at the chute that connected the flume and the constant head tank. The flow rate of the sediment slurry was adjustable and was controlled to maintain the upstream turbidity between 1500 and 2000 nephelometric turbidity units (NTU). Flow rate of the incoming sediment was measured at the start and the end of the experiment run and was averaged to determine the incoming sediment flow rate.

Hydrofloc 445L, an anionic polyacrylamide monomer (aPAM) flocculent manufactured by AquaBen Corporation, California was used for all the experiments. Additional information on flocculant selection can be found in Oklahoma Transportation Center report 'Design of Turbidity Controls for Oklahoma Highway Construction.' (Vogel et al, 2014). The flocculant was mixed with water optimally for 5-6 hours prior to running the experiment at the concentration of 30 g/L. The flocculant was injected in the flume with a peristaltic pump immediately before the oscillating grids. The flow rate of the flocculent was calibrated such that the concentration of the flocculent in the sediment water mixture would be 0.15 g/L. This required flocculant dosage was predetermined with the help of jar test.

The flume experiments were broadly classified as control and flocculation runs. No flocculant was injected for the control runs to determine the mass of sediment settling without flocculation. Control runs were conducted for high and low mixing intensity and for no mixing condition. All the control runs were replicated twice. Flocculation runs were conducted at high and low mixing intensities. All flocculation runs were replicated thrice for better repeatability. The speed of the oscillating grids was set at 99 rpm for low mixing intensity which corresponded to a velocity gradient (G) of 104 s^{-1} and 148 rpm for high mixing intensity which corresponded to a velocity gradient of 134 s^{-1} . These velocity gradients were calculated based on the equations presented by Liem et al. (1999).

Six samples were collected at an interval of one minute simultaneously from the top and bottom port in a high density polyethylene (HDPE) bottle having a volume of 250 ml, at each sampling station. ASTM D3977-97 Test A procedure was followed to determine the sediment concentration. A procedure was followed to determine the sediment concentration. However, instead of drying the samples in an evaporating dish at 105°C, they were dried in the sample bottles at a lower temperature of 90°C for duration of 48 hours, owing to the large sample size and lower melting point of the HDPE bottles. The same procedure was followed to determine the concentrations of the sediment that settled in the trays for both the all the experiment runs.

In addition, the inlet and the outlet turbidity measurement were recorded at every 30s during the experiment using Hydrolab MS5 multiparameter sondes (Hach Hydromet, Loveland, Colorado). A two point calibration procedure as recommended by the Hach Hydromet was carried out once every two weeks to ensure that the sensors were calibrated for turbidity measurements.

Background Information on Selected Soils from Oklahoma

Flume experiments were conducted on five soil types: Port A, Port B, Kamie B, Stephenville B and Norge B. Each soil was separated to remove the sand and large aggregates. The undispersed and the dispersed particle size distribution for parent and the separated soil slurry measured from pipette tests is shown in Figure 4.2 and Figure 4.3.

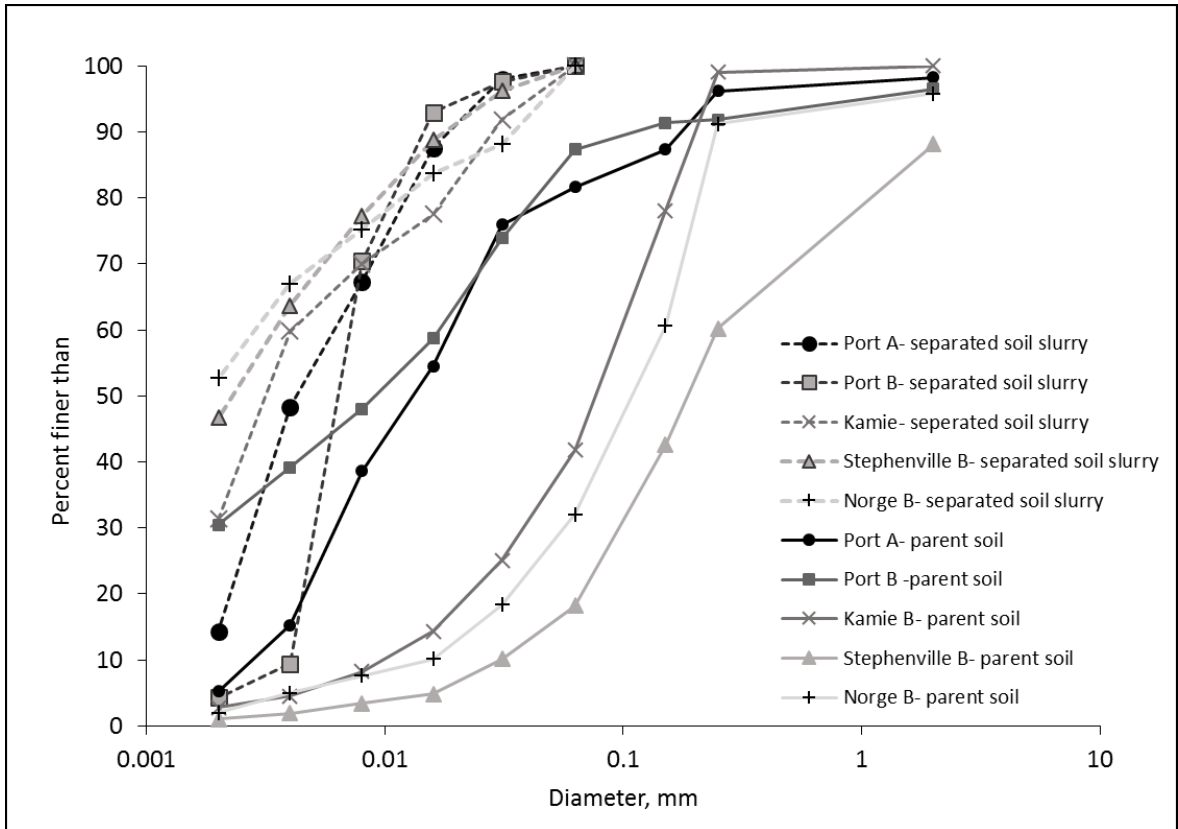


Figure 4.2. Undispersed sediment particle size distribution for all the soil for parent and separated soil slurry measured from pipette tests

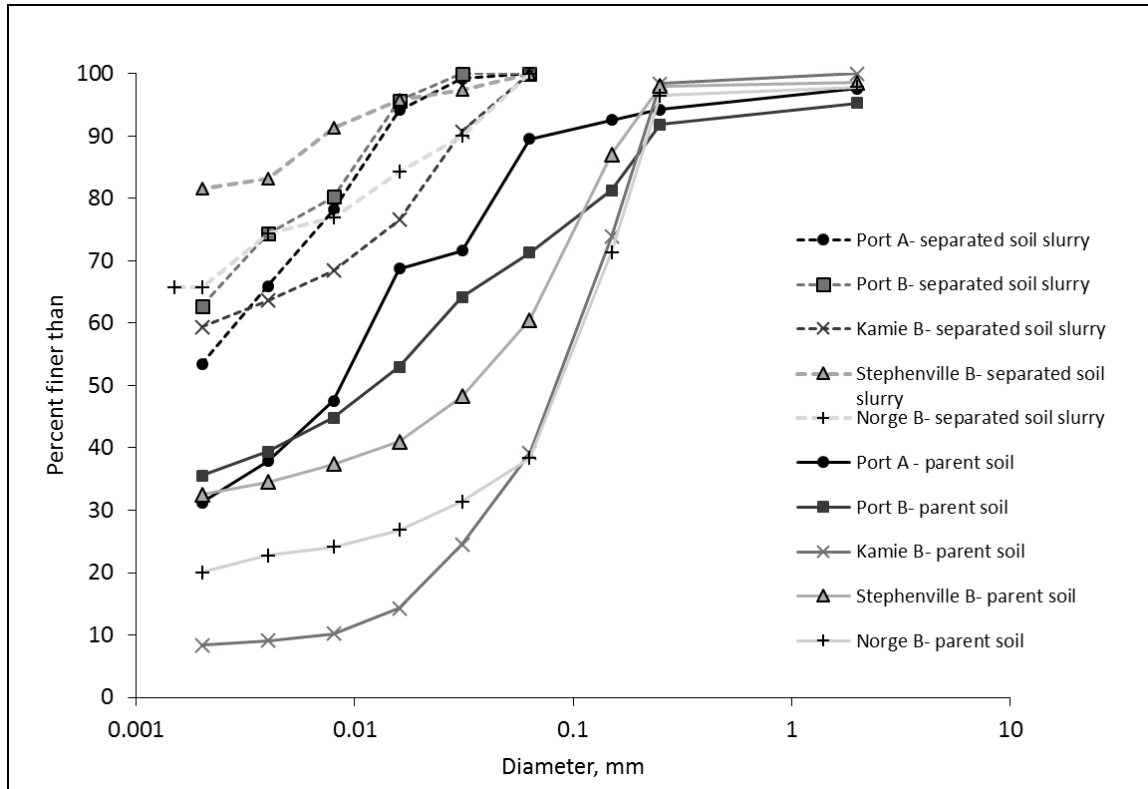


Figure 4.3. Dispersed sediment particle size distribution for all the soil for parent and separated soil slurry measured from pipette tests

Results and Discussion

Flume experiments were utilized to characterize the sediment removal and turbidity removal efficiency when using flocculants on runoff with suspended sediment deriving from selected soils using Hydrofloc 445L.

Sediment Removal

Figure 4.4 and 4.5 shows the difference observed between the sediment concentrations measured at the top and the bottom ports of the flume for a low mixing intensity control and flocculation run respectively for Port B soil. From Figure 4.4 it can be seen that the suspended sediment concentration measured at the top and the bottom of the flume were more or less similar in the range of 1 to 2.2 g/L. Since no flocculant was added, there was not a huge difference in the suspended sediment concentration measured at the top and bottom ports. However, the

suspended sediment concentrations measured at the top and bottom ports for the flocculation run were very different and can be seen in Figure 4.5. In Figure 4.5A, the suspended sediment concentration measured at the top port at a distance of 0.7 m and 1.6 m downstream was high compared to other sampling locations downstream. This was the zone where the flocculant and the sediment was mixed thoroughly and flocculation had begun. The effect of the flocculant on the sediment can be seen starting at distance of 3.5 m downstream, where the suspended sediment concentrations decrease, with the lowest measured at the outlet of the flume (8.9 m). In Figure 4.5 B, suspended sediment concentrations measured at the bottom port at 3.5 m and 5.3 m respectively, were low. The reason for this could have been that large flocs were yet to be formed and therefore there was not much settling of sediment at these locations. But again from, Figure 4.5 B, most of flocculated sediment settled at a distance of 7.2 m and therefore, the largest flocs might have formed at this location. This also, explains the low suspended sediment concentration measured at the bottom port at sampling location of 8.9m downstream.

The mass of the deposited sediment measured from the trays placed at the bottom of the flume was used to determine the effective sediment removal capacity. A box plot showing the range of the sediment removal efficiencies measured for all the flocculation runs is shown in Figure 4.6. The sediment removal efficiency for Port A soil was observed to be the lowest, with average sediment removal efficiency of 32%. Sediment removal efficiencies for Port B were in the range of 48 to 64 %, with average sediment removal efficiency of 56%. From Figure 4.2, the percentage of clay in separated slurry for Port A soil was greater than that for Port B. The possible reason for the huge difference in the flocculation efficiency could be due to the different clay minerals in the two horizons. The range of the sediment removal efficiency was observed to be largest for the Kamie B soil. The greater variability could be associated with the lower percentage of clay in Kamie B compared to the other four soils, which made the separation of finer particles relatively difficult. Stephenville B soil also had a larger range of sediment removal efficiency compared to Port A, Port B and Norge B soil. Norge B had the lowest range of the

sediment removal efficiency of any of the five soils tested. Overall average sediment removal efficiency using Hydrofloc 445 L was approximately 41%. The variability in the range of the sediment efficiencies observed could be attributed differences in the clay types in each soil and the percentage of the small aggregates.

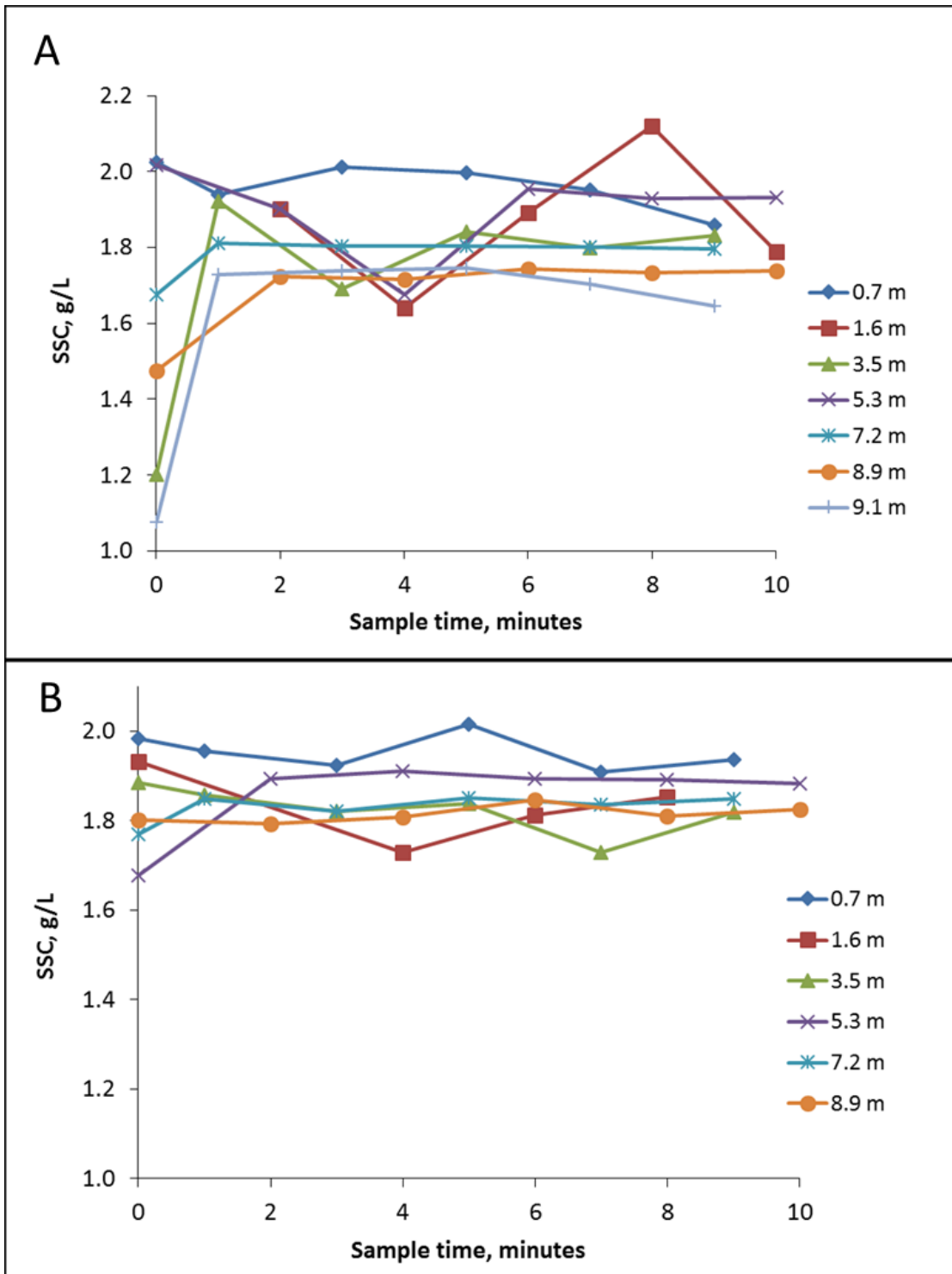


Figure 4.4. Suspended sediment concentration (SSC) for low mixing intensity control run
 A) Top port and tailgate B) Bottom port.

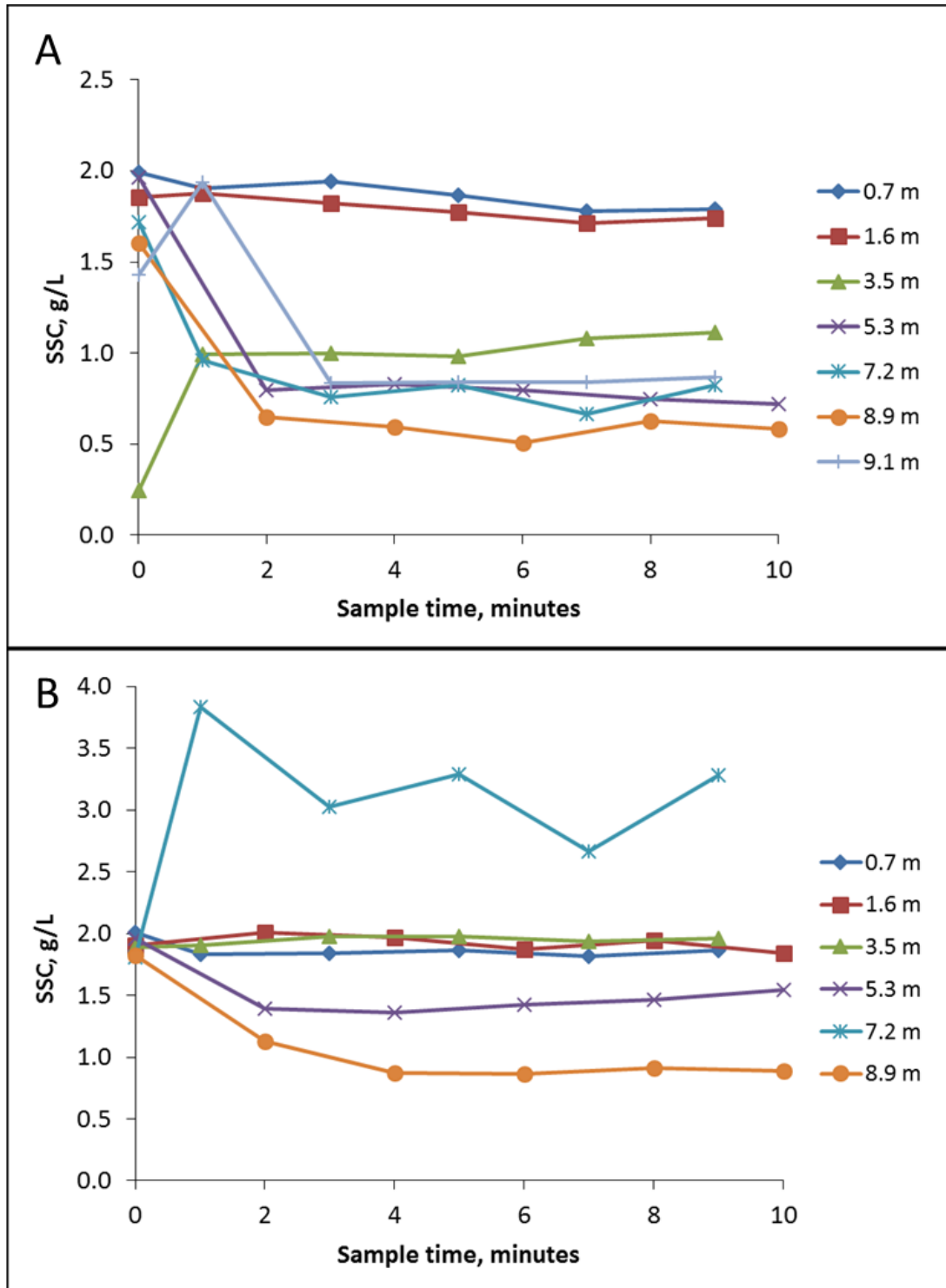


Figure 4.5. Suspended sediment concentration (SSC) for low mixing intensity flocculation run for Port B soil. A) Top port and tailgate B) Bottom port.

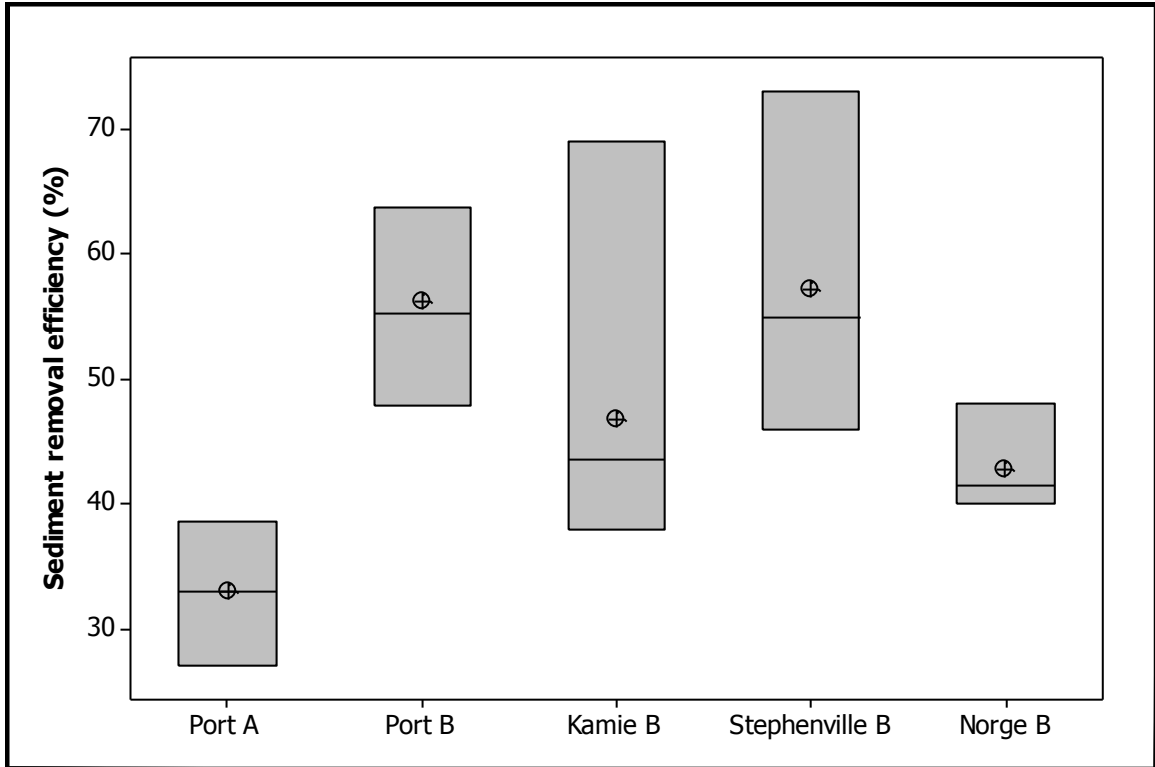


Figure 4.6. Range and the average percent sediment removal efficiency for all soils

Turbidity Removal:

A representative graph for the upstream and downstream turbidity measurements for the control run for Port B is shown in Figure 4.7 and for a flocculation run for Port B is shown in Figure 4.8. The upstream and downstream turbidities were recorded an interval of 30 seconds for all the experiment runs. The effect of the addition of the flocculant can be seen by the reduction in the downstream turbidity in Figure 4.8 compared to that in Figure 4.7. Table 4.2 shows the average input and output turbidities for the five soils and Figure 4.9 shows a box plot of the range of the upstream and downstream turbidities measured for the soils. The overall turbidity reduction for was in the range of 71% and 80%. The highest average turbidity reduction of 79% was observed for Stephenville B soil, which also had the highest average sediment removal efficiency. The range of the upstream turbidity was the largest for Kamie B soil. As explained previously, this was due to the lower percentage of clay in the soil and the difficulty in separation

of the finer particles. With the highest flow rate of the incoming soil slurry, the maximum turbidity range that could be achieved for the Kamie B soil was in the range of 1300-1500 NTU, with an average turbidity in the range of 1200- 1400 NTU. The average turbidity reduction efficiency for Kamie B soil was 77%. Port A soil had the lowest turbidity reduction efficiency of 71%. The average turbidity reduction for Port B soil was 75% and that for Norge B soil was 73%. The overall average turbidity reduction for all the soils using Hydrofloc 445 L was 76%. Research study done by Barrett et al., 1995 on silt fences on three different soil types, showed that the turbidity reduction was lower than 30%. Therefore, in comparison with the research done by Barrett et al., 1995, turbidity reduction due to flocculation treatment is larger.

Table 4.2. Average turbidity measured at the inlet and outlet of the flume for all the soils.

Soil	Average upstream turbidity (NTU)		Average downstream turbidity (NTU)	
	Low mixing intensity	High mixing intensity	Low mixing intensity	High mixing intensity
Port A	1584	1526	400	436
Port B	1771	1751	485	360
Kamie B	1284	1402	360	259
Stephenville B	1644	1559	352	316
Norge B	1618	1681	490	395

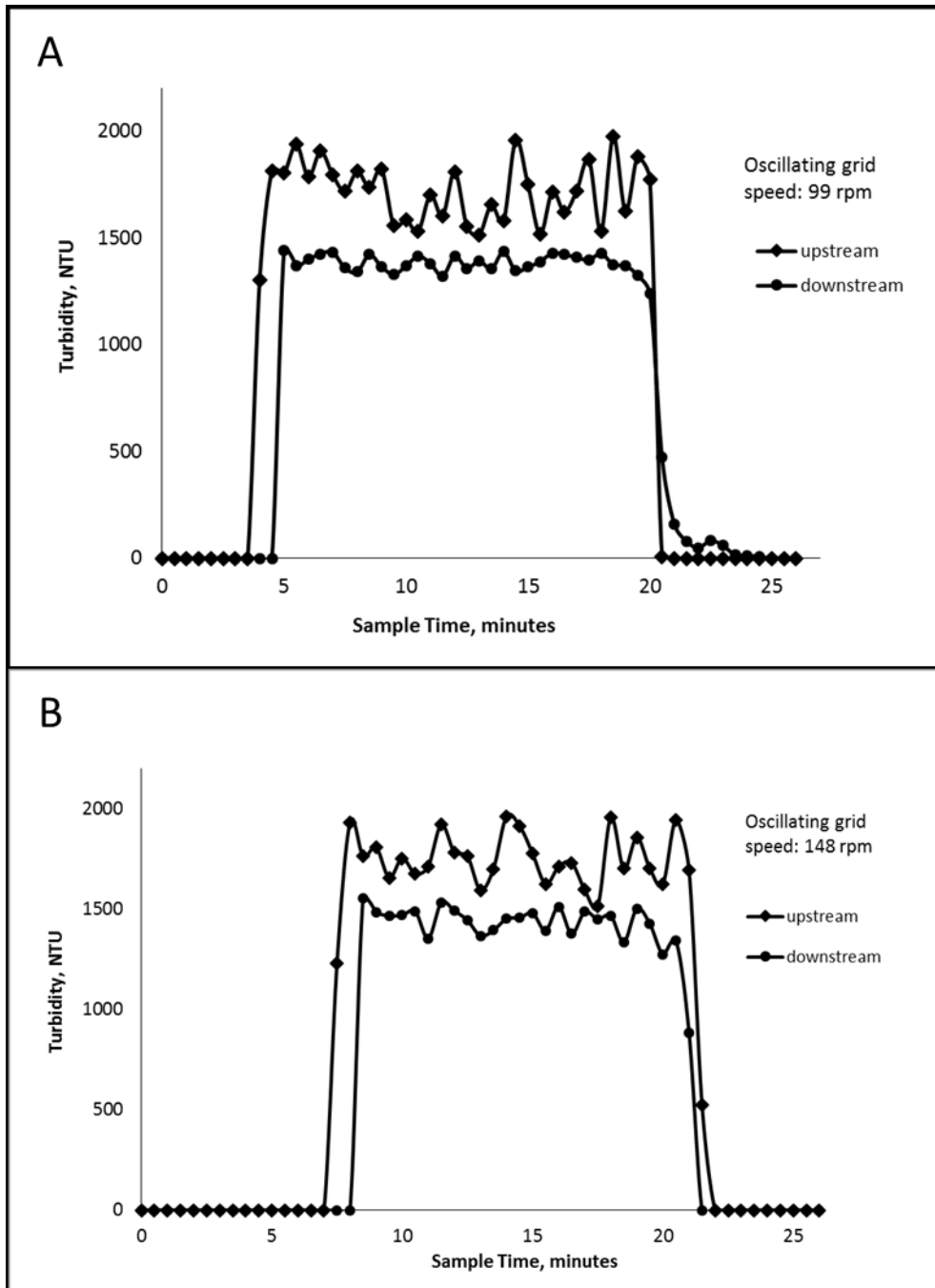


Figure 4.7. Upstream and downstream turbidity measurement results for Port B soil for control runs: A) Low mixing intensity run B) High mixing intensity run.

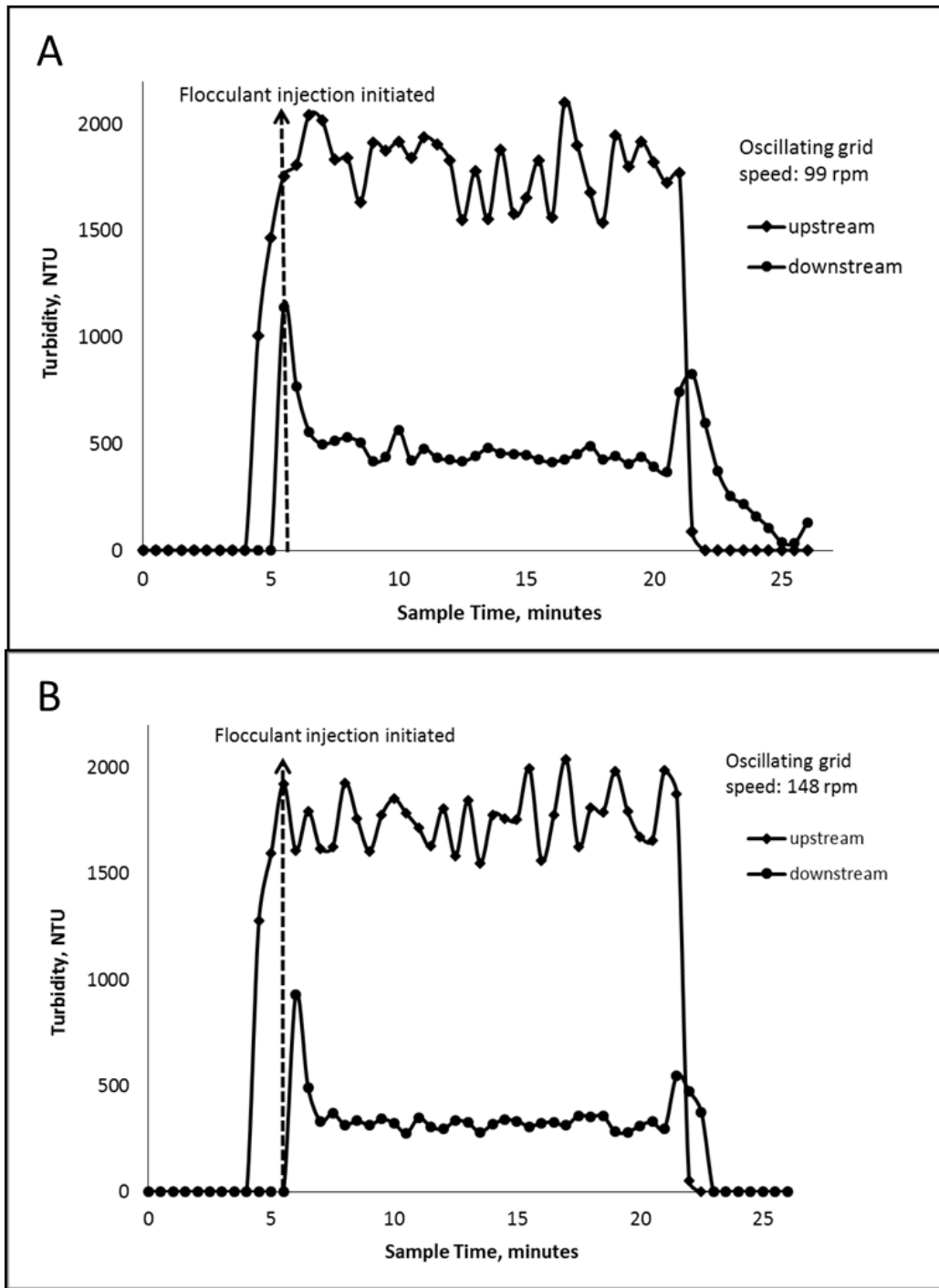


Figure 4.8. Upstream and downstream turbidity measurement results for Port B soil for flocculation runs: A) Low mixing intensity run B) High mixing intensity run.

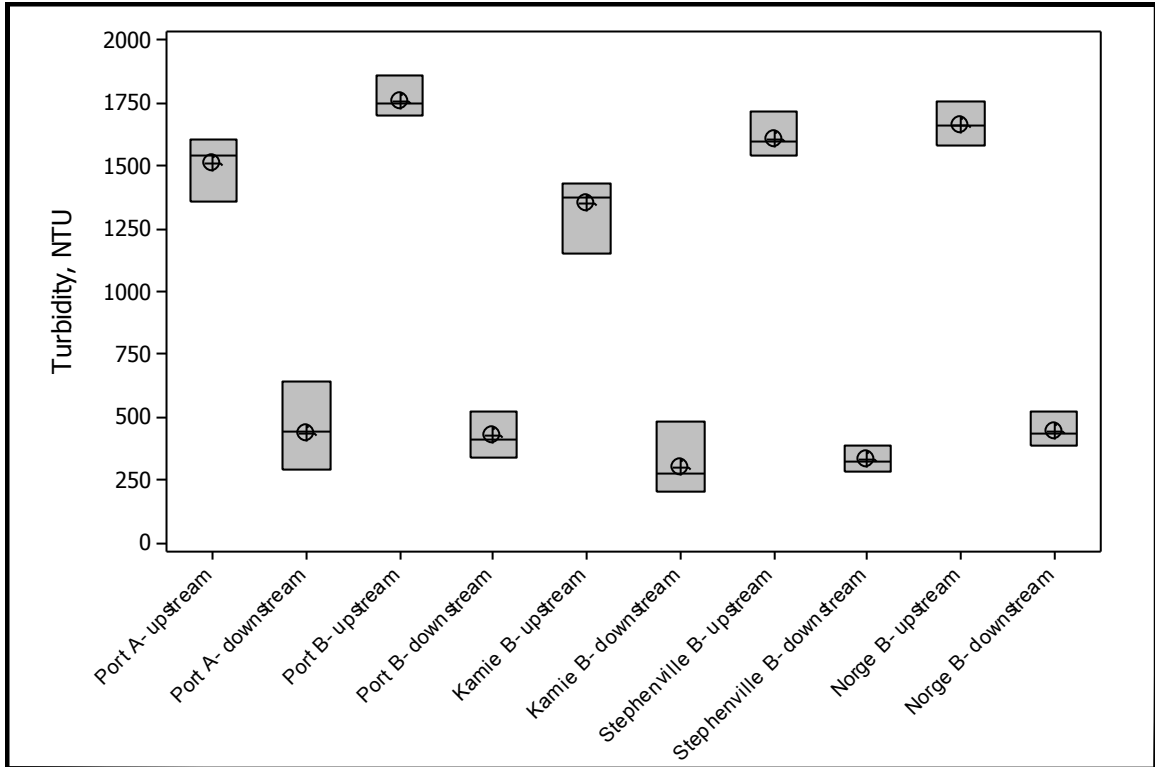


Figure 4.9. Range and average of upstream and downstream turbidity measured for all the soils.

The overall average turbidity reduction was 76%, while the average sediment mass removed was 41%. Finer suspended sediments have a greater impact on the turbidity measurement. Therefore, greater turbidity reductions relative to the suspended sediment reduction was due to the flocculation of finer silts and clays in the flow. The average reduction in the suspended sediment concentration at the outlet of the flume were in the range of 55 to 60%

The low and high mixing intensities did not have a significant effect on the sediment removal efficiency. The results of a paired t-test on the sediment removal efficiencies at low and high mixing intensities, gave a P-value of 0.342 at 95% confidence interval. Therefore, high mixing intensities may not be required for flocculation using Hydrofloc 445 L. Lower mixing intensity which can provide initial uniform mixing could be sufficient to achieve the same sediment and turbidity reduction.

Conclusions

The flume investigations were utilized to characterize flocculation both spatially and temporally for five soils from Oklahoma. The uniqueness of the apparatus and the experiment procedures allowed the control of the input variables, yet allowed for the simulation of suspended sediment distributions in the flow similar to those observed in construction site runoff. Turbidity reduction was in the range of 71 to 80 percent, which is better than traditional stormwater control techniques (Barrett et al., 1995 and Millen et al., 1997). The sediment removal efficiency was in the range of 30 to 60 percent and the average sediment removal efficiency was 41%. The largest mean turbidity and sediment removal efficiencies were measured for Stephenville B soil. The lowest sediment removal efficiency and turbidity reduction was measured for Port A soil compared to all other soils, which were from B horizon, showing that subsurface soils flocculate better because the percentage of clay tends to increase with distance below the surface. The sediment removal efficiency at low and high mixing intensities did not vary greatly, thus showing that the selected mixing intensities did not have a huge impact on flocculation of the sediment. Thus, either mixing intensity is acceptable to mix the flocculant and the sediment uniformly and could be used to achieve the same flocculation efficiencies.

CHAPTER V

MODELING OF CHEMICAL FLOCCULATION FOR SEDIMENT RUNOFF FROM CONSTRUCTION SITES

Abstract:

The flocculation model of Krishnappan and Marsalek (2002) was modified to predict flocculation of sediment using polymer flocculant. Flocculation efficiencies of suspended sediment deriving from five soils from Oklahoma were used to inversely estimate the stickiness coefficient for those soils. The trend of predicted flocculated sediment distribution was similar to that observed in the flume experiments, with R-squared values and NSE values greater than 0.xx and 0.xx, respectively, for three of the five soils. Thus, the predicted spatial and temporal distribution of the flocs was consistent with both, the theory of flocculation and the experimental observations. The range of the stickiness coefficient values for all the soil was in the range of 0.2 to 1.0. A low value of the stickiness coefficient indicated low flocculation efficiency. Estimated stickiness coefficients for Port A horizon soils were lower than the B horizon soils, likely because of the higher organic content usually associated with topsoil, which could have inhibited flocculation.

The modeled flocculation efficiency for the Port B horizon and Stephenville B horizon was lower than measured, likely because of inadequate characterization in the model of differential settling within the flume. In addition, a sensitivity analysis was performed on the model with respect to the stickiness coefficient and the turbulent energy dissipation rate. Flocculation efficiency was not sensitive to change in the both these parameters.

Keywords: flocculation, stormwater, sediment, sensitivity, mathematical model

Stormwater runoff from construction sites carry suspended sediment that is often comprised of clay and colloidal sized particles that remain in suspension for prolonged periods increasing their turbidity of the receiving water bodies. The most commonly used sediment control techniques on construction sites, such as silt fences, sedimentation ponds and check dams rely on ponding of stormwater runoff, to allow the particles to settle out. Though these techniques are capable of trapping sand sized particles easily, they are ineffective in trapping particles in the size range of fine silt and clay. In order to capture these fine particles it is necessary to enhance the settling rates of the particles. Flocculation treatment increases settling velocities of the clay particles. The most commonly used flocculants for construction sites are the anionic polyacrylamide monomers (aPAMS). However, each construction site is unique depending upon the area, variability in the soil type and the climatic conditions. Therefore, it is advantageous to have a capability to predict the amount of sediment that can be trapped in the stormwater runoff using mathematical modeling. Mathematical models defining the physical processes affecting flocculation can be incorporated in software routines, can be used as design tool to size the flocculation systems on constructions sites.

Review of Flocculation Models:

Flocculation is a physicochemical process where destabilized suspended particles can interact with each other by two most common phenomenon. Interactions of the particles occur either due to their random motion in the fluid system, which is known as perikinetic flocculation or because of change in the velocity gradients due to induced mixing conditions, which is known as orthokinetic flocculation (Thomas et al, 1999). In either case, the most basic mathematical representation for the rate of flocculation is given as

$$\frac{dn}{dt} = \alpha K(i,j)n_i n_j \quad (5.1)$$

where, $\frac{dn}{dt}$ is the rate of flocculation, and

α is the stickiness coefficient.

Theoretically, α is defined as the probability of two particles sticking successfully to form a floc. $K(i,j)$ is defined as the rate of particle collisions and n_i and n_j are defined as the number of particles in size class of i and j respectively (Thomas et al., 1999, Amirtharajah et al., 2007). While Equation 5.1 defines the factors that affect the rate of floc formation, it does not define how the particles growth. The development of the mathematical models to predict particle growth due to flocculation began in the 1916, with the classical population balance theory proposed by Smoluchowski (1916) and is given by

$$\frac{\partial n(x_i, t)}{\partial t} = \frac{1}{2} \sum_{j=1}^{i-1} A(x_i - x_j, x_j) n(x_i - x_j, t) n(x_j, t) - \sum_{j=1}^{\infty} A(x_i, x_j) n(x_i, t) n(x_j, t) \quad (5.2)$$

where, A = coagulation kernel

x_i x_j = particles in size class .

This flocculation model applicable only to laminar flows. Most of the flocculation processes in our world are orthokinetic in nature. Thus, a number of flocculation models were developed for make Smoluchowski's model applicable to orthokinetic flocculation. Flocs in sediment runoff are composed of clay, silt and particulate organic matter. They are characterized by their size, shape and specific gravity in fluid system. These properties are both time and space variant and therefore affect the transport phenomenon of the sediment (Maerz et al, 2011). Therefore, most of the existing flocculation models involve some types of empirical or semi-empirical relations to characterize floc size and type. Initial research work done by Camp and Stein (1943) showed that the rate of orthokinetic flocculation was a function of root mean square velocity gradient ' G '. Kramer and Clark (1997) showed that the velocity gradient ' G ' defined by Camp and Stein (1943) was an average value for the reactor and that was highly dependent upon the local hydrodynamics of the fluid system within reactor. They also showed that mean value ' G ' overestimated or underestimated the rate of flocculation. Model's based on Smoluchowski's theory of population balance are often referred to as size class based models (Maerz et al., 2011). Size class based models are useful in studying the time evolution of the flocs and they distribute the flocs depending upon different size classes. One parameter that characterizes a floc is its fractal dimension. The fractal dimension is dependent on the size and the shape of the floc. Maerz et al., (2011) suggested that the fractal dimension is a sensitive parameter to characterize growth of flocs. Winterwerp (1998), Maggi et al., (2007), and Son and Hsu (2009) proposed their models based on fractal theory. However, these models are also semi-empirical in nature and require complex experimental measurements to predict the time evolution of flocs. Models presented by both Son and Hsu (2009) and Winterwerp (1998) did not produce good satisfactory results for the floc size distribution in mixing tanks (Son and Hsu, 2009). Moreover, fractal theory is very complex and needs complicated image processing techniques for floc size measurement. Argaman and Kaufman (1970) proposed that rate of floc formation as shown in Equation 5.3, is directly proportional to the mean square turbulent velocity.

$$H_{1F} = -4\pi K_s \alpha R_f^3 n_1 n_f [u'^2]_a \quad (5.3)$$

where, K_s = Parameter that relates the effectiveness of floc formation,

$[u'^2]_a$ = mean square turbulent velocity,

R_f = Radius of the floc,

n_1 = Number of primary particles, and

n_f = Number concentration of flocs.

Their proposed rate of floc breakup is given

$$B_{1T} = B \frac{R_f^2}{R_1^2} n_f [u'^2]_a \quad (5.4)$$

where, B = Floc breakup constant and R_1 is the radius of the primary particle.

The Argaman and Kaufman (1971) model is well suitable for mixed reactor based processes where the rate of flocculation can be based on the ratio of the number concentration of the primary particles in the influent and effluent. It also does not represent the time evolution of the flocs.

Krishnappan and Marsalek (2002) developed a flocculation model to study the effect of cohesive sediment transport in an on-stream stormwater detention pond. Their modeling procedure assumed the growth of the particles in a geometric progression having a discrete size class range, which gave the model a simplistic approach. The model assumes that the mass of the particles in size range j is conserved when they coagulate to form new particles in higher size class range i . Their flocculation equation was,

$$\frac{dN}{dt} = - \sum_{j \neq 1} \beta_{i,j} K_{i,j}^{eff} n_i n_j + \sum_{j < 1} \beta_{i,j} f_{i,j} K_{i,j}^{eff} n_i n_j + \sum_{j < i-1} \beta_{i-1,j} (1 - f_{i-1,j}) K_{i-1,j}^{eff} n_{i-1} n_j \quad (5.5)$$

where, $\beta_{i,j}$ = Coagulation coefficient,

$K_{i,j}^{eff}$ = Effective collision frequency,

The effective collision frequency is the weighted sum of the collision frequencies due to Brownian motion, laminar or turbulent shear, inertia of turbulent flow and differential settling and is given by

$$K_{i,j}^{eff} = K_{i,j}^{BR} + \sqrt{(K_{i,j}^{SH})^2 + (K_{i,j}^{IN})^2 + (K_{i,j}^{DS})^2} \quad (5.6)$$

Where, $K_{i,j}^{BR}$, $K_{i,j}^{SH}$, $K_{i,j}^{IN}$ and $K_{i,j}^{DS}$ are the collision frequency functions due to Brownian motion, laminar or turbulent shear, inertia of turbulent flow and differential settling. The equations the collision frequencies for the four mechanisms are shown in Table 5.1. $f_{i,j}$ is the fraction of flocs formed due to interactions of the particles and n_i and n_j are the number of particles in the size class i and j .

Table 5.1: Collision frequency functions (Krishnappan and Marsalek, 2002)

Brownian Motion	$K_{ij}^B = \frac{2 B_z T (r_i + r_j)^2}{3 \rho \nu r_i r_j}$ <p> $B_z = \text{Boltzmann constant}$ $T = \text{Temperature (Kelvin)}$ $\rho = \text{density of water (ML}^{-3}\text{)}$ $\nu = \text{kinematic viscosity of water (L}^2\text{T}^{-1}\text{)}$ $r_i r_j = \text{radii of the particles in } i, j \text{ size class}$ </p>
Laminar or Turbulent shear	$K_{ij}^{SH} = \frac{4}{3} \left(\frac{\varepsilon}{\nu} \right)^{0.5} (r_i + r_j)^3$ <p> $\varepsilon = \text{turbulent energy dissipation rate (L}^2\text{T}^{-3}\text{)}$ </p>
Inertia of Turbulent flow	$K_{ij}^{IN} = 1.21 \frac{\rho_s}{\rho_j} \left(\frac{\varepsilon^3}{\nu^5} \right)^{0.25} (r_i + r_j)^2 \text{abs}(r_i^2 - r_j^2)$ <p> $\rho_s = \text{density of the floc (ML}^{-3}\text{)}$ $\rho_j = \text{density of the primary particle (ML}^{-3}\text{)}$ </p>
Differential settling	$K_{ij}^{DS} = \frac{2\pi g \rho_s - \rho_w}{9\nu \rho_w} (r_i + r_j)^2 \text{abs}(r_i^2 - r_j^2)$ <p> $\rho_w = \text{density of water (ML}^{-3}\text{)}$ $g = \text{acceleration due to gravity (LT}^{-2}\text{)}$ </p>

Flocculation Model Description

The framework utilizing the geometric progression for the floc growth of Krishnappan and Marsalek (2002) model was used to develop a new model to characterize floc formation using chemical flocculant. All primary particles were assumed to be clay having a characteristic radius of 1 μm . Particles larger than 1 μm were distributed as flocs having primary clay particles given by (Krishnappan and Marsalek, 2002).

$$r_f = r_1 \cdot 2^{(i-1)/3} \quad (5.7)$$

where, r_f is the radius of the floc, r_1 is the radius of the primary clay particle and i is the size class of the particle.

Krishnappan and Marsalek (2002) characterized the formation of flocs for cohesive sediment naturally, without the addition of chemical flocculant. Flocs formed naturally have different densities compared to those formed used chemical flocculant. Their modeled densities were based on empirical constants that were characteristic to natural flocculation. Their equation for specific gravity of the flocs is given by

$$SG_f = 1 + (SG_p - 1)exp(-bd^c) \quad (5.8)$$

where SG_f and SG_p are the specific gravities of the flocs and primary clay particles respectively, d is the diameter of the particle in microns and b and c are empirical constants. The values of b and c as shown in equation 5.7 greatly affect the predicted density of the flocs. For natural flocculation the value of b and c determined by Krishnappan and Marsalek (2002) were 0.02 and 1.45. These values will not hold true for flocs formed by chemical flocculation, since they are larger in size and are more porous. The following subsection will briefly describe the methodology for determination of b and c values for characterizing flocs formed by liquid flocculant Hydrofloc 445L as described in Chapter IV.

Determination of b and c

The settling velocities of the flocs were used to calibrate the values of b and c . To measure the settling velocities of the flocs formed using the liquid flocculant Hydrofloc 445L, as described in Chapter IV, a jar test according to the ASTM D2035- 13 was performed along with a pipette test. A 2 liter sediment solution having a concentration of 400g/L was prepared from separated soil slurry of Port B soil as described in Chapter IV. 10 mL of 30g/L of Hydrofloc 445L solution was added to the sediment solution to give a flocculant dosage of 0.15 g/L. The flocculant and the sediment solution were thoroughly mixed for 30 seconds and then the particles were allowed to settle. Using the pipette test samples were collected at different time intervals till a duration of 2 hours, starting at the immediate time of stoppage of mixing, at distance of 0.1m,

0.05m, 0.03m and 0.02m below the water surface. The sampling depth was then divided by the sampling time to determine the measured settling velocity of the particles. The predicted settling velocity for our flocculation model, ω_f (m/s) is given by

$$\omega_f = 10^{Y_f} \quad (5.9)$$

where; Y_f is a dimensionless function of the modeled floc diameter (mm) and the specific gravity of the flocs. A Matlab code then used to calibrate the values of b and c , such that the predicted settling velocities were as close as possible to the actual measured settling velocities. The values of b and c were determined to be 0.013 and 0.72, and matched the measured settling velocities with root mean square error of 0.00004. Depending upon the b and c values, the settling velocities of the flocs formed using Hydrofloc 445L were predicted over the entire particle size range from 1 μm to 2mm as shown in Figure 5.1. These settling velocities are compared with the settling velocities for the flocs as predicted by Lau and Krishnappan (1997) and Tambo and Watanabe (1979). From Figure 5.1 it can be seen that the settling velocities of the flocs formed using Hydrofloc 445L are much higher compared settling velocities of natural flocs (Lau and Krishnappan, 1997) and those formed by aluminum sulfate (Tambo and Watanabe, 1979).

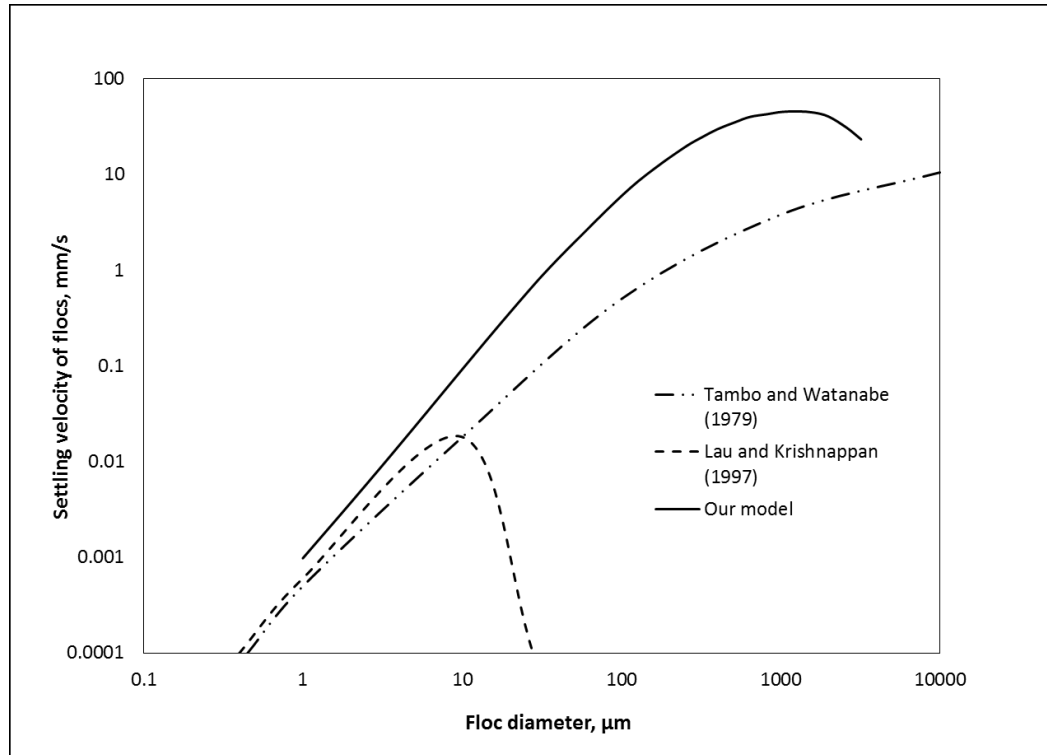


Figure 5.1: Settling velocities of flocs for three different relationships: i) Lau and Krishnappan (1997), ii) Tambo and Watanabe (1979) iii) Our model

Population balance equation to determine the rate of flocculation:

The Krishnappan and Marsalek (2002) flocculation model assumed that the mass of the primary particles is conserved after formation of the flocs. Therefore, their model does not present a mass balance for total number of primary clay particles present in the flocs. This methodology works for low number concentration of the primary clay particles for natural flocculation as measured by Krishnappan and Marsalek (2002). However, the suspended sediment concentration for stormwater runoff from construction sites can be in range of 200 -20,000 mg/L, and the number concentration of the primary clay particles could be greater than 10^{12} particles. Therefore, at such high concentrations of clay particles, the particle interactions exceed the total number of particles available for flocculation, creating negative number concentrations of the particles and inducing errors in the mass balance. On the other hand, to solve the problem of the negative numbers, if, for example these high number concentrations of primary clay particles such as 10^{12} are entered

as parts per million, then the number concentrations are low enough to not generate negative particle but they are so low that they do not form large number of flocs in higher size range of 1mm and greater. This results in prediction of very low flocculation efficiency and it would not be possible to match the same sediment removal efficiencies as were measured in Chapter IV using chemical flocculant. Therefore, to solve the problem of high primary clay concentrations, the population balance equation by the Krishnappan and Marsalek (2002) was modified to predict the rate of flocculation by preserving the total number of primary clay particles in the flocs. Thus, the mass of the floc formed was calculated on the basis of the total mass of all primary clay particles present in the floc. The modified equation for the population balance to determine the rate of flocculation is given by

$$\begin{aligned} \frac{dN}{dt} = & - \sum_{j=i}^{N_{max}} 2^{i-1} \beta_{i,j} K_{i,j}^{eff} n_i n_j + \sum_{j=1}^i 2^{j-1} \beta_{i,j} f_{i,j} K_{i,j}^{eff} n_i n_j \\ & + \sum_{j=1}^i 2^{j-1} \beta_{i-1,j} (1 - f_{i-1,j}) K_{i-1,j}^{eff} n_{i-1} n_j \end{aligned} \quad (5.10)$$

where $K_{i,j}^{eff}$ = Effective collision frequencies, which was calculated using the equation 5.6, and $\beta_{i,j}$ is the coagulation factor given by

$$\beta_{i,j} = \alpha \left(1 - \frac{R}{S+1} \right)^n \quad (5.11)$$

where α is the stickiness coefficient. R is the number of primary particles contained in any floc of size i,j . 'S' is the number of particles in the largest floc at any time.

The size of the flocs is controlled by the surface shear forces. The surface shear forces are controlled by the turbulent energy dissipation rate ' ε ' (m^2s^{-3}). Lower the value of ε larger is the floc size. However, lower ε , means lesser particle interactions and therefore the flocs reach an equilibrium size. Tapp et al (1981) showed that velocity gradient ' G ' which is the function of the

turbulent energy dissipation rate is inversely proportional to the radius of the flocs. For example, in a flume apparatus as described by Chapter IV, the turbulent energy dissipation rate can be controlled by controlling the mixing intensity. In an open channel flow the turbulent energy can be controlled with the help of energy dissipaters such as stilling basins where the depth of the flow increases and have static grids or baffles which will help in decreasing the turbulence gradually. With that background on modified flocculation model, the methodology used to predict the stickiness coefficient will be presented.

Determination of Stickiness Coefficient using the Flocculation Model

The stickiness coefficient value was predicted for the five soils: Port A horizon (Port A), Port B horizon (Port B), Kamie B horizon (Kamie B), Stephenville B horizon (Stephenville B) and Norge B horizon (Norge B) as described in Chapter IV. All the model equations were coded in a Matlab. As described in Chapter IV, flume experiments were conducted to measure the sediment removal efficiencies for each soil. To compare the predicted and the measured sediment removal efficiency, a batch reactor model approach was applied on this flume. The concept of the batch reactor approach was to divide the entire flume into a series of individual reactors, having equal volume. The average velocity of the flow was 0.061 m/s. Based on the average velocity it took 150 s for the sediment to flow out of the flume. The flume was therefore divided into 10 reactors, such that all the reactors not only had equal volume but also had equal retention time of 15 s. Also, as described in Chapter IV, the flow depth was 0.3m. This flow depth was divided into four equal layers each having a width of 0.07m. Therefore, to summarize, the entire flume was divided into 10 reactors each having four layers and the flocculation model equations were applied to each layer within the reactor for duration of 15 seconds. At the start of the simulation, the number of particles in each size class were distributed equally in all the layers in first reactor, assuming that they were all uniformly mixed. At the end of the simulation for an

individual reactor, an undispersed particle size distribution of unsettled particles was predicted. This particle size distribution coming out of one reactor was the input for the successive reactors.

As described earlier, the turbulent energy dissipation rate ϵ not only controlled the particle interactions but also the size of the flocs. ϵ within the mixing zone was determined using equations presented by Liem et al., 1999. ' ϵ ' for low mixing intensity (99 rpm, G: $104s^{-1}$) was $0.012 \text{ m}^2/\text{sec}^3$ and for high mixing intensity (148 rpm; G: $134s^{-1}$) was $0.02 \text{ m}^2/\text{sec}^3$. ϵ decreases as turbulence decays with the distance downstream, thus affecting the floc formation and the sediment removal efficiency with the distance downstream. Turbulent velocity measurement were taken in the flume which were used to determine average ϵ values at different distances downstream as shown in Table 5.2. Thus as can be seen from Table 5.2, each reactor had a specific ϵ value depending upon the distance, where it was located. Collision frequencies due to Brownian motion were set to zero assuming that its effect is negligible. The output and input concentrations were used to determine the effective stickiness coefficient α , depending upon the measured and the predicted values.

Table 5.2. Average turbulent energy dissipation rates ' ϵ ' with distance downstream.

Distance Downstream from start of flume (in meters)	Turbulent energy dissipation rate (m^2/sec^3)
0 to 0.9	0.012 (low mixing intensity) 0.020 (high mixing intensity)
0.9 to 3.6	0.015
3.6 to 6.3	0.0046
6.3 to 9	0.00084

Results and Discussion

Estimation of Stickiness Coefficient

Figure 5.2 compares the cumulative distribution of measured sediment removal efficiencies as shown in Chapter IV with those predicted using the flocculation model. Table 5.3 shows the R^2 and the NSE values for the observed and the modeled values.

Table 5.3. NSE and R^2 values for predicted and measured sediment removal efficiencies for all the soil (NSE: Nash Sutcliffe Efficiency; R^2 : Coefficient of determination).

Soil	NSE	R^2
Port A	0.91	0.9
Port B	0.46	0.66
Kamie B	0.95	0.95
Stephenville B	-0.19	0.18
Norge B	0.96	0.96

From Table 5.3, it can be seen that the for Port A, Kamie B and Norge B soils, NSE values from measured and predicted sediment removal efficiencies are close to 1. The R^2 values for these soils are also high, indicating that a close match between the predicted and the measured sediment removal efficiencies. For Stephenville B soil the NSE value was below zero. From Figure 5.3, for Stephenville B soil it can be seen the even for the highest predicted value of α of 1, the predicted mass of the sediment trapped was about 32% less than the actual measured mass. During the actual experiment smaller aggregates and finer silts might have been swept up by the larger flocs leading to higher measured mass by differential settling.

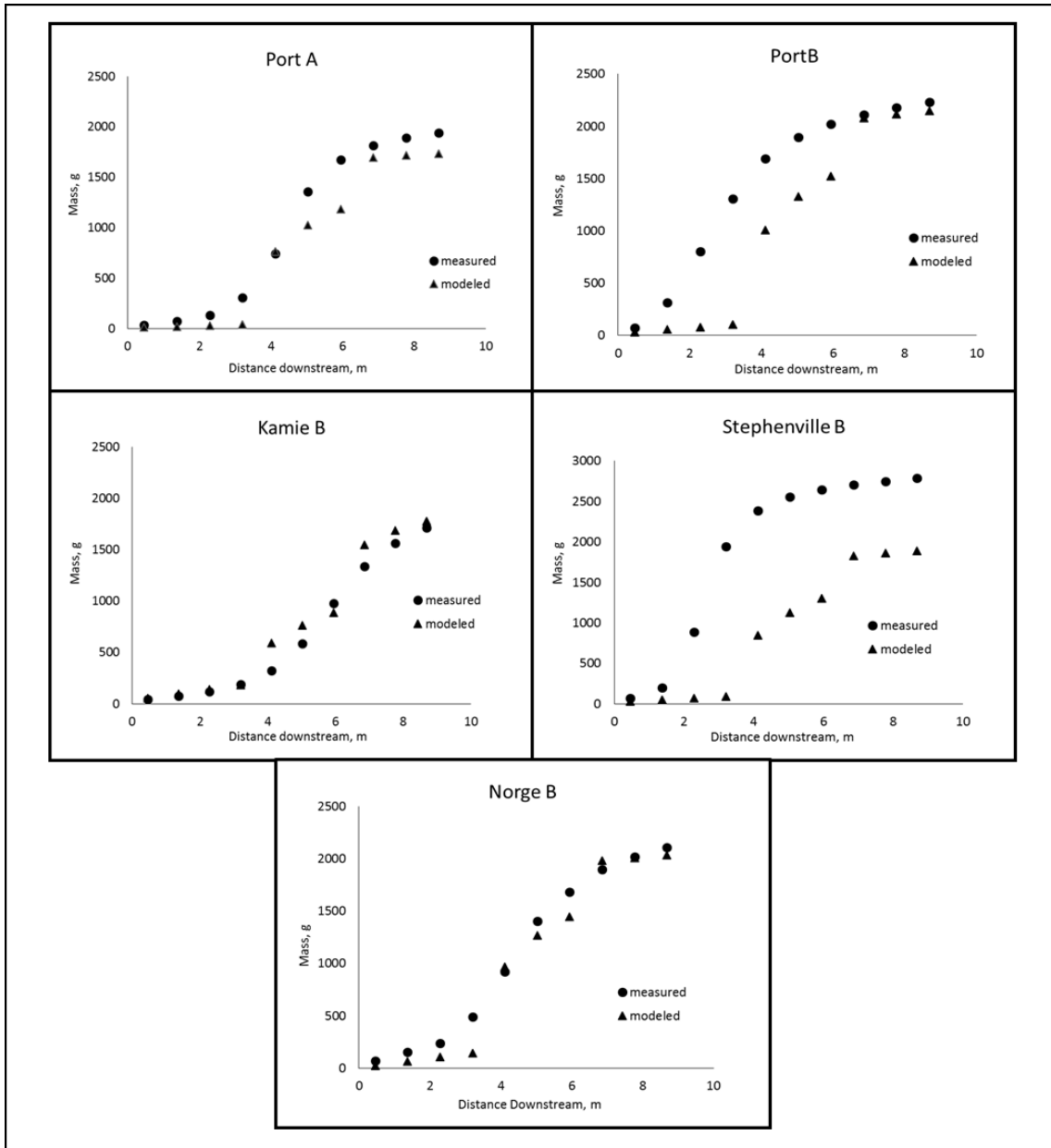


Figure 5.2. Measured vs modeled cumulative distribution of flocculated sediment for all the soils

The trend of the cumulative distribution for predicted sediment deposition on the downstream side of the flume for most of the soils shows that sediment deposition occurs further downstream compared to the measured sediment depositional position. The reason for this is that the turbulent energy dissipation rate ϵ that controls the particle interactions also controls the effective size of the flocs. The minimum value of ϵ in the mixing zone is $0.012\text{m}^2/\text{sec}^3$. This corresponds to an effective floc size of 0.016 mm. The particles have low settling velocities and do not settle out within the reactor during their retention period of 15 s. They are advected further downstream where ϵ is lower and they can react to form large flocs.

The total error between the measured and predicted mass for all the five soils for all the flocculation runs along with the stickiness coefficient is summarized in Table 5.4. The stickiness coefficient value determines the overall degree of flocculation. As mentioned earlier, the stickiness coefficient values asymptote at a value of 1. Above that value there was no change observed in the mass of the sediment trapped. For some runs where the stickiness coefficient was 1 and the error was greater than 10%, the predicted mass was the maximum mass that could be flocculated. .

Table 5.4. Stickiness coefficient values and total error for low and high mixing intensity runs for all soils. (Low mixing intensity: 99 rpm; high mixing intensity: 148 rpm).

Soil	Mixing Intensity	Stickiness coefficient	Observed mass (g)	Predicted mass (g)	Total error (%)
Port A	Low	1	1837	1640	10.7
	High	1	1609	1618	-0.52
	Low	0.2	1708	1728	-1.17
	F4	0.5	1197	1257	-4.9
	Low	1	1575	1428	9.3
	High	0.3	1311	1317	-0.41
Port B	Low	1	2676	1322	50.6
	High	1	2961	2847	3.84
	Low	1	1847	1384	25.1
	F4	1	1975	1966	0.46
	Low	1	1674	1526	8.85
	High	1	1920	1473	23.31
Kamie B	Low	0.2	1551	1570	-1.2
	High	0.2	1291	1350	-4.5
	Low	1	2892	1792	38.03
	F4	1	3483	1907	45.3
	Low	1	2932	1951	33.5
	High	1	4115	2031	50.64
Stephenville B	Low	1	2487	1739	30.1
	High	1	2730	1606	45.7
	Low	1	3317	1517	54.3
	F4	1	3181	1734	45.5
	Low	1	2556	1731	32.3
	High	1	2392	1694	29.2
Norge B	Low	1	2574	2049	20.4
	High	1	2674	1863	35.2
	Low	1	2511	1872	23.6
	F4	1	1806	1677	7.1
	Low	1	2051	2016	1.7
	High	1	2110	2035	3.6

Sensitivity Analysis:

Parameters selected for the sensitivity analysis were ' α ' and ' ϵ '. Both these parameters were changed by -50, -40, -30, -20, -15, -10, -5, -2, 2, 5, 10, 15, 20, 30, 40 and 50 percent to see the effect on the actual flocculation efficiency which was calculated as the ratio of predicted

settled mass to that the total mass incoming mass of the sediment. While changing one parameter, the other parameter was kept constant. The sensitivity analysis was conducted on Port B slurry as described in Chapter IV.

Model Response to Change in Stickiness Coefficient ' α '

Figure 5.3 shows the graph of the change in the flocculation efficiency with the change in the ' α ' values which has been divided into three linear ranges, due to the trend they follow. The 'higher range of alpha' series shows the first linear range where the values of α are in the range of 0.6 to 1.5. The slope the trend line for this range is very small indicating that the flocculation efficiency remains nearly constant. For the 'middle range of alpha' series as shown in Figure 5.3, the flocculation efficiency increases steadily. For this series, the values of α are in the range of 0.2 to 0.6. For value of α below 0.1, the flocculation efficiency decreases sharply. For a value of α of 0.09, the flocculation efficiency was close to 7%. This shows that at very low α values, there is very little or no effect of the flocculant.

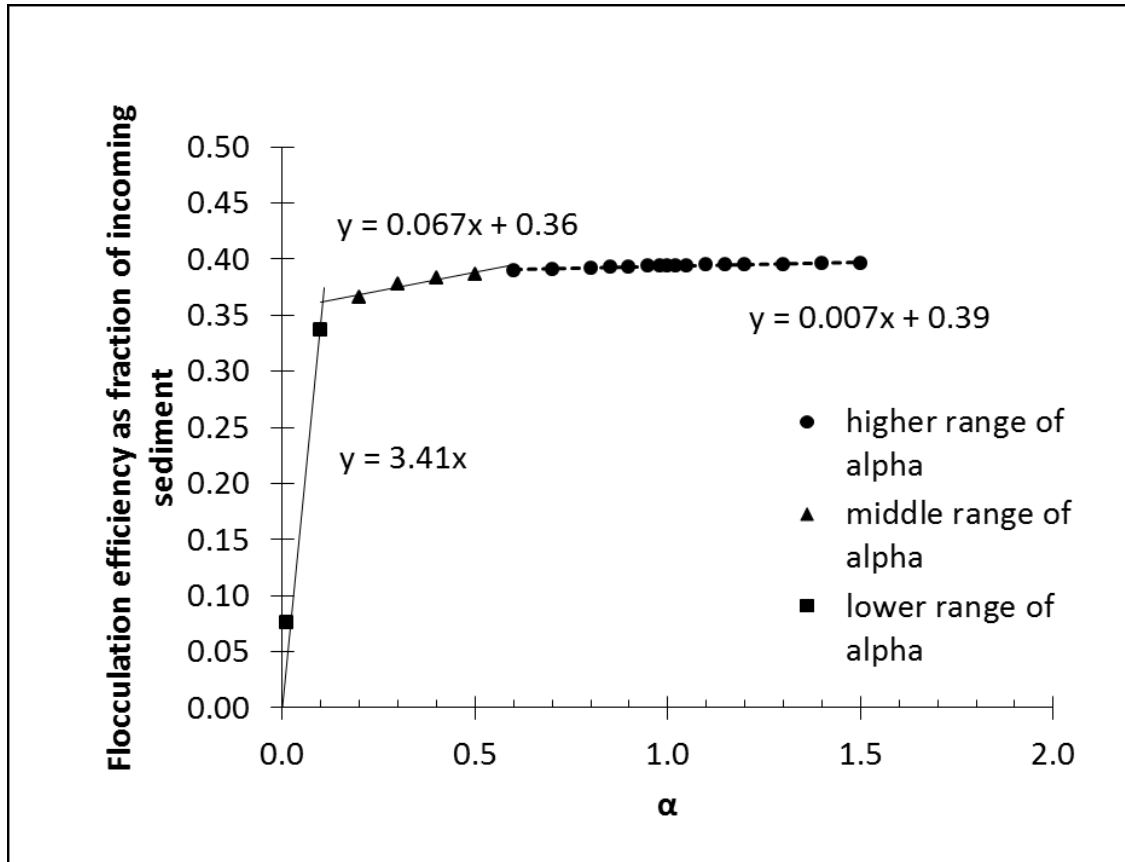


Figure 5.3. Change in flocculation efficiency with change in stickiness coefficient ' α '.

Model Response to Change in Turbulent Energy Dissipation Rate ' ϵ '

Figure 5.4 shows the graph of the change in the flocculation efficiency with the change in the turbulent energy dissipation rate ' ϵ '. The turbulent energy dissipation rate acts in two ways in formation of the flocs. It controls the number of particle interactions and at the same time it also has a growth limiting effect on the flocs. For the highest value of the stickiness coefficient of 1, there was no change in the flocculation efficiency with respect to the change in turbulent energy dissipation rate. Therefore, the model is not sensitive to a small change in the turbulent energy dissipation rate. This can also be related to the sediment removal efficiencies at low and high mixing intensities as presented in Chapter IV. In Chapter IV, it was concluded that low and high mixing intensity did not significantly affect the flocculation efficiency. Therefore, the change in

the turbulent energy dissipation rate has to be very large to significantly impact the flocculation efficiency.

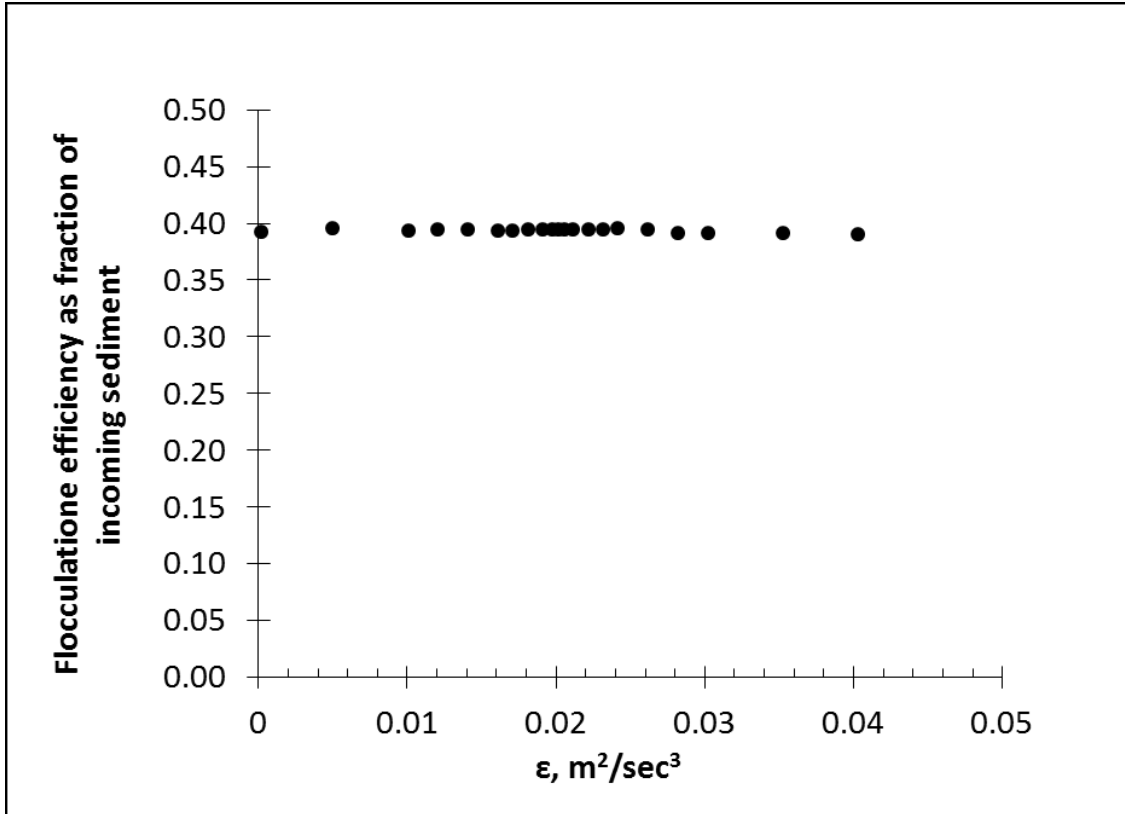


Figure 5.4. Change in flocculation efficiency with change in turbulent energy dissipation rate ' ϵ '

Conclusions

A model based on fundamental flocculation theory to predict the efficiency of sediment removal using polymer flocculant has been developed. The model has a simplistic mathematical approach and therefore can be used to predict the flocculation efficiency for different soil types and the model is capable of dealing with very high concentrations of clay particles as are typically seen in stormwater runoff from construction sites. The model can predict the spatial and temporal distribution of the flocculated particles that settle out; this distribution was similar to that

observed in flume experiments. Model results did under-predict sediment removal for a subset of soils, perhaps because of inadequate considerations for differential settling within the model. For the sensitivity analysis, in the higher range of stickiness coefficient the flocculation efficiency remained more or less constant. The flocculation efficiency reduced sharply for lower values of stickiness coefficient. Also, at higher values of the turbulent energy dissipation rate, the flocculation efficiency was low which increased with decrease in the turbulent energy dissipation rate. However at very low values of turbulent dissipation rate, the flocculation efficiency decreased again, as the number of particle interactions reduced. In conclusion, the flocculation model, has provided a fundamental base for predicting the flocculation efficiencies using chemical flocculant. Due to the simplistic approach, the model could be coupled with watershed models that can be used as a design tool to predict the flocculation efficiency of sediment runoff on field sites based on the individual characteristics of each site.

CHAPTER VI

THE SPATIAL AND TEMPORAL HYDRODYNAMICS OF A CIRCULAR JAR TEST: IMPACTS ON FLOCCULATION ESTIMATION

Abstract

Jar tests are widely used in water and wastewater industry to determine the optimum flocculant dosage. Recently, they have been utilized as a rough estimate to determine the flocculant dosage in control of sediment in stormwater runoff from construction sites. Turbulence of the runoff affects formation and the flocs and their transport both spatially and temporally. Previous research has shown that the most important parameter that affects the formation and the breakage of the flocs is the turbulent energy dissipation rate. In a stormwater sedimentation channel in the field, the turbulent energy dissipation rate changes with the distance downstream affecting the size of flocs. A study based on the principle of geometric and dynamic similitude was carried out on a circular jar test apparatus in the laboratory to characterize the turbulent energy dissipation spatially and temporally. This study was a first step in understanding the size distribution of flocs depending upon the turbulent energy dissipation rate and thus could be used to predict floc size distribution in the field depending using laboratory jar tests. The turbulent energy dissipation rate varied greatly both spatially and temporally within the jar test. It was observed that most of the turbulent energy dissipation rate decayed very quickly within first 30 seconds after the mixing was stopped, and then remained relatively constant irrespective of the mixing speed. For the same power input per volume, the turbulent energy dissipation rate scaled as the cube of the rotational speed times the square of the impeller diameter (N^3D^2).

Keywords: jar-test, hydraulic profile, turbulent kinetic energy, dissipation rate of turbulent kinetic energy

Introduction

The process of flocculation is a physicochemical process in which two factors play a major role: optimum flocculant dose and mixing intensity. The mixing intensity gives rise to turbulent forces which allow the formation and the breakage of the flocs. Most of the particle interactions occur with the distance that is equivalent to their size range. (Stanley and Smith, 1995). Therefore, from a turbulent flow perspective, large eddies are responsible for the bulk transport of the particles, while the smaller eddies are responsible for the particle interactions. Most of the kinetic energy is dissipated within the range of smaller eddies and therefore the particle interactions are controlled by the rate of dissipation of kinetic energy. Previous research (Wu and Patterson 1989; Kresta 1998; Cheng et al 1997; Bouyer et al 2005) on measurement of turbulence by rotating impellers within confined tanks have shown that local dissipation rates have greater impact on floc formation than average dissipation rates. The most common technique used to predict the optimum flocculant dose is jar-test (Stanley and Smith 1981; Camp and Stein, 1943; Saffman and Turner, 1956). However jar-tests are known to over-predict or under-predict the flocculation efficiencies because of the challenges in scaling (Kresta, 1998) and as shown by Camp and Stein (1943), turbulence within the mixing tank is not homogenous. The intensity of turbulence decreases away from the impeller zone into the bulk fluid.

With advances in technology, the measurement techniques to characterize turbulence have become better and more detailed analysis of the turbulence characteristics can be performed with the help of acoustic and laser Doppler velocimetry, particle tracking and hot wire anemometry. Laser Doppler velocimeter (LDV), particle image velocimeter (PIV) and hot wire anemometers provide very good spatial and temporal resolution however they are not very suitable for measurement having suspended sediment as they tend to make the fluid opaque which

makes creates difficulty in measurements (Garcia et al., 2005). A flocculation system only deals with suspended matter and therefore an Acoustic Doppler Velocimeter (ADV) can be used due to its relatively low cost compared to LDV and anemometers. It has a sampling volume of $9 \times 10^{-8} \text{ m}^3$ which can capture information on the turbulence characteristics. The ADV can capture a significant range of the total kinetic energy in the system, but the measurement values are biased towards high values (Lohman et al., 1994). While the ADV may exhibit decreased accuracy of the sensor due the Doppler noise and also can be a somewhat intrusive measurement technique, the advantages of the ADV outweigh its disadvantages for turbulence measurements in fluids with suspended sediments relative to the other techniques.

Spatial and temporal hydrodynamics within a rotating impeller-based reactor are governed by the range of scales of turbulence that exist within the reactor. The three main length-scale ranges of the turbulent flow are integral, inertial, and viscous dissipation as shown in Figure 5.1 (Stanley and Smith, 1995; Hinze, 1959). In the integral range, large eddies are formed and they transfer energy to smaller eddies. During this stage the turbulence is anisotropic (Stanley and Smith, 1995). The turbulent length-scale range from the inertial subrange to the viscous dissipation range is called the universal equilibrium range. Here, the turbulence is isotropic (Stanley and Smith, 1995). It is the inertial subrange where most of the particle interactions take place for floc formation or breakup. The largest scale of turbulence called the integral length scale is generally equal to $1/0^{\text{th}}$ of the impeller diameter (De Silva, 2006; Kresta, 1998). All these length scales are dependent on a time scale ' τ ' which represents the decay of the kinetic energy. In impeller zone the mean turbulent velocities are comparable to the rotational speed of the impeller (Stanley and Smith, 1995). The smallest scale of motion, also called as the Kolmogorov's length scales, are governed by the viscous forces; the motion of the impeller has no effect on them (Kresta, 1998).

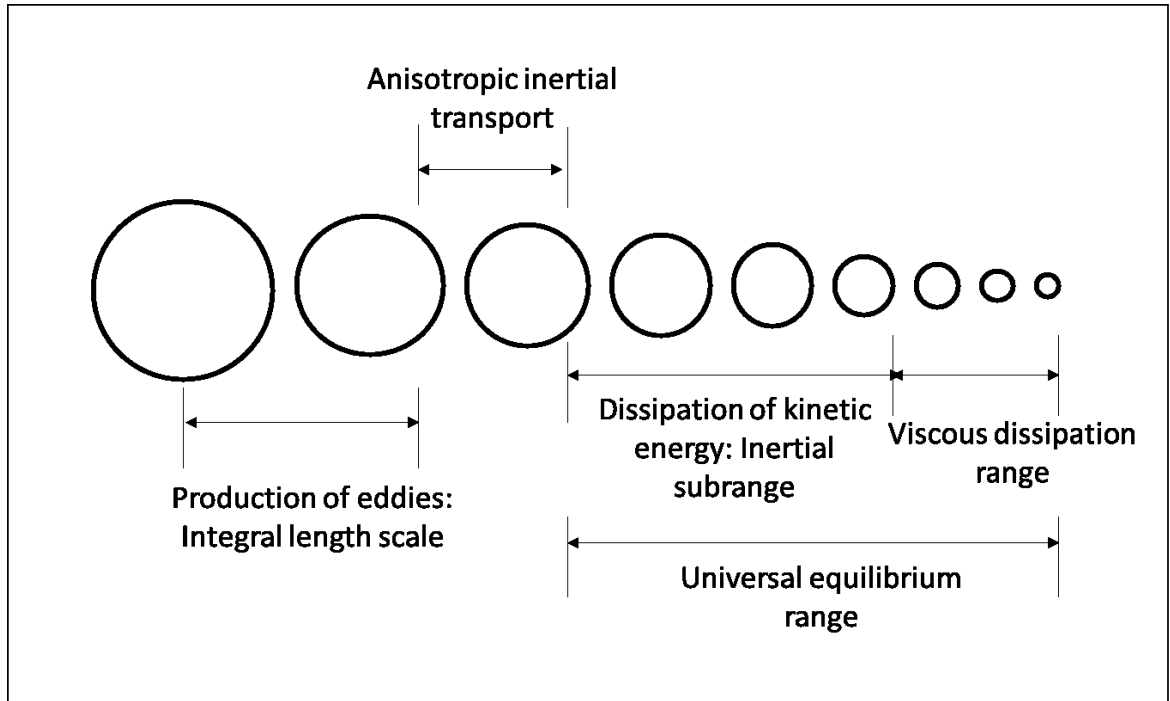


Figure 6.1. Schematic diagram showing different length scales of turbulence measurements by the acoustic Doppler velocimeter (ADV).

As the turbulence decays, within the jar the turbulent energy dissipation rate decreases. The dissipation rate of the vessel determines the velocity gradient of the tank, which is given by the following equation 6.1

$$G = \sqrt{\frac{\varepsilon}{\nu}} \quad (6.1)$$

where: G = velocity gradient (sec^{-1})

ε = turbulent energy dissipation rate (m^2/sec^3), and

ν = kinematic viscosity (m^2/s)

Tapp (1981) showed that the average floc size was directly proportional to tank average velocity gradient G ,

$$R_f = \frac{1}{G} \quad (6.2)$$

where R_f = radius of the floc (cm)

Flocculation has recently found application in control of sediment in stormwater runoff from construction sites. For this application there were mixing devices in a field flocculation system for sediment control, which induced turbulence by redirecting flow to enhance interactions between sediment particles. A traditional jar test apparatus was used to initially estimate the optimum flocculant dosage for this system. A useful, cost-effective method for predicting the sediment-removal efficiency of this field system would be to use a jar test to simulate the field processes. By comparing the spatial and temporal velocity profiles between and jar test and any other field or laboratory application with an alternate geometry, the jar-test procedure could theoretically be used to estimate flocculation effectiveness.

Measurement of spatial and temporal velocities with suspended sediment is difficult due to the limitations of opacity of the fluid and contamination of sensors from the sediment. Acoustic Doppler velocimeters (ADV) are not affected by opacity or contamination due to suspended sediment and can be useful in measuring turbulence. However, ADV is large in size and cannot be inserted in a standard 2 L. Similitude studies can be utilized to solve this problem. Similitude studies are often used to upscale reactors. Therefore, to characterize the turbulence within a jar test apparatus, a geometrically upscaled jar test apparatus can be used, which will allow turbulence measurements using ADV. Additionally, applying the principles of dynamic similitude to the laboratory scale reactors research has shown that if ratio of the tank diameter to the diameter of the blade is held constant, the turbulent energy dissipation rate within the tank can be described as a function of the impeller blade diameter and the impeller speed.(De Silva, 2006, Wu et al 1989, Kresta, 1996).

The focus of the research paper is to measure the spatial and temporal turbulent energy dissipation rate in an up-scaled circular jar-test apparatus using an ADV and then by using the

principles of geometric and dynamic similitude predict the turbulent energy dissipation rate in a 2 L circular jar test vessel and thus the floc size distribution.

Methodology

A Sontek YSI 16 MHz, Acoustic Doppler velocimeter (ADV) (San Diego, CA) was used to measure the three dimensional instantaneous velocity field in the upscale jar test apparatus, designed based on the principles of geometric and dynamic similitude. Most traditional jar tests apparatus have a flat blade impeller where the length of the blade D is three times the width W . The conventional Phipps and Bird jar test apparatus has a standard 2 L square jar. Instead of using a square geometry for upscale prototype, a circular geometry was found more convenient. Therefore, the design of the upscale jar-test vessel was based on the geometric scaling of a 2 L PYREX circular glass beaker. The PYREX circular beaker from here onwards will be referred as the model jar test vessel. The upscale jar-test vessel was a circular smooth plastic tank. Since, the principle of dynamic similitude was also applied the ratio of the vessel diameter to the blade diameter was kept constant. The ratio of D_p/D_j was equal to 5:1 where; D_p is the diameter of the blade in the upscale jar-test vessel and D_j is the diameter of the blade in the model jar test. Table 6.1 shows the actual dimensions of the prototype and the actual jar test apparatus.

Table 6.1. Dimensions of the model and the upscale prototype jar test apparatus.

Dimensional Parameter	Model Jar test	Upscale prototype
Tank diameter (m)	0.114	0.57
Impeller diameter (m)	0.076	0.38
Blade width (m)	0.025	0.13

Considering the upper edge of the blade as zero level, velocity measurements were taken at three different speeds of 18 rpm, 36 rpm and 54 rpm, at a distance of $z_1 = 0.1$ m, $z_2 = 0.08$ m, $z_3 = 0.05$ m and $z_4 = 0.03$ m above the blade. These sampling locations are shown in Figure 6.2. The sampling frequency of the ADV was 10Hz. The impeller was set into motion at the given rotational speed. The turbulence was allowed to be completely developed for a period of 120 s. The ADV was then inserted in the flow field at a fixed location as shown in Figure 6.2 and instantaneous velocity measurements were recorded continuously for a period of 60 s. The impeller was stopped after that duration and the velocity measurements were recorded for the next 600 s.. Measurement of the spatial distribution of the velocities simultaneously with and time requires more than one sensor therefore it was assumed that at a contour level the epsilon did not change with space. Therefore the measurements carried out at the fixed test locations were assumed to be representative of the velocity fields measured anywhere at that contour level.

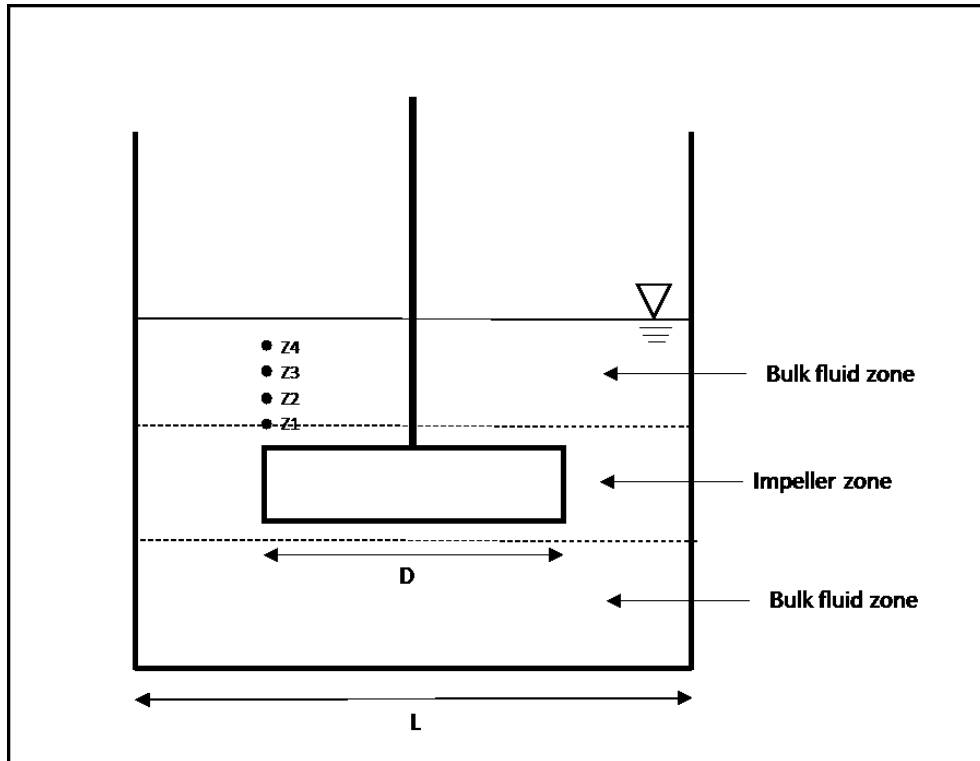


Figure 6.2: Frontal view of the prototype jar test apparatus showing velocity measurement locations. z_1 : 0.03 m; z_2 : 0.05 m; z_3 : 0.08 m ; z_4 0.1 m above the blade.

Analysis and Discussion

Mixing Condition Analysis

To characterize the turbulence it is important to analyze the length scales.. These length scales are directly related to the root mean square velocities of the turbulent fluctuations. Figure 6.3 shows the profile of the velocities measured in the radial, axial and tangential direction that were measured in the prototype jar test apparatus with the ADV. In general, from Figure 6.3 it can be seen that the root mean square values of the velocity fluctuations measured at a distance of 0.03 m and 0.05 m above the blade are greater than those measured at distance of 0.08 m and 0.1 m above the blade because of the proximity of the impeller. .

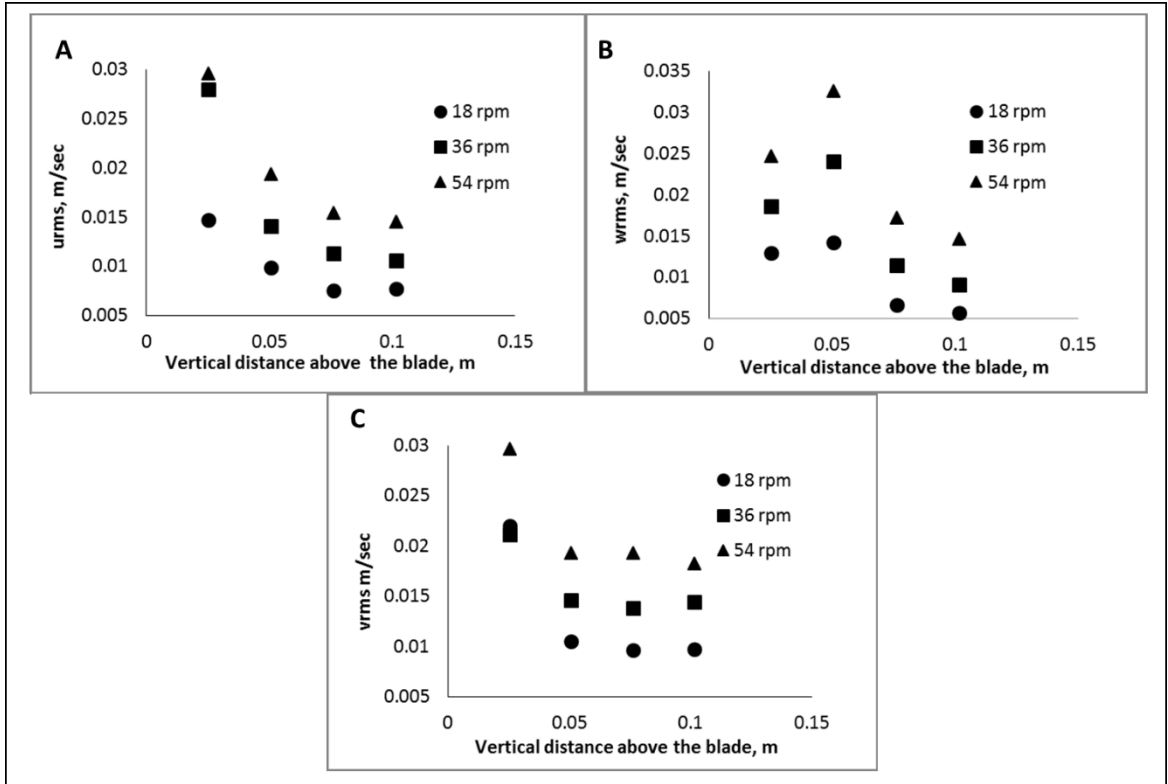


Figure 6.3. Root mean square turbulent velocity profiles A) Radial; B) Axial; C) Tangential.

The radial and tangential velocities approximately decrease as a power function of the distance away from the blade which can be represented as shown in Equation 6.3

$$\sqrt{\overline{u'^2}} = f(z^{-p}) \quad (6.3)$$

where $\overline{u'^2}$ = mean square of the fluctuating component of the velocity (m/sec)

z = Vertical distance above the impeller (m).

As the total turbulent kinetic energy (TKE) for isotropic turbulence is calculated by Equation 6.3 it can be seen the TKE has a similar profile as shown in Figure 6.4.

$$k = \frac{3}{2} \overline{u'^2} \quad (6.4)$$

where k = Total turbulent kinetic energy (TKE) (m^2s^{-2}).

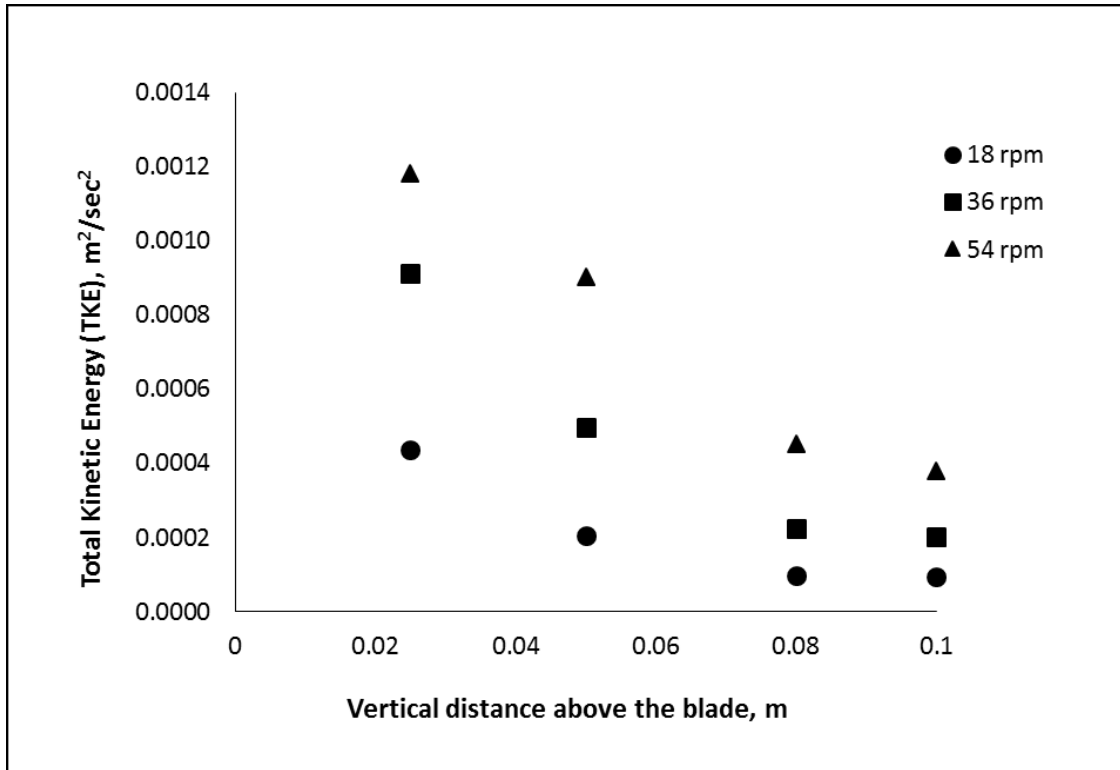


Figure 6.4. Profile of Total Kinetic Energy (TKE) at different vertical distances above the blade at different speeds.

During mixing it was assumed that the turbulent properties do not change with time for the entire mixing duration. Therefore the turbulence properties were deduced considering that the turbulence is independent of time. Table 6.2 shows all the average turbulence parameters deduced from the velocity measurements. The integral length scale ‘L’ was calculated using equations 6.5.

$$L = \tau * U_c \quad (6.5)$$

where τ = Decay time (seconds)

τ is computed from the autocorrelation function of the fluctuating components of the instantaneous velocity. U_c is the convective velocity which was computed from equation 6.6 deduced by Wu et al (1989).

$$U_c = \sqrt{\overline{U_r^2} + u_r'^2} \quad (6.6)$$

where $\overline{U_r^2}$ = mean square radial velocity

$u_r'^2$ = square of the fluctuating components of the radial velocity.

Table 6.2: Average turbulence properties: (TKE : Total kinetic energy; ε : Turbulent energy dissipation rate; N: rotational speed; z: vertical distance above the blade; L: Integral length Scale, τ : Time scale; G: Velocity gradient; η : Kolmogorov's length scale; λ : Taylor's length scale).

N (rpm)	z (m)	TKE (m ² sec ⁻²)	ε (m ² sec ⁻³)	L (m)	τ (s)	G (sec ⁻¹)	η (m)	λ (m)
18	0.1	0.000093	0.000026	0.035	0.41	4.8	0.00048	0.0064
18	0.08	0.000097	0.000029	0.033	0.38	5.10	0.00046	0.0061
18	0.05	0.000205	0.000027	0.024	0.29	10.60	0.00032	0.0043
18	0.03	0.000438	0.000043	0.021	0.18	21.11	0.00023	0.0034
36	0.1	0.000202	0.000075	0.04	0.24	8.15	0.00037	0.0055
36	0.08	0.000226	0.000084	0.041	0.24	8.65	0.00036	0.0055
36	0.05	0.000496	0.000413	0.027	0.18	19.19	0.00024	0.0036
36	0.03	0.000915	0.000542	0.026	0.16	21.96	0.00024	0.0035
54	0.1	0.00038	0.000189	0.057	0.19	11.45	0.00031	0.0054
54	0.08	0.000453	0.000189	0.051	0.19	12.96	0.00029	0.0052
54	0.05	0.000903	0.000845	0.032	0.13	27.41	0.0002	0.0035
54	0.03	0.001184	0.001300	0.031	0.17	34.06	0.00018	0.0032

The diameter of the impeller was 0.381m. The average length scales in the impeller zone were close to D/10 as shown by Zhou and Kresta (1996). Also the ratio the integral length 'L' scales to the Taylor's scale' λ ' was approximately constant which indicate isotropic condition (Pope, 2000). Figure 6.5 shows the turbulent energy dissipation rate profile for mixing conditions. From Figure 6.5 it can be seen that there is significant difference in the dissipation rate away from the blade in the bulk fluid. This difference also increases with the increase in the rotational speed. The turbulent flow Reynolds number were in the range of 290 to 1400.

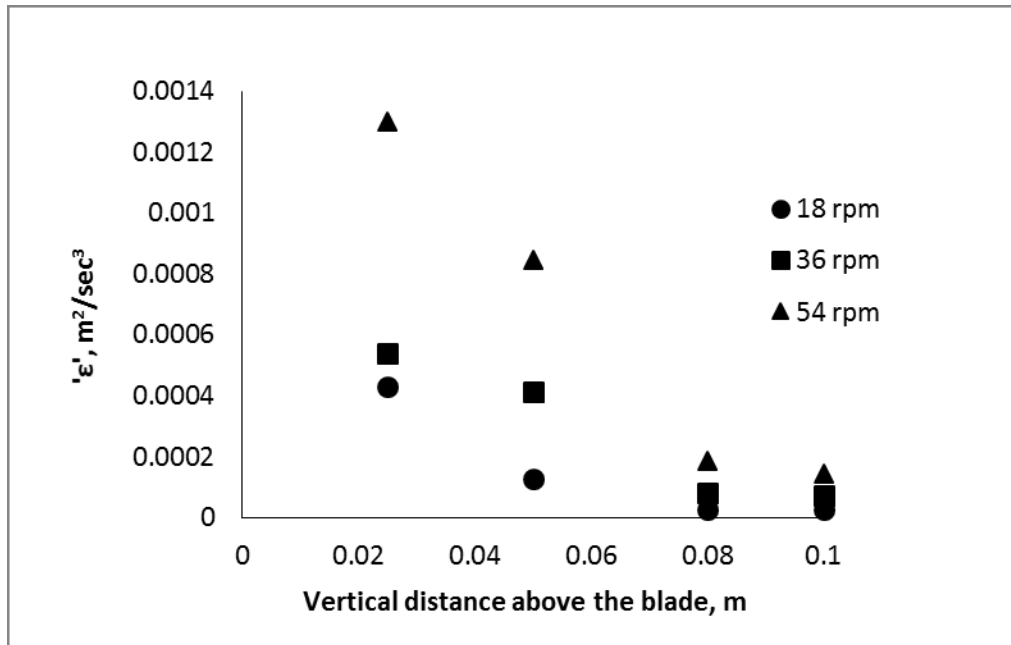


Figure 6.5. Profile of turbulent energy dissipation rate as distance above the blade at different speeds.

Settling Condition Analysis

The turbulent energy dissipation rate can also be represented as the rate of decay of the kinetic energy. So to study the temporal change in the turbulence, the kinetic energy profiles were examined to see the rate of change of the kinetic energy. Figure 6.6 shows a typical profile of the kinetic energy and how it changes within the entire duration of the experiment.

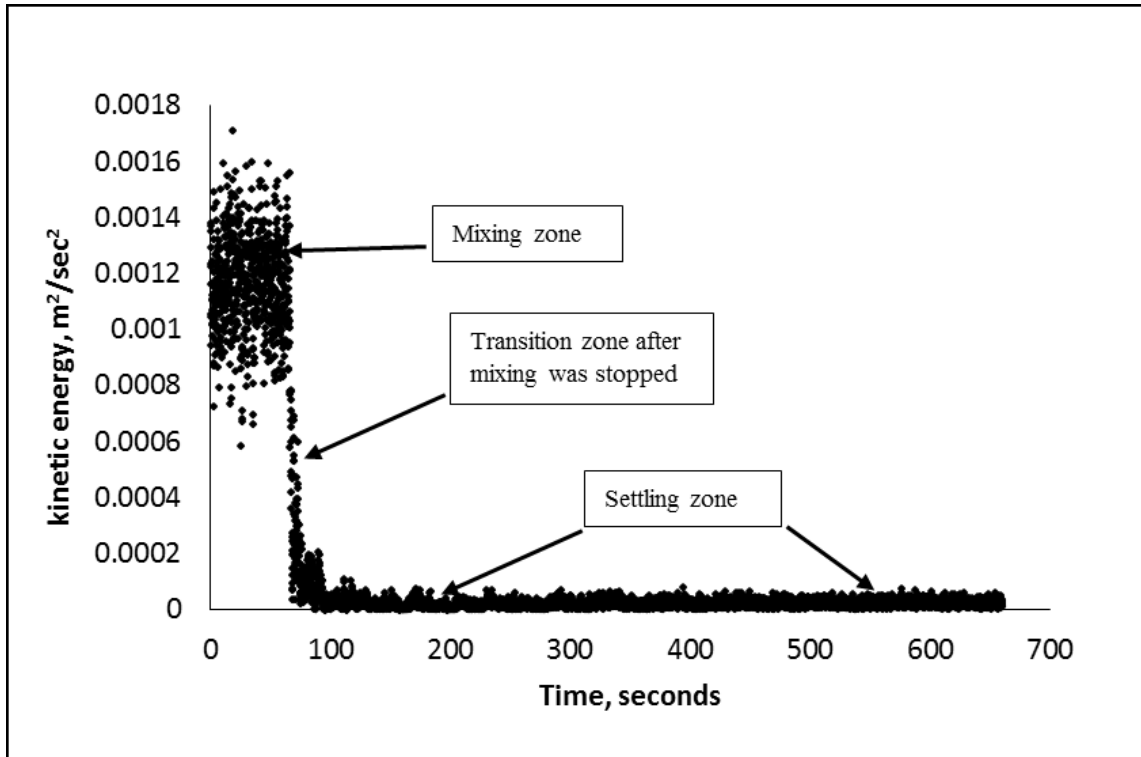


Figure 6.6: Kinetic energy profile across the entire measurement duration

From Figure 6.6 it can be seen that during the first 60 seconds, the mixing is uniform and the Total kinetic energy (TKE) is more or less constant. After the mixing is stopped there is a very sharp drop in the kinetic energy. It takes approximately 30 s for the kinetic energy to come down to a level where again it remains fairly constant. The root means square velocity profiles in the settling zone did not show continuous decay with respect to time and therefore turbulence in the settling zone was assumed to be stationary independent of the time. The same principles of isotropic stationary turbulence were applied on two different time sets, 100 to 300 s and 300 s to 600 s. No significant difference in the turbulent energy dissipation rates were observed. Figures 6.7 shows the temporal profiles of the turbulent energy dissipation rates for different speeds and different depths measured with respect to time in the prototype jar test apparatus.

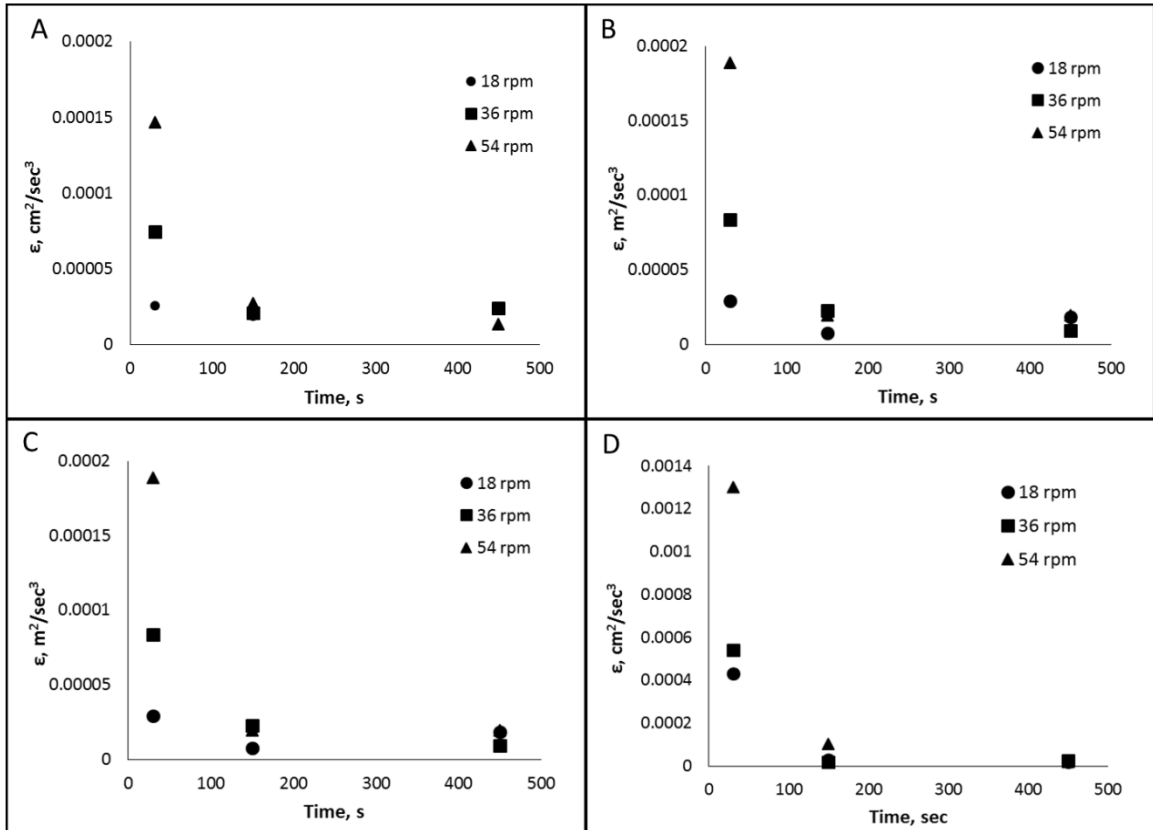


Figure 6.7: Temporal profiles of the turbulent energy dissipation rate at different distances above from the blade at different speeds in prototype jar test apparatus A) 0.1m B) 0.08 C) 0.05 m D) 0.03 m .

Similar to the mixing zone, the ratio the integral length scale ‘L’ to the Taylor’s length scale ‘ λ ’ in the settling zone was fairly constant, indicating that the turbulence was isotropic. Maximum energy dissipation occurred within the first 30 seconds after the mixing was stopped. The decay of the turbulence is a power function of the time. Dissipation rates are maximum near the impeller zone during the mixing conditions. At 18 rpm, due to the low rotational speed there is not much difference in the rate of change of epsilon at the farthest distance of 0.1 m from the impeller. Irrespective of the impeller speed, the turbulent energy dissipation rate was more or less similar in the settling zone. This supports the flocculation theory that the initial high mixing conditions helps in increasing the number of particle interactions. It can also be observed in the jar test procedure when the coagulant is added and mixed initially for the brief duration,

immediately after the stoppage of mixing, large flocs are formed and they begin to settle very quickly. This can be seen from Figure 6.6 that during the first few seconds, there is a sharp reduction in the turbulent energy dissipation rate which leads to large effective floc diameter (Tapp et al, 1981). From the trend of the decay of turbulence it can be said that the turbulence dissipation rate decreases as some power function of time which would depend upon the geometry of the reactor and blade and also the mixing speed. However, for scaling, if the geometric and dynamic similarity is maintained, the turbulence decay rate should be similar.

Geometric Scaling of Turbulence Parameters

Since it is not possible to physically insert the ADV probe in the actual jar test apparatus to measure the turbulence parameters, the measurements as described in the methodology were conducted in an upscaled prototype of the cylindrical jar test where the dynamic similarity was maintained by keeping a constant ratio between the tank diameter and the impeller diameter. Due to the design of mounting of the impeller on the prototype tank, higher speeds could not be used to measure turbulent velocity as the motor noise was increasing proportionately and also the motion of the impeller blade appeared to be non-uniform. Considering these parameters the speeds selected for the prototype motion were 18 rpm, 36 rpm and 54 rpm. Based on these speeds, the impeller Reynolds numbers for the both the tanks are shown in Table 6.3.

Table 6.3. Reynolds number in the actual and the prototype jar test.

Impeller Speed	Reynolds number in prototype (NRe_p)	Reynolds number in actual jar test (NRe_j)
18 rpm	43374	1743
36 rpm	86749	2891
54 rpm	130124	3469

Since the impeller Reynolds number scales as the square of the impeller diameter it can be seen from Table 6.3 that the Reynolds number in the actual jar test are 25 times lower than those in the prototype for the same rotational speed 'N'. For turbulent flow the impeller Reynolds number NRe should be greater than 10,000 (Reynolds and Richards, 1996). For laminar flow the NRe is less than 10 (Reynolds and Richards, 1996). Therefore it can be seen from Table 6.3 that even though the flow is fully turbulent in prototype apparatus, it is still in the transitional stage in the actual jar tests at the same mixing speed. Therefore, the turbulent energy dissipation rate scales will not match and if the dissipation rate has to be maintained constant, the rotational speeds for the actual jar test would have to be adjusted to match the scale of the turbulence in the prototype. Based on the principles of geometric and dynamic similitude, it is shown that as long as the ratio of the blade diameter to the tank diameter remains constant the turbulence parameters scale as \bar{U}/ND , u'/ND and ε/N^3D^2 (Wu et al., 1989; Zhou and Kresta, 1986). Therefore to maintain a constant turbulent energy dissipation rate in the actual jar test apparatus, the rotational speeds that would be needed are as shown in Table 6.4.

Table 6.4: Comparison of rotational speeds in prototype with the scaled rotational speeds needed in actual jar test apparatus for constant turbulent energy dissipation rates.

Rotational Speed in prototype	Required rotational speed in actual jar test for same 'ε'
18 rpm	53 rpm
36 rpm	105 rpm
54 rpm	158 rpm

For the constant calculated turbulent energy dissipation rate the approximate temporal floc size distribution that could be expected in model jar test apparatus as a function of the distance away from the blade as shown in Figure 6.8. It can be seen from Figure 6.8 floc sizes are small at start of the mixing due to high 'ε' values. The floc growth is significant in the first 30 seconds and then tend to reach a relatively equilibrium floc size. The floc sizes were calculated using equation 6.2. Also the impeller was turned on for duration of 60 ss. From Figure 6.8, it can also be seen that the floc sizes for the average 'G' values are low compared to the actual floc size. The reason for this is that the average 'G' values are calculated from the average power dissipated per volume, which is a function of the rotational speed and the impeller diameter. Therefore, the average 'G' value is more representative of the turbulence near the impeller than the bulk fluid. Therefore, with average 'G' values, low floc sizes are obtained. One consequence of this could be using more flocculant which would lead to overdosing.

To summarize, the spatial and temporal floc size distribution is different and once the turbulence decays the flocs reach an equilibrium floc size. The turbulent energy distribution profiles could be determined in the field and could be correlated with the turbulent energy dissipation rate profiles in the jar test not only to optimize the flocculant dosage but also size the mixing devices, so as to achieve maximum possible flocculation efficiency.

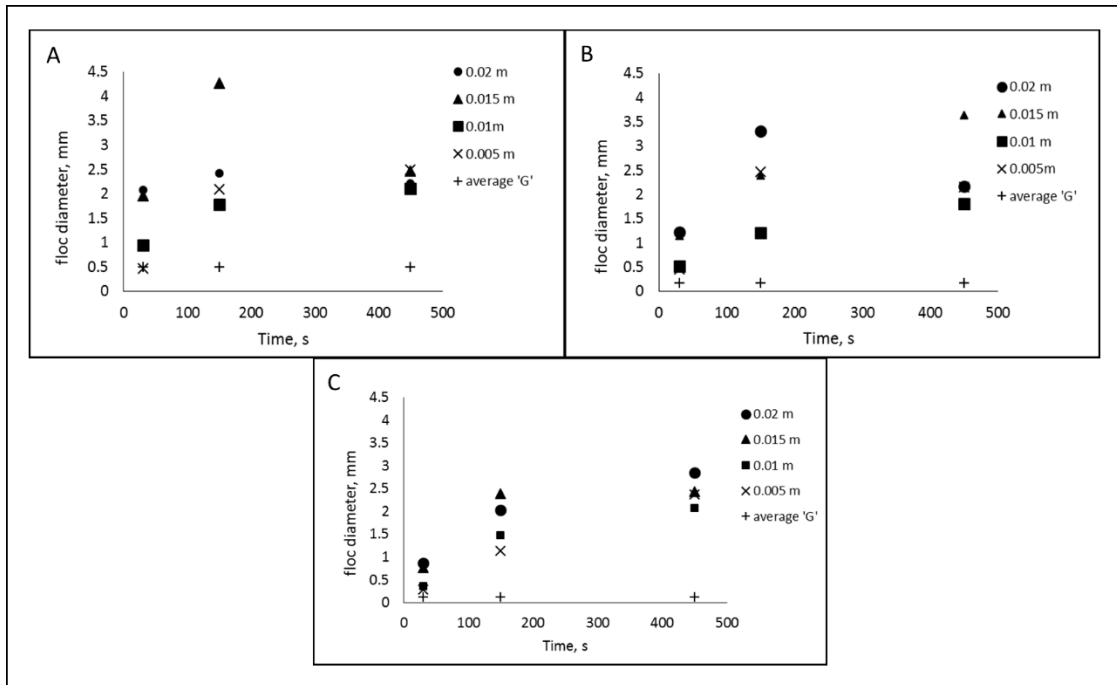


Figure 6.8: Floc size distribution at various rotational speeds for change in ‘ ϵ ’ with time and vertical distance from blade for the model jar test apparatus A) 53 rpm; B) 105 rpm C) 158 rpm

Conclusions:

Similitude studies on jar tests have shown that local turbulent energy dissipation rate ‘ ϵ ’ within the jar test varies significantly with the distance away from the impeller from the blade and therefore a vessel average ‘ ϵ ’ value cannot be used to represent the overall scale of turbulence within the jar. Again, after mixing is stopped there is a sharp decrease in ‘ ϵ ’ which leads to formation of large flocs as observed in jar-test experiments. Irrespective of the rotational speed of the impeller, ‘ ϵ ’ remains fairly constant once the mixing is stopped.. Average ‘ G ’ values predict lower size of floc and are more representative of the turbulent energy dissipation rate in the impeller zone than the bulk fluid. Overall, if the ratio of the impeller diameter with respect to the tank diameter is kept constant, turbulence parameters can be scaled to predict floc size distributions. Finally, The turbulent energy distribution profiles could be determined in the field and could be correlated with the turbulent energy dissipation rate profiles in the jar test not only

to optimize the flocculant dosage but also size the mixing devices, so as to achieve maximum possible flocculation efficiency..

CHAPTER VII

CONCLUSIONS AND FUTURE RESEARCH RECOMMENDATIONS

The overall research objective was to measure and predict sediment reduction using flocculation to control sediment from construction site to reduce the turbidity. Flume experiments were conducted to measure the flocculation efficiency of five soils from Oklahoma. A mathematical model was developed based to predict the flocculation efficiency of sediment using polymer flocculant and the flume experiments were used to calibrate the model. Finally, turbulence within a jar test was characterized through similitude comparisons.

Conclusions

- 1) The first research objective was to conduct flume experiments to determine the flocculation efficiency for five soils from Oklahoma. The overall conclusions of this research objective are
 - The flume experiment design and procedures allowed the spatial and temporal characterization of flocculated settled mass and suspended sediment concentration to determine the flocculation efficiency.

- The flume apparatus design was unique such that it allowed the control of the variables including turbidity and particle size distribution of the incoming sediment so as to simulate suspended sediment concentrations and distributions representative to those typically observed construction site runoff in the field.
 - The average reduction in the turbidity for all the five soils was 76 percent, while the average sediment removal rate was 41%. Thus, liquid polymer flocculant was more effective in removing fine particles that are a primary source of the turbidity compared to conventional sediment techniques that are currently commonly used.
- 2) The second objective was to develop a flocculation model based to predict the flocculation efficiency and estimate stickiness coefficient for five soils from Oklahoma. The overall conclusions for this research objective are
- A mathematical model was modified based on the research work done by Krishnappan and Marsalek (2002) to predict the flocculation efficiency of sediment using polymer flocculant with sediment runoff having concentration of clay particles.
 - The model has a simplistic mathematical approach based on the fundamental theory of flocculation and therefore can be used to predict the flocculation efficiency of different sediment types and flocculants.
 - The predicted spatial and temporal distribution of the flocculated sediment was similar to that observed in the flume experiments, and the accuracy of the prediction was high for soils where settling was not dominated by differential settling. Thus, the model is consistent with both the theory of flocculation and the experimental observations. Improvements to the model that would make it even more widely applicable would be to better characterize differential settling of the flocculated particles.

- Finally, the model can be coupled with watershed models and thus can be used a design tool to predict the flocculation efficiency of sediment runoff on remote field sites based on the individual characteristics of the site.
- 3) The third research objective of the research study to quantify the spatial and temporal turbulence energy dissipation rate in a round jar test and the impact it has on floc size distribution. The overall conclusions for this objective were
- Similitude studies of a jar test showed that the floc size distribution varies greatly due to spatial and temporal variability in the turbulent energy dissipation rate.
 - The variability of this local turbulence greatly affects the floc size distribution. An average value of the velocity gradient ‘ G ’ that is conventionally used in the jar test procedures may predict lower floc sizes and may lead to overdosing on the flocculant.
 - Determination of the temporal change of the turbulent energy dissipation rate was a unique aspect of this study. Results indicate that irrespective of the rotational speed, the total kinetic energy within the jar test dissipated, which caused rapid decrease in the turbulent energy dissipation rate. This promoted formation of larger flocs than estimated using the average turbulent energy dissipation rate.
 - The temporal decay of the turbulent energy dissipation rate in a jar test can be used to represent the spatial decay in the flume or the field apparatus. Therefore, the nature of the turbulence and the floc size distribution in the field stormwater runoff can be predicted using the laboratory jar test.

Recommendations for Future Work

The research on flocculation treatment for control of sediment from construction sites is very dynamic. Follow-up and related research questions that have potential for further investigation include:

1. The scale of the flume experiments conducted to support the flocculation modeling work was large. A controlled laboratory scale experiments where physical characteristic of the flocs, such as density settling velocities, could be determined experimentally could improve the prediction accuracy. In other words, better calibration data will lead to better model results.
2. Conduct tests to measure the stickiness coefficient directly rather than estimate it. . These tests may require understanding the clay mineralogy and determining the effect of flocculant concentrations on different clay minerals to optimize flocculant dosage.
3. For the flume experiments, an average shear rate was used for every reactor. In future versions of the flocculation model, coupling a turbulent advection dispersion model, such as the $k-\epsilon$, would lead to better prediction of the transport phenomenon.
4. For the upscaled jar-test apparatus, turbulence measurement using a sensor that has a high sampling rate of 1Khz is recommended so that to increase the spatial and temporal accuracy of measurement of the turbulent energy dissipation rate. Turbulence measurements should have more than 10 -15 replicates to check for repeatability and ensure better accuracy of measurement
5. Combining this model with an algorithm to predict turbidity from particle size distributions would expand the useful of this model for turbidity prediction.

To conclude, it is prudent to have a scientific approach in the methodology used to control sediments entrained in stormwater runoff. The research work done has helped in

understanding the overall process of flocculation and use of polymer flocculants in controlling sediment in stormwater runoff. The flocculation model is a useful tool for predicting the sediment removal efficiencies from stormwater runoff from construction sites and can be used to optimize flocculant dosage and size stormwater structures

REFERENCES

- Argaman, Y., & Kaufman, W. J. (1970). Turbulence and flocculation. *Journal of the Sanitary Engineering Division*, 96(2), 223-241.
- Amirtharajah, A., & Clark, M. M. (1991). *Mixing in coagulation and flocculation*. American Water Works Association.
- Ayesa, E., Margeli, M. T., Florez, J., & Garcia-Heras, J. L. (1991). Estimation of breakup and aggregation coefficients in flocculation by a new adjustment algorithm. *Chemical Engineering Science*, 46(1), 39-48.
- Barrett, J.E., Kearney, J.E., McCoy, T.G., Malina, J.F., Charbeneau, R.J and Ward, G.H., (1995). An Evaluation of the Performance of Geotextiles for Temporary Sediment Control. *Center for Research in Water Resources, College of Engineering, The University of Texas at Austin, CRWR 261*
- Barvenik, F. W. (1994). Polyacrylamide characteristics related to soil applications. *Soil Science*, 158(4), 235-243.
- Batchelor, G. K. (2000). *An Introduction to Fluid Dynamics*. Cambridge University Press.
- Bhardwaj, A. K., & McLaughlin, R. A. (2008, October). Storm water turbidity control by flow energy dissipation and chemical treatment in stilling basins. In *2008 Joint Meeting of The Geological Society of America, Soil Science Society of America, American Society of Agronomy, Crop Science Society of America, Gulf Coast Association of Geological Societies with the Gulf Coast Section of SEPM*.
- Bushell, G.C, Yan, Y.D, Woodfield, D, Raper, J, Amal, R,2002. On Techniques for the measurement of the mass fractal dimension of the aggregates. *Advances in Colloid Interface Science*, 95(2002)1-50.
- Bouyer, D., Escudié, R., & Liné, A. (2005). Experimental analysis of hydrodynamics in a jar-test. *Process Safety and Environmental Protection*,83(1), 22-30.
- Bouyer, D., Line, A., Cockx, A., & Do-Quang, Z. (2001). Experimental analysis of floc size distribution and hydrodynamics in a jar-test. *Chemical Engineering Research and Design*, 79(8), 1017-1024.
- Caddy, J. F. (1973). Underwater observations on tracks of dredges and trawls and some effects of dredging on a scallop ground. *Journal of the Fisheries Board of Canada*, 30(2), 173-180.

- Camp, T. R., & Stein, P. C. (1943). Velocity gradients and internal work in fluid motion. *Journal of the Boston Society of Civil Engineers*, 85, 219-37.
- Canning, D.J 1988. Construction Erosion Control: Shorelands Technical Advisory Paper No.3. *Shorelands and Coastal Zone Management Program, Washington Department of Ecology, Olympia, WA*
- Canli, M., & Atli, G. (2003). The relationships between heavy metal (Cd, Cr, Cu, Fe, Pb, Zn) levels and the size of six Mediterranean fish species. *Environmental pollution*, 121(1), 129-136.
- Celik, I. B. (1999). Introductory turbulence modeling. *Western Virginia University*
- Chen, S., & Eisma, D. (1995). Fractal geometry of in situ flocs in the estuarine and coastal environments. *Netherlands Journal of Sea Research*,33(2), 173-182.
- Cheng, C. Y., Atkinson, J. F., & Bursik, M. I. (1997). Direct measurement of turbulence structures in mixing jar using PIV. *Journal of Environmental Engineering*, 123(2), 115-125.
- Clark, M.M., 1996. Transport Modeling for Environmental Engineers and Scientists. John Wiley & Sons, Inc.
- Colomer, J., Peters, F., & Marrasé, C. (2005). Experimental analysis of coagulation of particles under low-shear flow. *Water Research*, 39(13), 2994-3000.
- Cornwell, D. A., & Bishop, M. M. (1983). Determining velocity gradients in laboratory and full-scale systems. *Journal (American Water Works Association)*, 470-475.
- Davis, M. L., & Cornwell, D. A. (1998). *Introduction to Environmental Engineering* (Vol. 3). New York: McGraw-Hill.
- De Silva, I. P. (2006). Turbulence dissipation in stirred jars. *Journal of engineering mechanics*, 132(11), 1260-1268.
- Dyer, K. R., & Manning, A. J. (1999). Observation of the size, settling velocity and effective density of flocs, and their fractal dimensions. *Journal of Sea Research*, 41(1), 87-95.
- Faucette, L. B., Sefton, K. A., Sadeghi, A. M., & Rowland, R. A. (2008). Sediment and phosphorus removal from simulated storm runoff with compost filter socks and silt fence. *Journal of Soil and Water Conservation*, 63(4), 257-264.
- Garcia, C. M., Cantero, M. I., Niño, Y., & Garcia, M. H. (2005). Turbulence measurements with acoustic Doppler velocimeters. *Journal of Hydraulic Engineering*, 131(12), 1062-1073.
- Green, V. S., & Stott, D. E. (1999, May). Polyacrylamide: A review of the use, effectiveness, and cost of a soil erosion control amendment. In *The 10th International Soil Conservation Organization Meeting* (pp. 384-389).

- Gregory, J., & O'Melia, C. R. (1989). Fundamentals of flocculation. *Critical Reviews in Environmental Science and Technology*, 19(3), 185-230.
- Ha, H. K., & Maa, J. P. Y. (2010). Effects of suspended sediment concentration and turbulence on settling velocity of cohesive sediment. *Geosciences Journal*, 14(2), 163-171.
- Haan, C. T., Barfield, B. J., & Hayes, J. C. (1994). Design hydrology and sedimentology for small catchments. *Elsevier*.
- Harper, H. H. (2007). Current research and trends in alum treatment of stormwater runoff. In *Proceedings of the 9th Biennial Conference on Stormwater Research & Watershed Management* (pp. 2-3).
- Hinze, J. O. (1959). Turbulence, 1975. *New York*.
- Horner, R. R., Guedry, J., & Kortenhof, M. H. (1990). Improving the cost effectiveness of highway construction site erosion and pollution control. *Washington State Department of Transportation*.
- Jarvis, P., Jefferson, B., Gregory, J., & Parsons, S. A. (2005). A review of floc strength and breakage. *Water Research*, 39(14), 3121-3137.
- Johnston Jr, S. A. (1981). Estuarine dredge and fill activities: A review of impacts. *Environmental Management*, 5(5), 427-440.
- Jury, W. A., & Horton, R. (2004). Soil Physics. *Hoboken*.
- Jun Nan, Weipang He, Juanjuan Song, Xinxin Song, 2009. Fractal Growth and Characteristics of Floccs in Flocculation Process in Water Treatment. International Conference of Energy and Environmental Technology ICEET.2009.379
- Kang, J., McCaleb, M. M., & McLaughlin, R. A. (2013). Check dam and polyacrylamide performance under simulated stormwater runoff. *Journal of Environmental Management*, 129, 593-598.
- Kang, J. H., Li, Y., Lau, S. L., Kayhanian, M., & Stenstrom, M. K. (2007). Particle destabilization in highway runoff to optimize pollutant removal. *Journal of Environmental Engineering*, 133(4), 426-434.
- Kusters, K. A., Wijers, J. G., & Thoenes, D. (1997). Aggregation kinetics of small particles in agitated vessels. *Chemical Engineering Science*, 52(1), 107-121.
- Khelifa, A., & Hill, P. S. (2006). Models for effective density and settling velocity of floccs. *Journal of Hydraulic Research*, 44(3), 390-401
- Kranenburg, C. (1994). The fractal structure of cohesive sediment aggregates. *Estuarine, Coastal and Shelf Science*, 39(6), 451-460.
- Kresta, S. (1998). Turbulence in stirred tanks: anisotropic, approximate, and applied. *The Canadian Journal of Chemical Engineering*, 76(3), 563-576.

- Krishnappan, B. G., & Marsalek, J. (2002). Modelling of flocculation and transport of cohesive sediment from an on-stream stormwater detention pond. *Water Research*, 36(15), 3849-3859.
- Krone, R. B. (1978). Aggregation of suspended particles in estuaries. *Estuarine Transport Processes*, 177, 190.
- Lau, Y. L., & Krishnappan, B. G. (1997). Measurement of size distribution of settling flocs. *National Water Research Institute, Environment Canada, CCIW, Burlington, Ont., Canada 1997*.
- Lee, K. C., & Yianneskis, M. (1998). Turbulence properties of the impeller stream of a Rushton turbine. *AIChE journal*, 44(1), 13-24.
- Liem, L. E., Smith, D. W., & Stanley, S. J. (1999). Turbulent velocity in flocculation by means of grids. *Journal of Environmental Engineering*, 125(3), 224-233.
- Lick, W., & Lick, J. (1988). Aggregation and disaggregation of fine-grained lake sediments. *Journal of Great Lakes Research*, 14(4), 514-523.
- Maerz, J., Verney, R., Wirtz, K., & Feudel, U. (2011). Modeling flocculation processes: Intercomparison of a size class-based model and a distribution-based model. *Continental Shelf Research*, 31(10), S84-S93.
- Maggi, F., Mietta, F., & Winterwerp, J. C. (2007). Effect of variable fractal dimension on the floc size distribution of suspended cohesive sediment. *Journal of Hydrology*, 343(1), 43-55.
- Matsuo, T., & Unno, H. (1981). Forces acting on floc and strength of floc. *Journal of the Environmental Engineering Division*, 107(3), 527-545.
- McAnally, W. H., & Mehta, A. J. (2000). Aggregation rate of fine sediment. *Journal of Hydraulic Engineering*, 126(12), 883-892.
- McCave, I. N. (1984). Size spectra and aggregation of suspended particles in the deep ocean. *Deep Sea Research Part A. Oceanographic Research Papers*, 31(4), 329-352.
- McCave, I.N (1975). Vertical flux of particles in the ocean. *Deep Sea Research and Oceanographic Abstracts* 22, (7),. 491-502.
- Millen, J. A., Jarrett, A. R., & Faircloth, J. W. (1997). Experimental evaluation of sedimentation basin performance for alternative dewatering systems. *Transactions of the ASAE*, 40(4), 1087-1095.
- Newcombe, C. P., & MacDonald, D. D. (1991). Effects of suspended sediments on aquatic ecosystems. *North American Journal of Fisheries Management*, 11(1), 72-82.
- O'Melia, C. R. (1980). Aquasols: The Behavior of Small Particles in Aquatic Systems. *Environmental Science & Technology*, 14(9), 1052-1060.
- Palmer, H. D., & Gross, M. G. (Eds.). (1979). *Ocean dumping and marine pollution: geological aspects of waste disposal*. Dowden Hutchinson and Ross.

- Parker, D. S., Kaufman, W. J., & Jenkins, D. (1972). Floc breakup in turbulent flocculation processes. *Journal of the Sanitary Engineering Division*, 98(1), 79-99.
- Patil, S. 2011. Turbidity model for construction sites. *Proceedings EWRI International Meeting, Palm Springs, CA*
- Pope, S. B. (2000). *Turbulent flows*. Cambridge university press.
- Reynolds, T. D., & Richards, P.A (1996). Unit operations and processes in environmental engineering, 1996. *PWS-Kent, Boston*, 173.
- Rier, S. T., & King, D. K. (1996). Effects of inorganic sedimentation and riparian clearing on benthic community metabolism in an agriculturally-disturbed stream. *Hydrobiologia*, 339(1-3), 111-121.
- Richards, C., & Bacon, K. L. (1994). Influence of fine sediment on macroinvertebrate colonization of surface and hyporheic stream substrates. *Western North American Naturalist*, 54(2), 106-113.
- Roach, P. E. (1987). The generation of nearly isotropic turbulence by means of grids. *International Journal of Heat and Fluid Flow*, 8(2), 82-92.
- Ryan, P. A. 1991. Environmental effects of sediment on New Zealand streams: a review. *New Zealand journal of marine and freshwater research*, 25(2), 207-221
- Saffman, P., & Turner, J. S. (1956). On the collision of drops in turbulent clouds. *Journal of Fluid Mechanics*, 1(01), 16-30.
- Serra, T., Colomer, J., & Logan, B. E. (2008). Efficiency of different shear devices on flocculation. *Water research*, 42(4), 1113-1121.
- Simon, J. L., & Dyer, J. P. (1972). *An evaluation of siltation created by bay dredging and construction company during oyster shell dredging operations in Tampa Bay, Florida*. Final Research Report, University of South Florida, Tampa.
- Smoluchowski, M. V. (1916). Drei vortrage uber diffusion, brownsche bewegung und koagulation von kolloidteilchen. *Zeitschrift fur Physik*, 17, 557-585.
- Somasundaran, P., & Runkana, V. (2003). Modeling flocculation of colloidal mineral suspensions using population balances. *International Journal of Mineral Processing*, 72(1), 33-55.
- Son, M., & Hsu, T. J. (2009). The effect of variable yield strength and variable fractal dimension on flocculation of cohesive sediment. *Water Research*, 43(14), 3582-3592.
- Spicer, P. T., & Pratsinis, S. E. (1996). Shear-induced flocculation: the evolution of floc structure and the shape of the size distribution at steady state. *Water Research*, 30(5), 1049-1056.
- Stanley, S. J., & Smith, D. W. (1995). Measurement of turbulent flow in standard jar test apparatus. *Journal of environmental engineering*, 121(12), 902-910.

- Tapp, J.S., Barfield, B.J., Griffin, M.L. 1981. Suspended solids removal in pilot size sediment ponds using chemical flocculation. IMMR81/063
- Tambo, N., & Watanabe, Y. (1979). Physical characteristics of flocs—I. The floc density function and aluminum floc. *Water Research*, 13(5), 409-419.
- Thomas, D. N., Judd, S. J., & Fawcett, N. (1999). Flocculation modelling: a review. *Water Research*, 33(7), 1579-1592
- Thomas, D. G. (1964). Turbulent disruption of flocs in small particle size suspensions. *AIChE Journal*, 10(4), 517-523.
- Trent, L., Pullen, E. J., & Proctor, R. (1976). Abundance of macrocrustaceans in a natural marsh and a marsh altered by dredging, bulkheading, and filling. *Fish. Bull*, 74, 195-200.
- Tsai, C. H., Jacobellis, S., & Lick, W. (1987). Flocculation of fine-grained lake sediments due to a uniform shear stress. *Journal of Great Lakes Research*, 13(2), 135-146.
- US Environmental Protection Agency (USEPA). 2005. National Management Measures to Control Nonpoint Source Pollution from Urban Areas. Management Measure 8: Construction Site Erosion, Sediment, and Chemical Control. *EPA-841-B-05-004*, Washington, D.C. Retrieved from: http://water.epa.gov/polwaste/nps/urban/upload/urban_ch08.pdf on February 2, 2014
- US Environmental Protection Agency (USEPA). 2009. Effluent Limitations Guidelines and Standards for the Construction and Development Point Source Category. *EPA-HQ-OW-2008-0465*, Washington D.C. Retrieved from: <http://www.gpo.gov/fdsys/pkg/FR-2009-12-01/pdf/E9-28446.pdf> on June 5, 2014
- US Environmental Protection Agency (USEPA). 2014. Effluent Limitations Guidelines and Standards for the Construction and Development Point Source Category. *EPA-HQ-OW-2010-0884*, Washington D.C. Retrieved from: <http://www.gpo.gov/fdsys/pkg/FR-2014-03-06/pdf/2014-04612.pdf> on June 5, 2014
- Winterwerp, J. C. (1998). A simple model for turbulence induced flocculation of cohesive sediment. *Journal of Hydraulic Research*, 36(3), 309-326.
- Wood, P. J., & Armitage, P. D. (1997). Biological effects of fine sediment in the lotic environment. *Environmental management*, 21(2), 203-217.
- Wu, H., & Patterson, G. K. (1989). Laser-Doppler measurements of turbulent-flow parameters in a stirred mixer. *Chemical Engineering Science*, 44(10), 2207-2221.
- Wu, H., & Patterson, G. K. (1989). Laser-Doppler measurements of turbulent-flow parameters in a stirred mixer. *Chemical Engineering Science*, 44(10), 2207-2221
- Yeung, A., Gibbs, A., & Pelton, R. (1997). Effect of shear on the strength of polymer-induced flocs. *Journal of Colloid and Interface Science*, 196(1), 113-115.

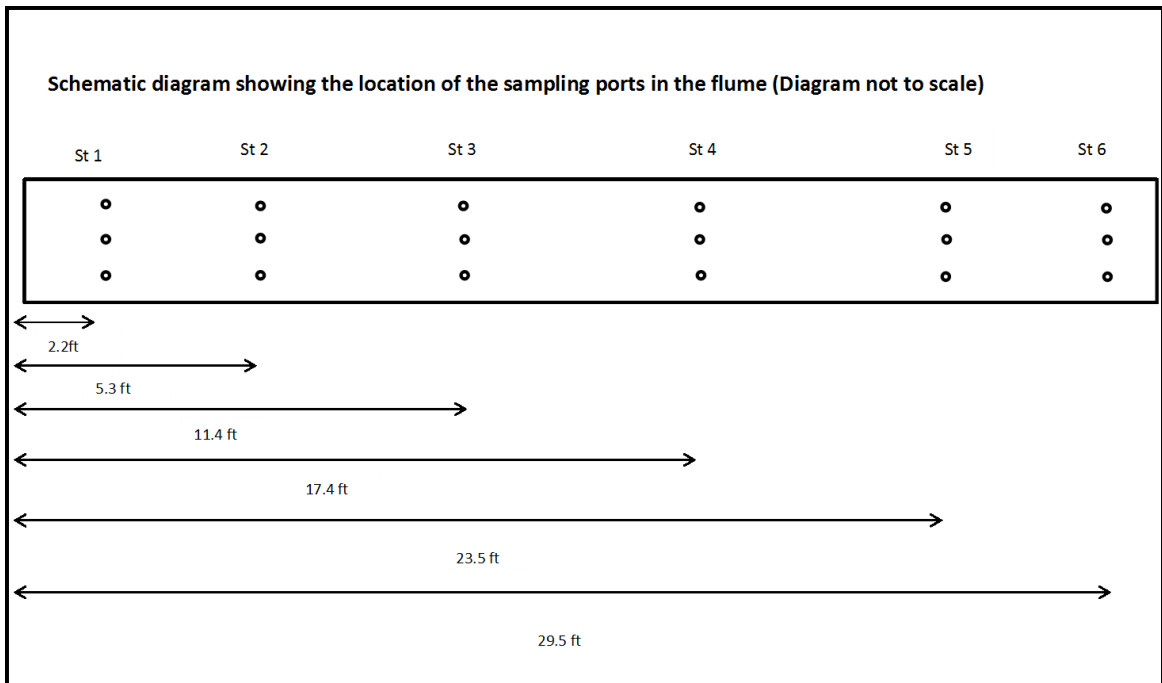
Yusa, M. (1977). Mechanisms of pelleting flocculation. *International Journal of Mineral Processing*, 4(4), 293-305.

Zhang, Z., Sisk, M. L., Mashmouhy, H., & Thomas, C. R. (1999). Characterization of the breaking force of latex particle aggregates by micromanipulation. *Particle & Particle Systems Characterization*, 16(6), 278-283.

Zhou, G., & Kresta, S. M. (1996). Impact of tank geometry on the maximum turbulence energy dissipation rate for impellers. *AIChE journal*, 42(9), 2476-2490

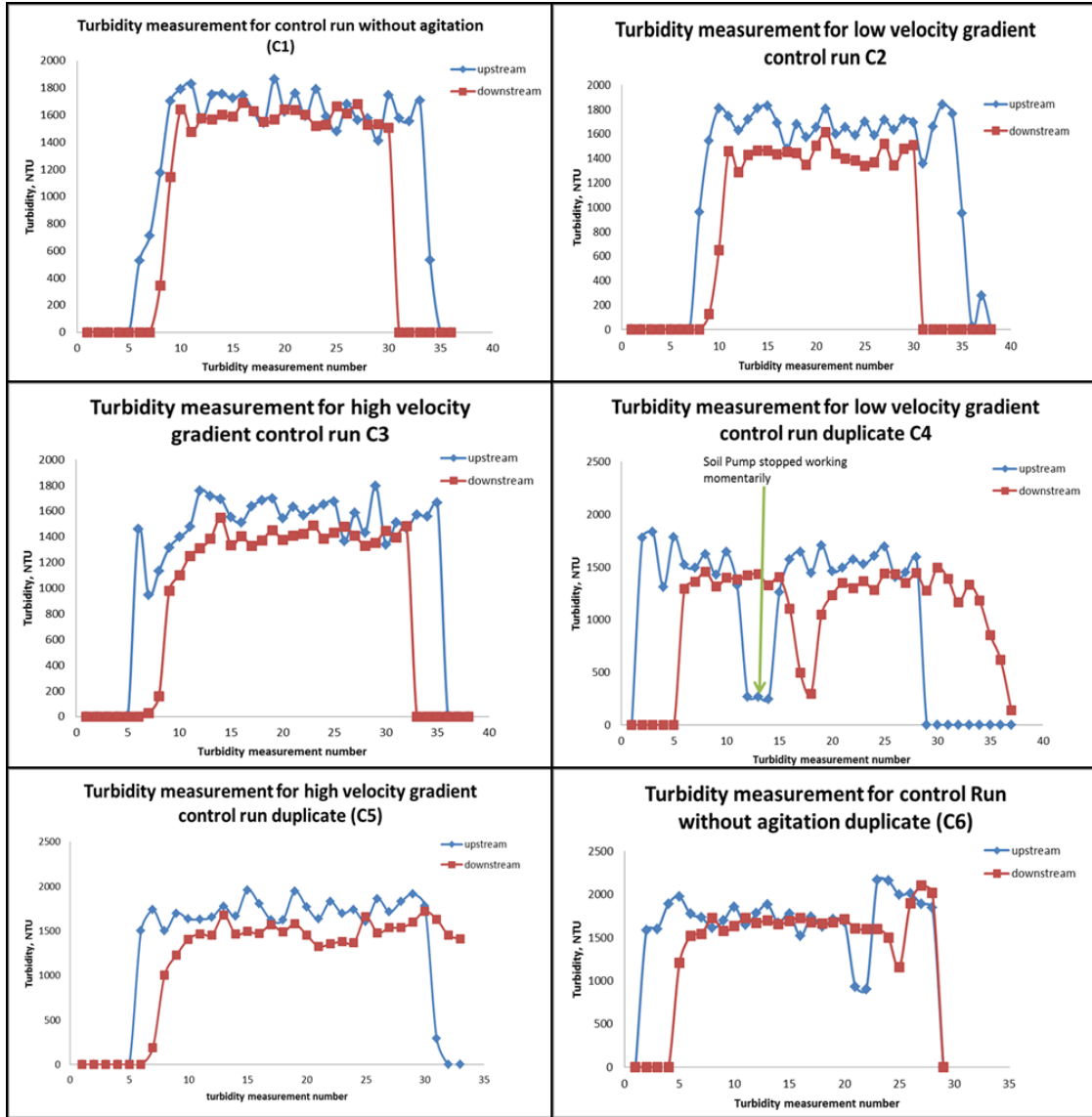
APPENDICES

Appendix I: Sediment Port Diagram

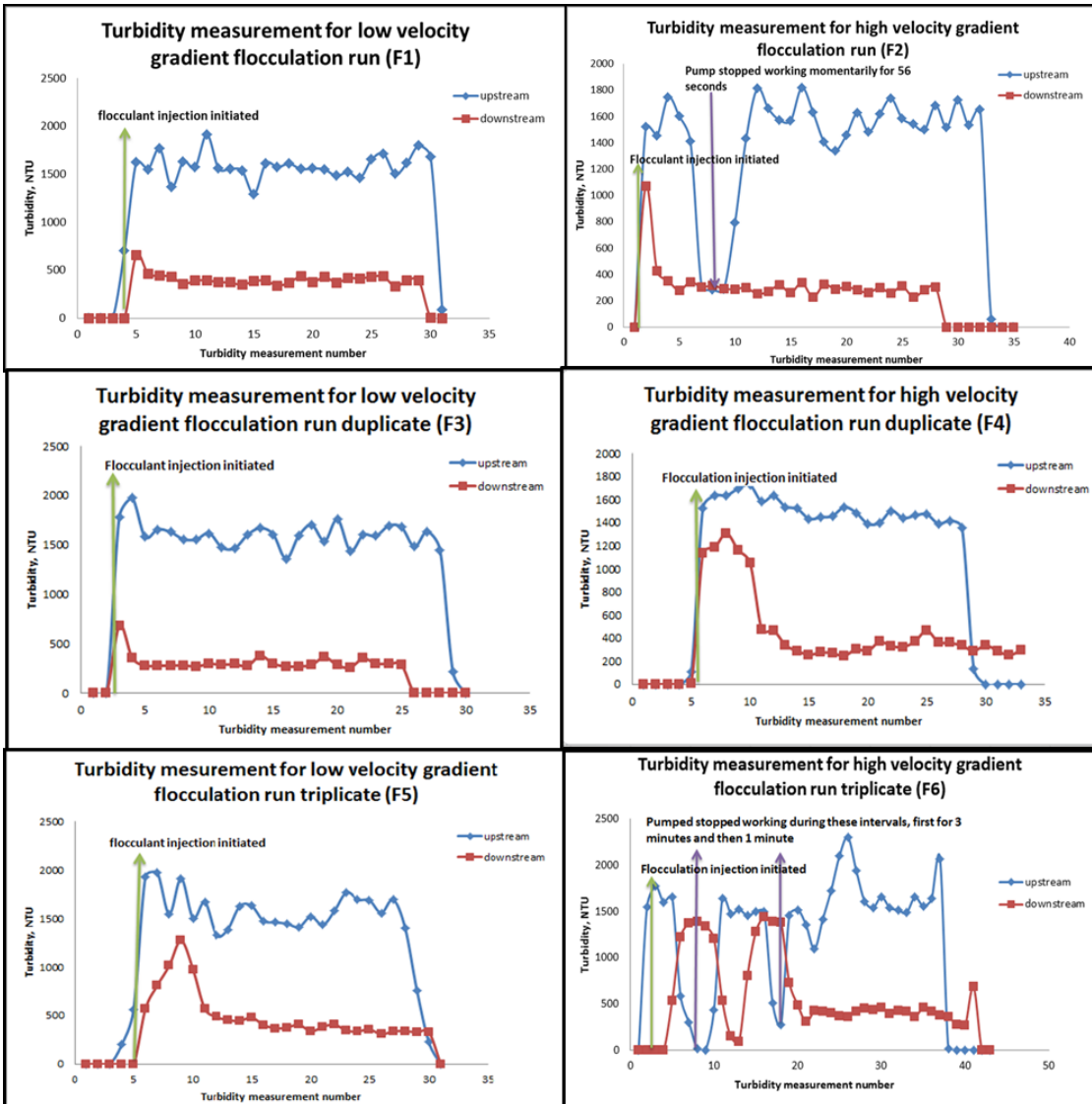


Appendix II: Turbidity measurements for Port A Soil

Turbidity Measurement for Control Runs

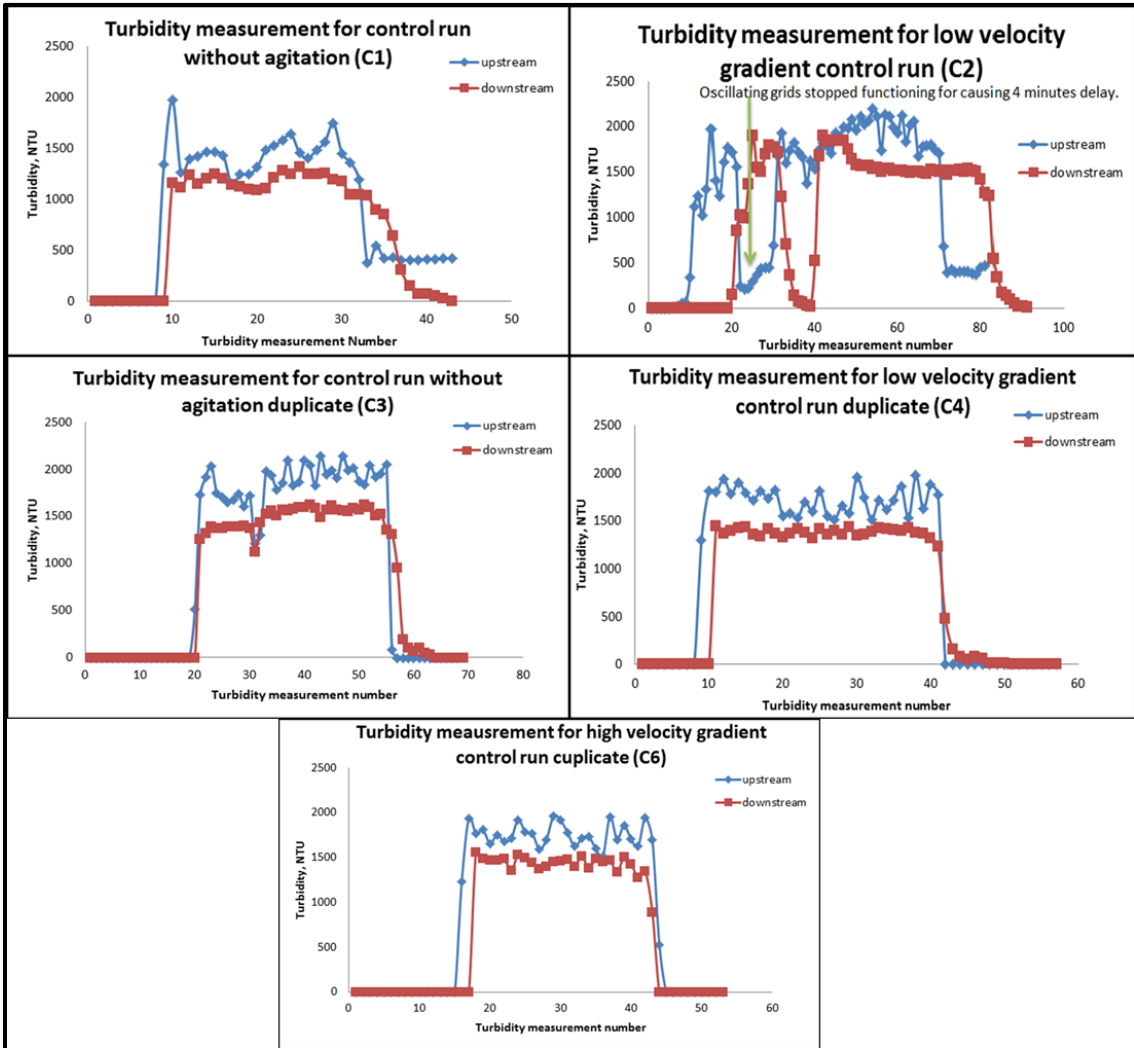


Turbidity Measurement for Flocculation Runs

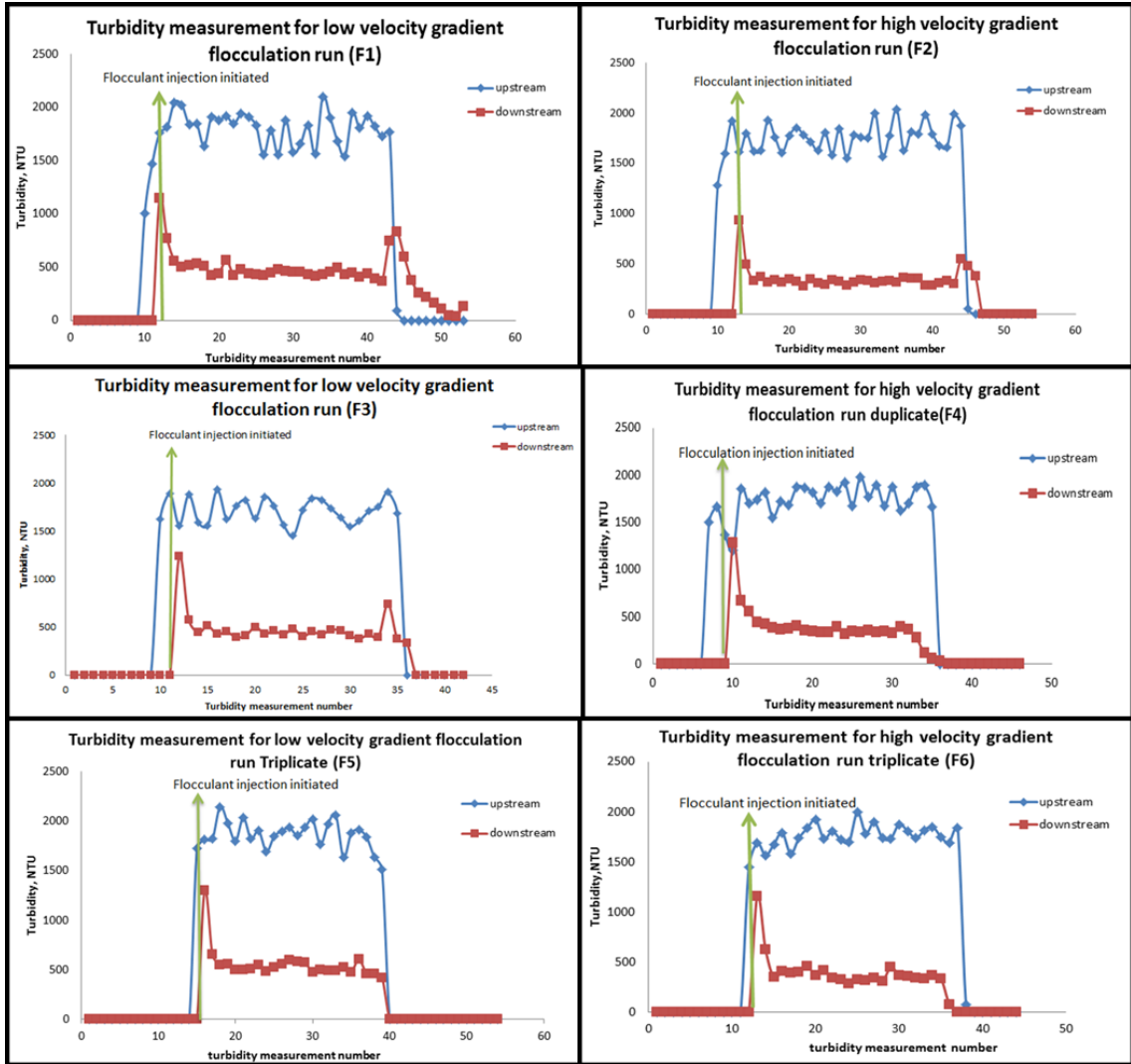


Appendix III: Turbidity Measurements for Port B soil

Turbidity measurements for control runs

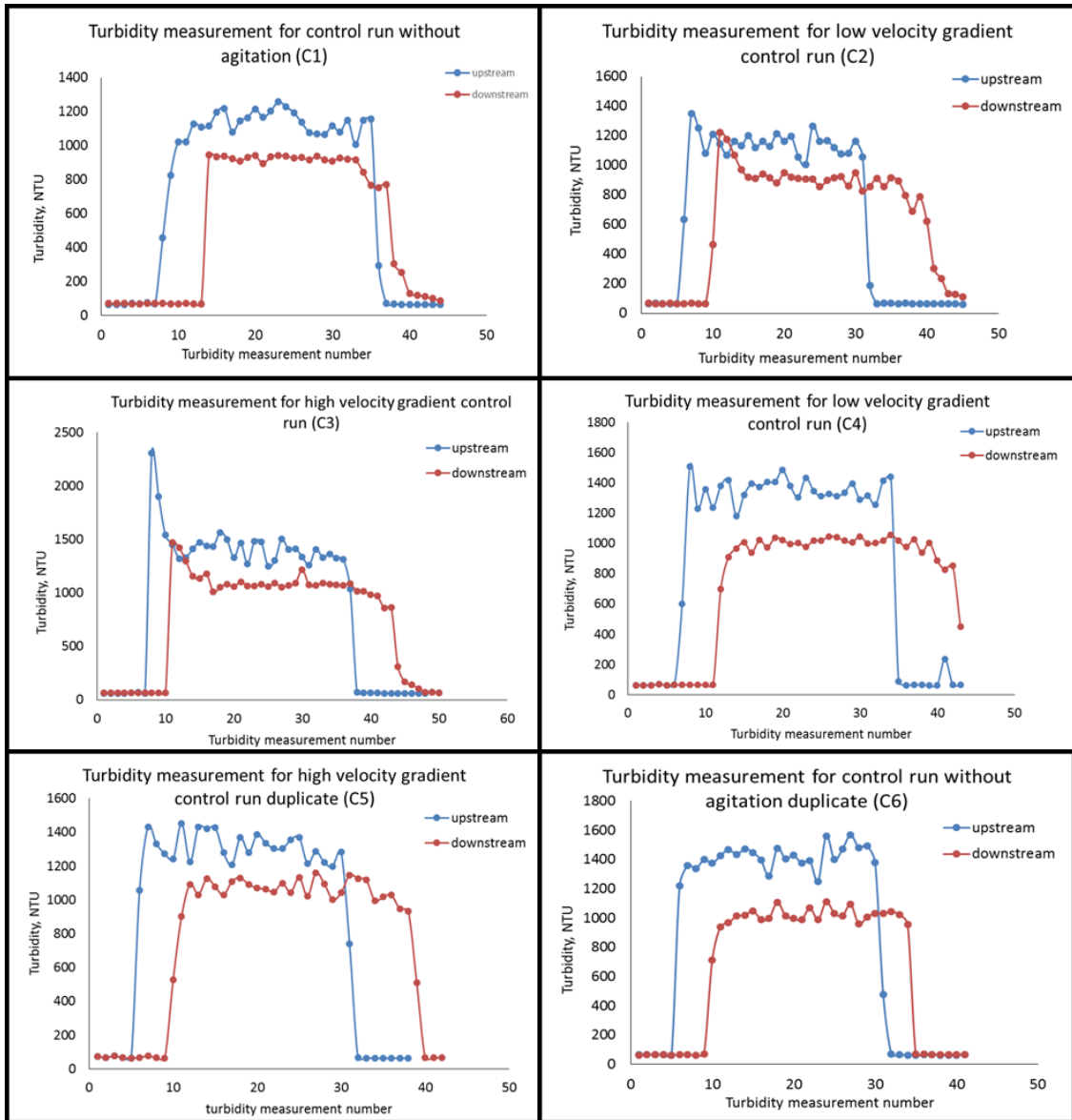


Turbidity measurements for flocculation runs:

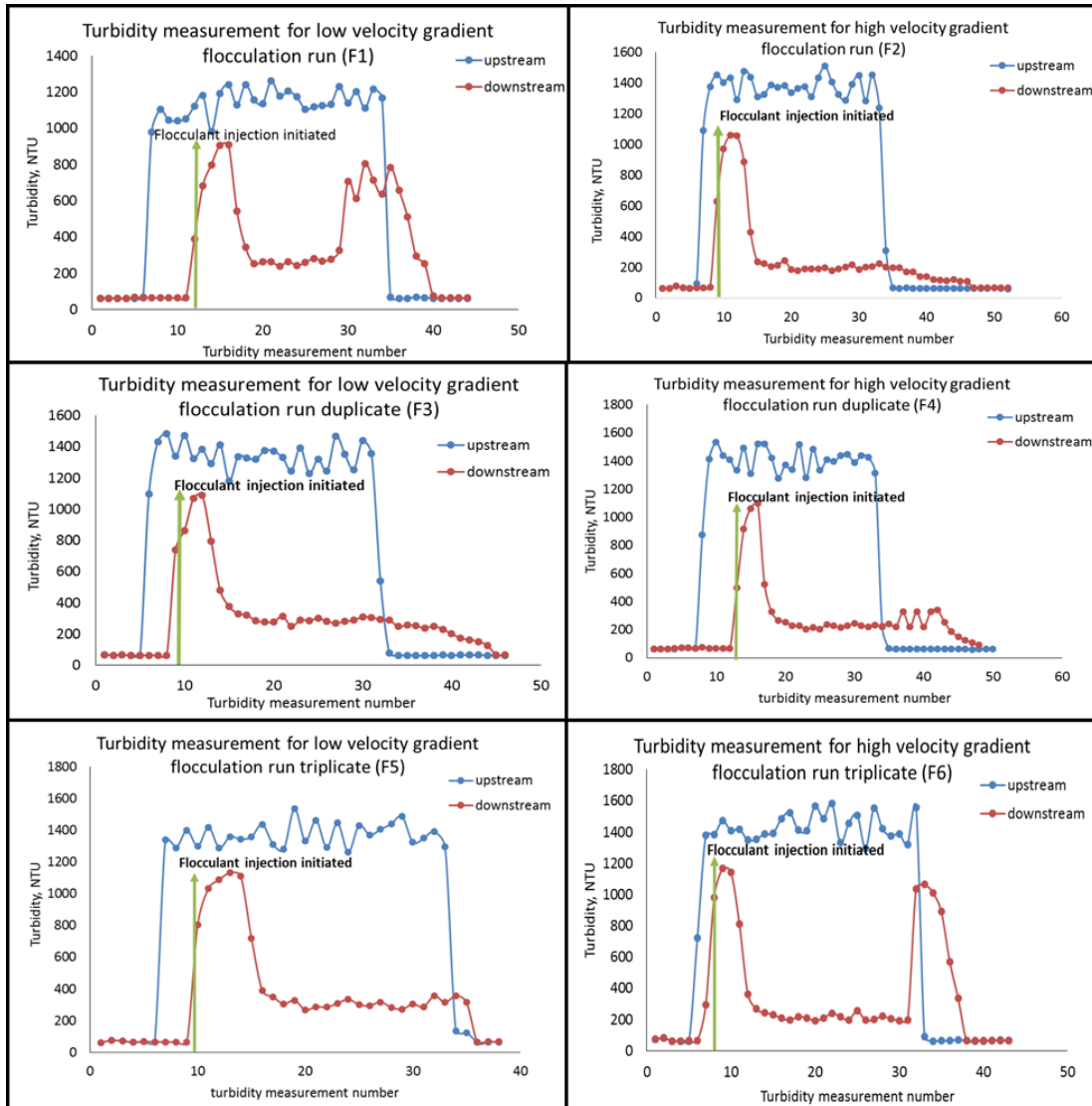


Appendix IV: Turbidity Measurements for Kamie B soil

Turbidity Measurement of Control Runs

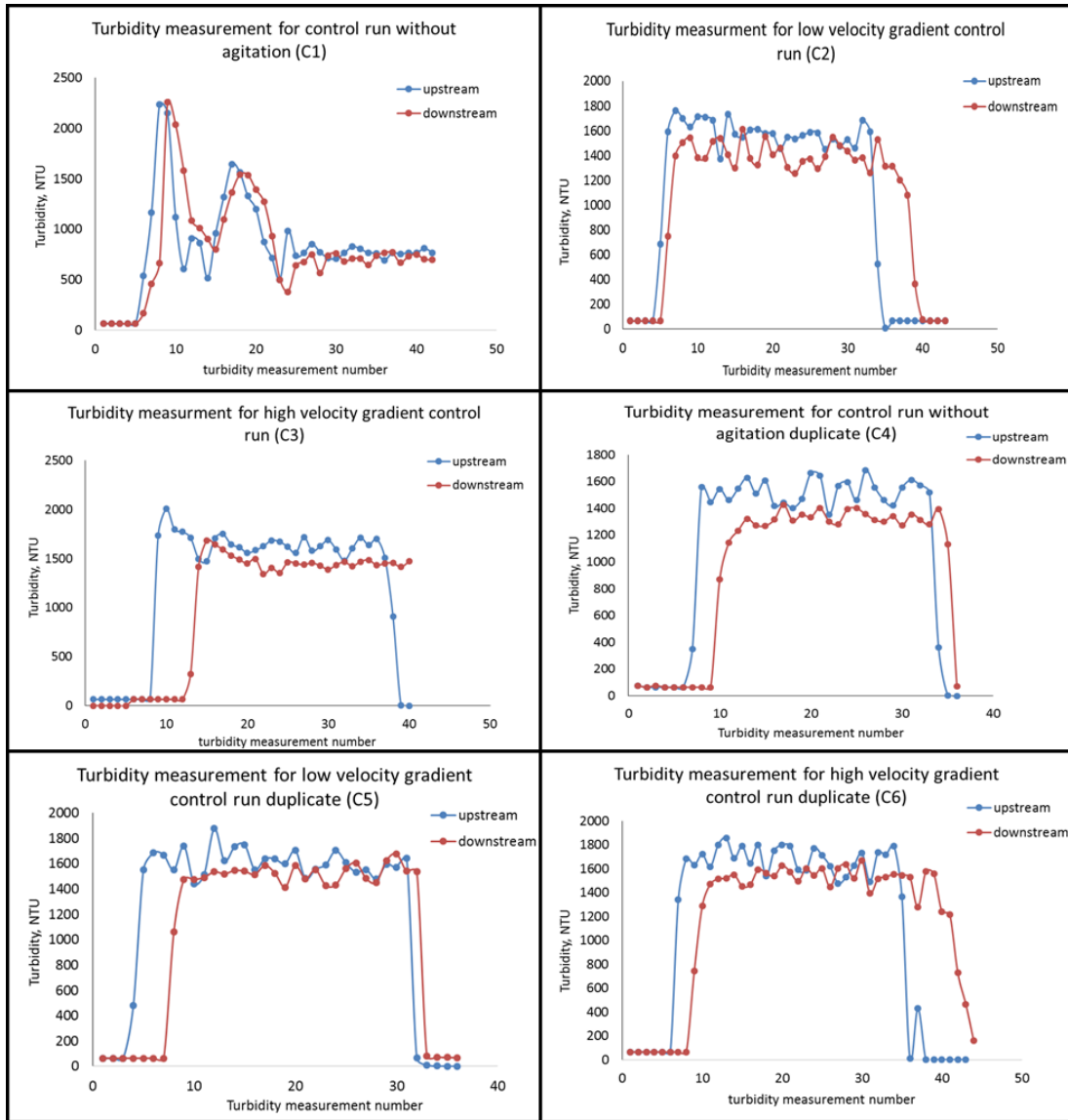


Turbidity Measurement for Flocculation Runs

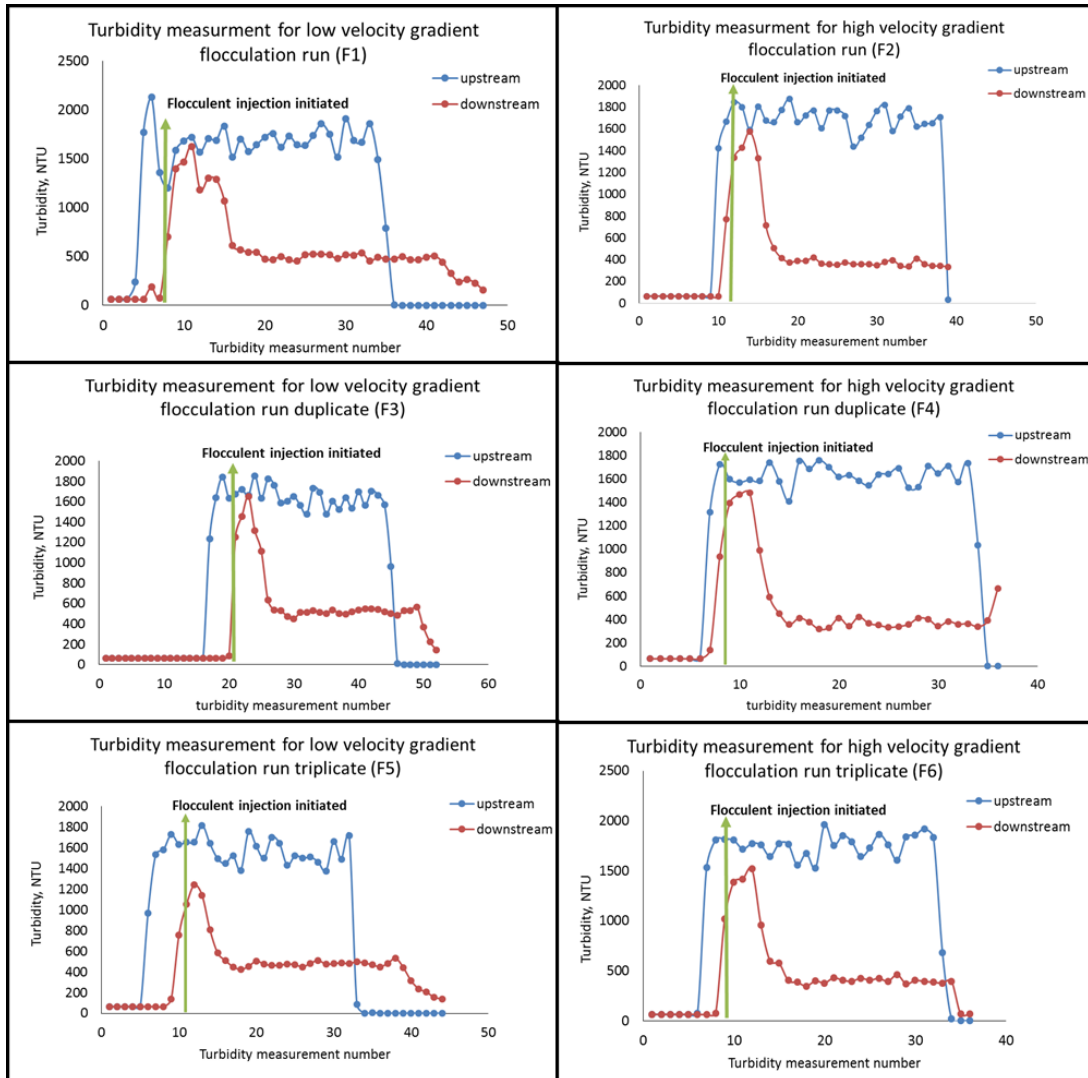


Appendix V: Turbidity measurement for Norge B soil

Turbidity measurements for Control Runs

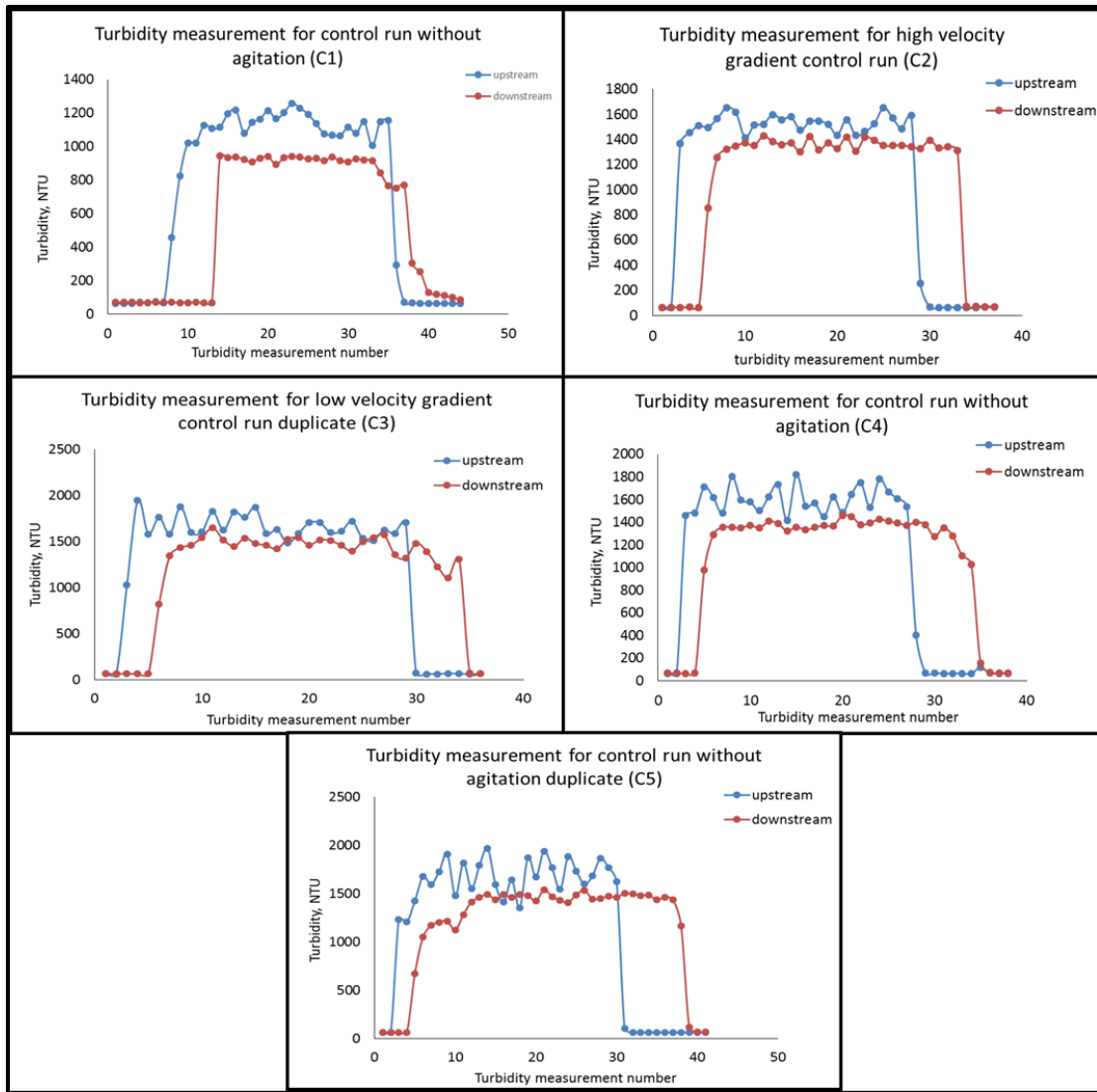


Turbidity measurement for Flocculation Runs:

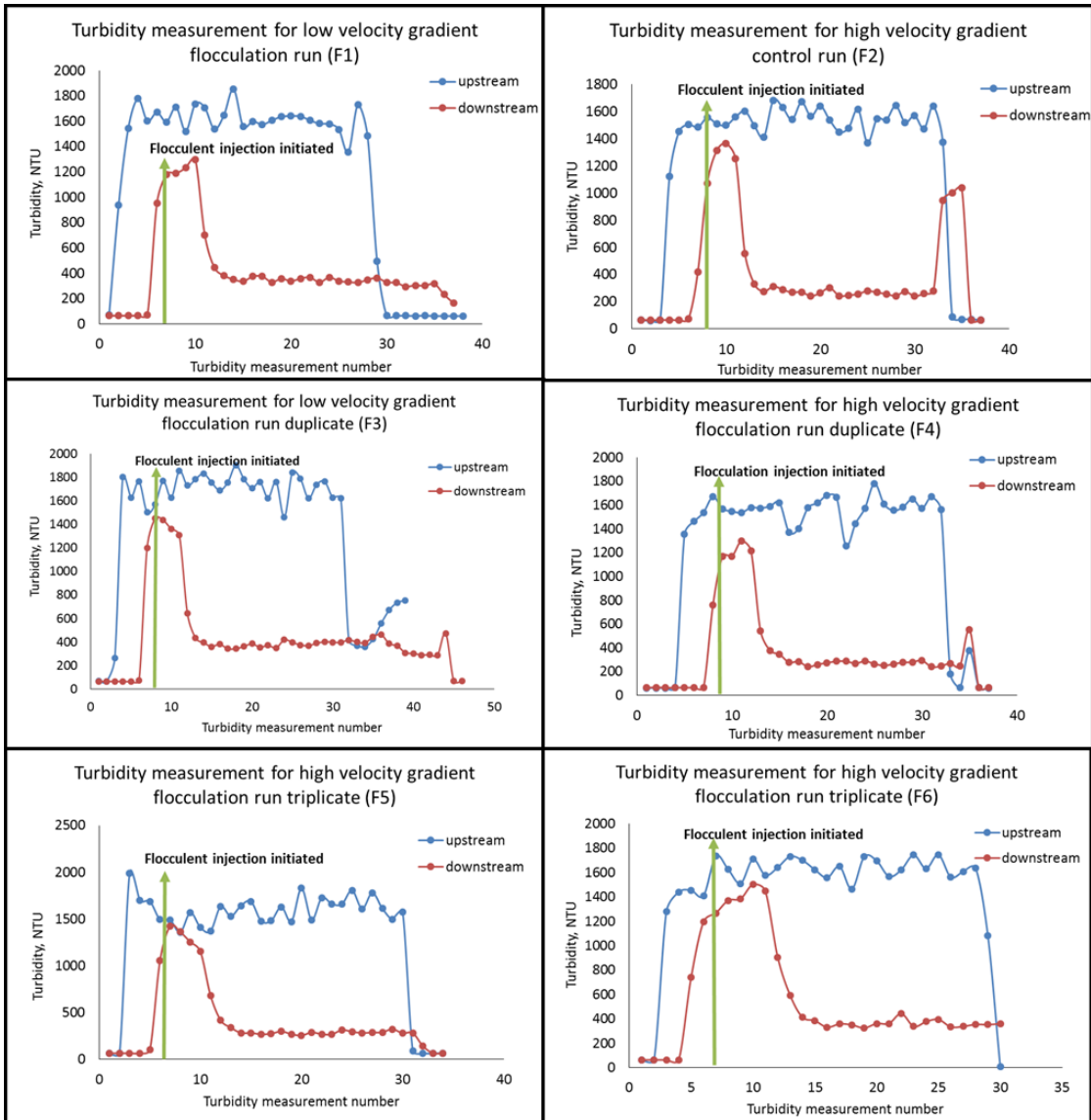


Appendix VI: Turbidity Measurements for Stephenville B soil

Turbidity Measurements for Control Runs

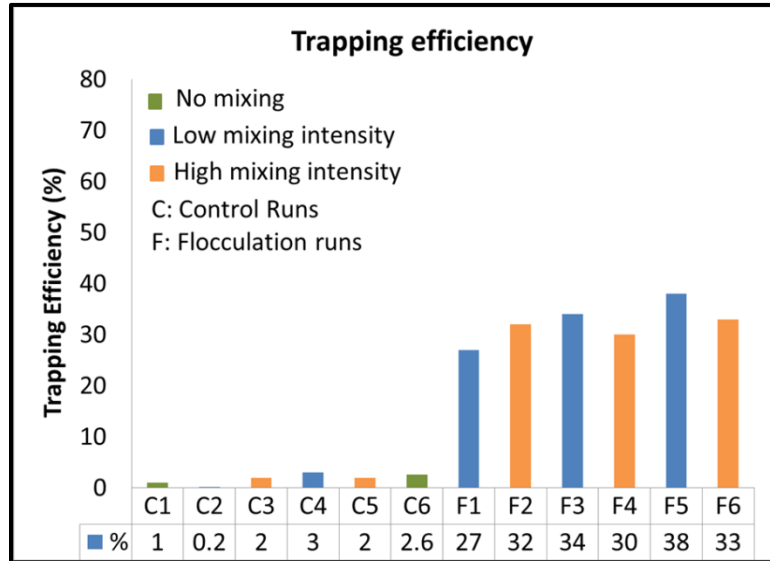


Turbidity Measurement for Flocculation Runs

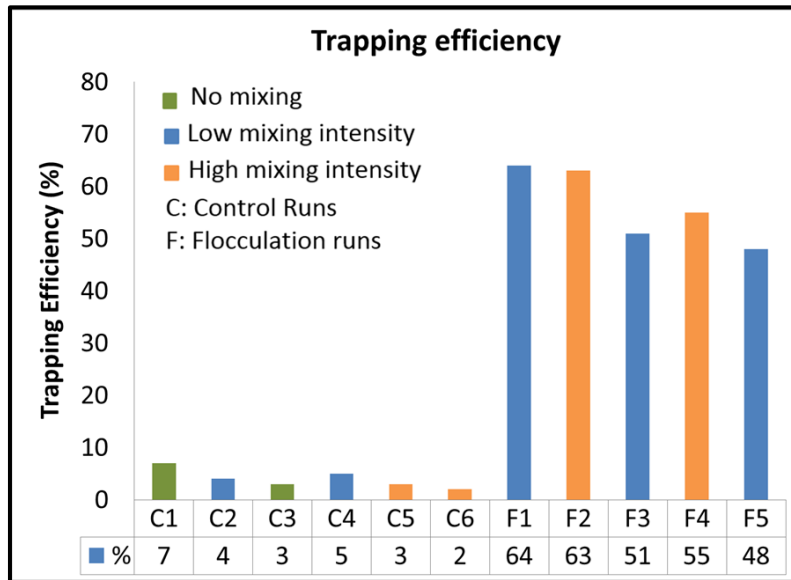


Appendix VII: Sediment removal efficiencies for all the soils

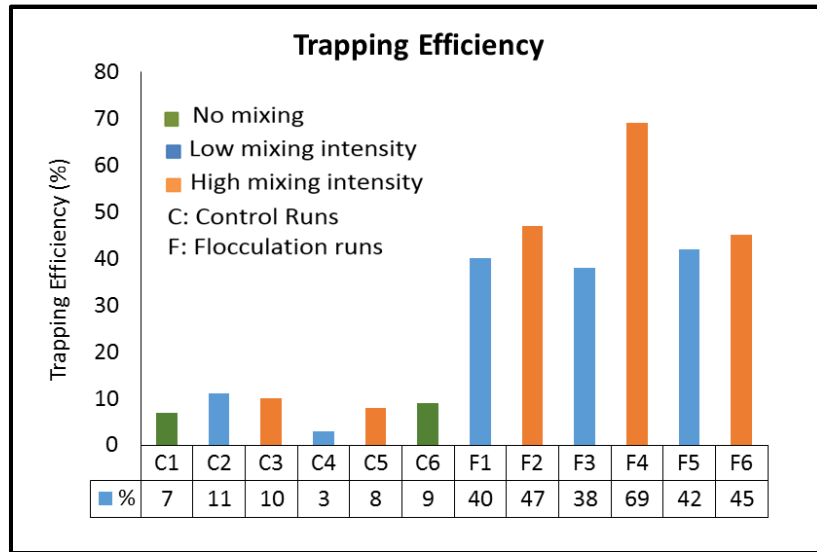
a) Sediment Removal Efficiency for Port A



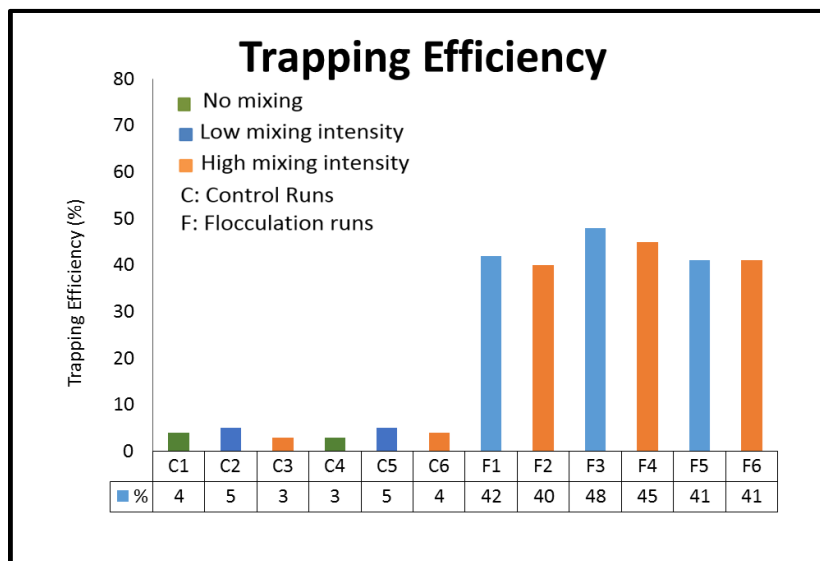
b) Sediment Removal Efficiency for Port B



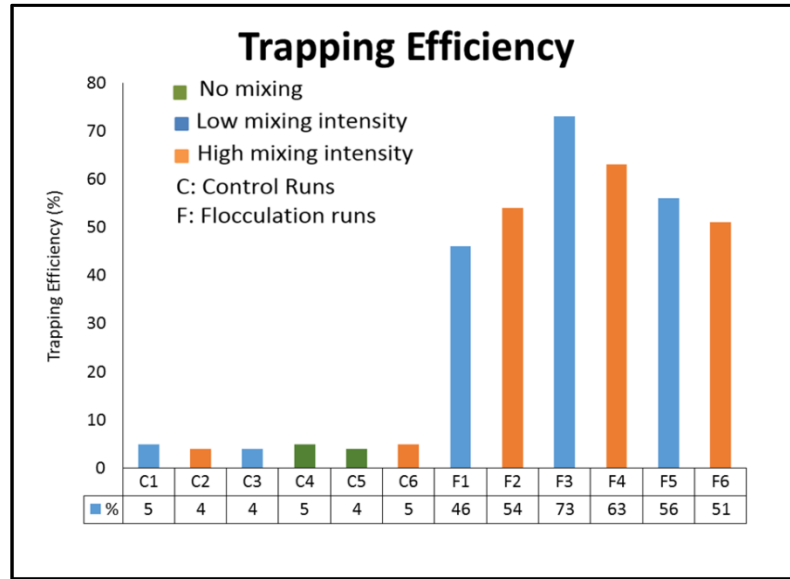
c) Sediment Removal Efficiencies for Kamie B



d) Sediment Removal Efficiencies for Norge B



e) Sediment Removal Efficiencies for Stephenville B



Appendix VIII: Matlab Codes for flocculation Model:

a) Matlab code for determination of flocs size, density

```
function [ flocradius, avgsg_floc, f, sg_floc ] = flocden( d1, Nbmax)
%flocden: this function calculates the size and the density of the
flocs
%and the fraction of the flocs.

% The calculations for floc density and radius and fraction of the
flocs are done based on
% Krishnappan and Marsalek (2002)

% Declaring all the variables needed for calculating the function.
flocradius = zeros(Nbmax,1);
vol = zeros(Nbmax,1);
sg_floc = zeros(Nbmax,1);
df = zeros(Nbmax,1);
avgsg_floc = zeros(Nbmax,Nbmax);
f = zeros(Nbmax,Nbmax);

b = 0.013; % Empirical constant
(Krishnappan & Marsalek, 2002)
c = 0.72; % Empirical constant
(Krishnappan & Marsalek, 2002)
sg_clay = 2.65; % specific gravity of
clay
sg_water = 1; % specific gravity of
water

for m1=1:Nbmax;
flocradius(m1) = (d1*0.0001/2)* 2.^((m1-1)/3);
vol(m1) = (4/3)*pi*flocradius(m1).^3;
df (m1) = (flocradius(m1)*2*10000); %
floc diameter in microns
sg_floc(m1) = sg_water + ((sg_clay-1)*exp(-b*(df(m1).^c))); %
density of floc in each bin (Krishnappan and Marsalek, 2002)
if df(1) == 1;
sg_floc(1) = 2.65;
end
end

% calculating the average specific gravity of flocs
for m1 = 1:Nbmax;
for n1 = 1:Nbmax;
avgsg_floc(m1,n1) = (sg_floc(m1)+sg_floc(n1))/2;
end
end

% Calculating the fractions of the flocs formed
for m2 = 1:(Nbmax-1);
```

```

    for n2 = 1:(Nbmax-1);
        f(m2,n2) = (avgsg_floc(m2)*vol(m2)+avgsg_floc(n2)*vol(n2)-
avgsg_floc(m2+1)*vol(m2+1))/(avgsg_floc(m2)*vol(m2)-
avgsg_floc(m2+1)*vol(m2+1));
        if m2 <= n2
            f(m2,n2) = 0;
            if m2 == n2;
                f(m2,n2) = 0;
            end
        end
    end
end
end
end

```

b) Matlab Code for Determination of Collision Frequencies

```

function [ numofbins, bins, Keff, beta ] = Coll_freq( epsilon, d1,
flocradius, alpha, avgsg_floc, Nbmax )
%The function calculated the number of the bins based on the shear
rate. It
%calculates the collision frequency and coagulation factor.

% Collision frequenyc abbreviations: Kb: Brownian motion, Kt: Laminar
or
% turbulent shear, Ki: Inertia due to turbulent flow, Kd: Differential
% settling, Keff: effective collision frequency.

% declaring the collision frequency variables

Kb = zeros(Nbmax,Nbmax);
Kt = zeros(Nbmax,Nbmax);
Ki = zeros(Nbmax,Nbmax);
Kd = zeros(Nbmax,Nbmax);
Keff = zeros(Nbmax,Nbmax);

R = zeros(Nbmax,Nbmax);
beta = zeros(Nbmax,Nbmax);

% Calculating the number of bins for a given shear rate

nu = 0.0112; % kinematic viscosity of water at 15.6C
in cm^2/s
G = sqrt(epsilon/nu); % velocity gradient calculation for the
reactor

dmax = 1/G; % Tapp et al 1981
bins = round(1 + 3*log(dmax/(d1*0.0001)));
if bins >= Nbmax;
    bins = Nbmax;
end
numofbins = bins+1; % number of bins +
ghostbin

```

```

% Calculating the collision frequencies

Bz = 1; % Boltzman Constant
T = 293; % Temperature in Kelvin
g = 981; % acceleration due to gravity in ft/sec^2
sg_water = 1; % specific gravity of water
sg_clay = 2.65; % specific gravity of clay
rho_water = 0.99; % density of water

for m2 = 1:bins;
    for n2 = 1:bins;
        Kb(m2,n2) = 0; % (2/3)*((Bz*T)/(rho_water*
nu))*((flocradius(m2)+flocradius(n2)).^2/(flocradius(m2)*
flocradius(n2)));
% Collision frequency function for Brownian motion
        Kt(m2,n2) =
((4/3)*(epsilon/nu)^0.5*(flocradius(m2)+flocradius(n2))^3);
% Collision frequency function for Turbulent shear
        Ki(m2,n2) =
(1.21*(sg_clay/sg_water)*(epsilon^3/nu^5)^0.25*(flocradius(m2)+flocradi
us(n2))^2*abs(flocradius(m2)-flocradius(n2))^2); %Collision
frequency function for Inertia of turbulent flow
        Kd(m2,n2) = ((2*pi*g/9*nu)*((avgsg_floc(m2)-
sg_water)/sg_water)*(flocradius(m2)+flocradius(n2))^2*abs(flocradius(m2
)^2-flocradius(n2)^2)); %Collision frequency function for
differential settling
        Keff(m2,n2) =
Kb(m2,n2)+sqrt(Kt(m2,n2)^2+Ki(m2,n2)^2+Kd(m2,n2)^2);
% Effective collision frequency function
    end
end

% calculating the coagulation factor

n_exponent = 6; %
Krishnappan and Marsalek, 2002 %
S = 2^(bins); %
Maximum number of particles in largest floc

for m3 = 1:bins;
    for n3 = 1:bins;
        R(m3,n3) = 2.^(m3-1)+2.^(n3-1);
        beta(m3,n3) = alpha*(1-(R(m3,n3)/(S+1)))^n_exponent; %
Calculation of beta values
    end
end

end

```

c) Matlab Code for Flocculation Routine

```

function [ error_correct ] = floccroutine(numpart_deltat, bins,
numofbins, Keff, beta, f, sumpp_deltat)
% Krishnappan and Marsalek routine to calculate the rate of
floculation.
% This function runs the flocculation routine to calculate the total
% number of flocs formed at time 't'

% Declaring variables
d1= 1;
Nbmax= 35;
deltat= 1;
squiggle = 1;
ghostbin = zeros (size(d1));

%-----%
---%
% Rate of loss
for m4 = 1:(Nbmax-1);
    for n4 = 1:(Nbmax-1);
        if m4 == n4
            rateofloss(m4,n4) = (-1)* 2^(m4-
1)*beta(m4,n4)*Keff(m4,n4)*((numpart_deltat(m4)^2)/4);
        else
            rateofloss(m4,n4)= (-1)*2^(m4-1)*beta(m4,n4)*Keff(m4,n4)*
numpart_deltat(m4)*numpart_deltat(n4);
        end
        if m4 > n4
            rateofloss(m4,n4)= 0;
        end
        totalloss(m4)= sum(rateofloss(m4,1:end));
    end
end

%-----%
---%
% Rate of gain
for m5 = 1:(Nbmax-1);
    for n5 = 1:(Nbmax-1);
        if m5==n5
            rateofgain(m5,n5)= 2^(n5-
1)*0.5*beta(m5,n5)*Keff(m5,n5)*(numpart_deltat(m5)^2/4);
        else
            rateofgain(m5,n5)= 2^(n5-
1)*beta(m5,n5)*f(m5,n5)*Keff(m5,n5)*numpart_deltat(m5)*numpart_deltat(n
5);
        end
        if n5>m5
            rateofgain(m5,n5)= 0;
        end
        totalgain(m5) = sum(rateofgain(m5,1:end));
    end
end

```

```

end

%-----
---%
% Rate of growth
for m6= 1:(Nbmax);
    for n6= 1:(Nbmax-1);
        if m6==1
            rateofgrowth(m6,n6)=0;
        end
        if m6>1
            if m6-1<n6
                rateofgrowth(m6,n6)=0;
            elseif m6-1==n6
                rateofgrowth(m6,n6)=2^(n6-1)*0.5*beta(m6-1,n6)*Keff(m6-1,n6)*(numpart_deltat(m6-1)^2/4);
            else
                rateofgrowth(m6,n6)= 2^(n6-1)*beta(m6-1,n6)*(1-f(m6-1,n6))*Keff(m6-1,n6)*numpart_deltat(m6-1)*numpart_deltat(n6);
            end
        end
        totalgrowth(m6)= sum(rateofgrowth(m6,1:end));
    end
end

%-----
---%
% Total rate of flocculation

for m7 = 1:(Nbmax-1);
totalrate(m7) = totalloss(m7)+ totalgain(m7) + totalgrowth(m7) ;
end
A= sum (totalrate);

%-----
---%
% Number of particles undergone flocculation
for m8 = 1:(Nbmax-1);
delta_nt(m8)= totalrate(m8).*deltat;
nplusedelta_nt(m8)= 2.^(m8-1).*numpart_deltat(m8)+delta_nt(m8);
end

%-----
---%
% Distribution of particles in ghostbin
%if bins==Nbmax;
ghostbin = totalgrowth(Nbmax)*deltat;
%end
sumofbins = sum(bins);
for m8 = 1:(Nbmax-1);
expGBN(m8) = exp(m8.*squiggle);
end

```

```

sum_expGBN = sum(expGBN);
for m8= 1:(Nbmax-1);
if ghostbin == 0;
numpart_ghostbin(m8)= 0;
else
numpart_ghostbin(m8)= ghostbin*(expGBN(m8)/sum_expGBN);
end
distpar_ghostbin(m8) = numpart_ghostbin(m8)+ nplusdelta_nt(m8);
end

%-----
---%
% Negative particles correction
for m9 = 1:(Nbmax-1);
if distpar_ghostbin(m9) > 0
    binshavingparticles(m9) = 1;
else
    binshavingparticles(m9) = 0;
end
end
sum_binshavingparticles = sum(binshavingparticles);

for m10 = 1:(Nbmax-1);
if distpar_ghostbin(m10) < 0
    negativeparticles(m10) = distpar_ghostbin(m10);
else
    negativeparticles(m10) = 0;
end
end
sum_negativeparticles = abs(sum(negativeparticles));

for m11 = 1:(Nbmax-1);
if distpar_ghostbin(m11) > 0
    positiveparticles(m11) = distpar_ghostbin(m11);
else
    positiveparticles(m11) = 0;
end
end
sum_positiveparticles = sum(positiveparticles);

for m12 = 1:(Nbmax-1);
    if binshavingparticles(m12)==1;
        negativecorrection(m12)= distpar_ghostbin(m12)-
((distpar_ghostbin(m12) /sum_positiveparticles)*sum_negativeparticles);
    else
        negativecorrection(m12) = 0;
    end
end
sum_negcorrec = sum(negativecorrection);

%-----
---%
% Error correction

```



```

error = zeros(size(d1));
error = sumpp_deltat - sum_negcorrec;

for m13 = 1:(Nbmax-1);
if error==0;
    error_correct(m13) = negativecorrection(m13);
else
    error_correct(m13)= negativecorrection(m13)+
negativecorrection(m13)*(error/sum_negcorrec);
end
end
sum_errorcorrect = sum(error_correct);

err_errcorrect = sumpp_deltat- sum_errorcorrect;

%-----
---%

% Number of flocs
%for m14= 1:(Nbmax-1);
    %flocs_t(m14)= error_correct(m14)/2.^(m14-1);

%end

end

```

d) Main code to calculate particle distribution and settling

```

%% Main code

clear all
clear variables
clc

%Defining all the input values

d1 = 1; % charactersitic
diameter of clay particles in microns % Maximum number
Nbmax = 35; % Stickiness
of bins % density in
alpha = 0.96; % density of water
coefficient %input('Enter the
rho_clay = 2.65; g/cm^3 %input ('Enter the
rho_water = 0.99; in g/cm^3
deltat= 1; time step:');
lasttime = 15; retention time for the reactor:');
retention time for the reactor:');

```

```

%-----
---%

% Number concentration of particles

sedflow = 11; % input('Enter the
sediment flow rate in lpm:');
massconcentration = 21; % input('Enter the
mass concentration in g/l:');
massflow = sedflow*massconcentration/60; % mass flow rate
grams per second

mass_clay = rho_clay*(4/3)*pi*(d1*0.0001)^3; % mass of single
clay particle in grams
pp = zeros(size(d1)); % primary
pp = (massflow/mass_clay); % primary
particles per second
totalpp = (massflow/mass_clay)*900; % total number of
primary particles
%pp = totalpp/60; % total primary
particles per second

%-----
---%

% Size, density, fraction function
[ floccradius, avgsg_floc, f, sg_floc ] = floccden( d1, Nbmax);

%-----
---%

% Declaring variables

numpart_deltat= zeros(Nbmax,1);
pp_deltat= zeros(Nbmax,1);
flocs_t= zeros(Nbmax,1);
settledparticles = zeros(Nbmax,1);
particlesinlayer2 = zeros(Nbmax,1);
particlesinlayer3 = zeros(Nbmax,1);
particlesinlayer4 = zeros(Nbmax,1);
unsettledparticles = zeros(Nbmax,1);
unsettledflocs = zeros(Nbmax,1);
settledflocs = zeros(Nbmax,1);
flocsinlayer2 = zeros(Nbmax,1);
flocsinlayer3 = zeros(Nbmax,1);
flocsinlayer4 = zeros(Nbmax,1);
sumpp_deltat = zeros (size(d1));

epsilon = zeros(size(d1));

%-----
---%

```

```

% Reactors
for r= 1:10

% Layers
for l= 1:4

% Time
for t=0:deltat:lasttime

    if r == 1;
        epsilon = 0.217;
    else if r > 1 && r <= 4;
        epsilon = 0.15;
    else if r > 4 && r <= 7;
        epsilon = 0.06;
    else if r > 7 && r <= 10;
        epsilon = 0.009;
    end
end
end
end

%-----
---%
% Collision frequency, coagulation factor function
[ numofbins, bins, Keff, beta ] = Coll_freq( epsilon, d1, floccradius,
alpha, avgsg_floc, Nbmax );

%-----
---%

% Calculation for the distrbition of the particles

Ni = zeros (Nbmax,1);
data = xlsread('Nicalculation.xlsx','Sheet1');
Ni = data(:,3);

for p3 = 1:(Nbmax-1);
    if t==0 && r==1;
        numpart_deltat(p3) = (Ni(p3)/4) + unsettledflocs(p3);
    else
        numpart_deltat(p3) = flocs_t(p3);
    end
pp_deltat(p3) = numpart_deltat(p3).*2^(p3-1);
end
sumpp_deltat = sum(pp_deltat);

```

```

%-----
---%

% Flocculation routine
[ error_correct ] = floccroutine(numpart_deltat, bins, numofbins, Keff,
beta, f, sumpp_deltat);

%-----
---%

for m15= 1:(Nbmax-1);
    flocc_t(m15)= error_correct(m15)/2.^(m15-1);
end

%end of time loop
end
% Routine for interpolating for calculating the settling velocities of
the
% flocc from the submerged specific gravities of the flocc
data = xlsread('den2.xlsx','Sheet5');           % importing data from
spreadsheet
x1d = data(2: Nbmax+1,1);                       % array of diameters
x2d = data(1, 2:end);                           % array of densities
yd = data(2:Nbmax+1, 2:end);                   % array of the
calculated Y values

X = zeros(size(x1d));
X = log10(x1d);                                % calculating the value
of X

%m = (1: length(x1d))';
Y= zeros(size(x1d));
Y = interpn(x1d,x2d,yd,x1d,sg_floc,'linear');  % calculating the values
of Y

w = zeros(size(Y));
w = (10.^Y);                                  % Calculating the
settling velocity;

% calculating the settling depth
ds = zeros (size(w));
ds = 15*w*12;                                 % settling depth of each
particle in inches

for m14 = 1:(Nbmax-1)

if ds(m14)<= 12
    unsettledparticles(m14)= 2.^(m14-1)*flocc_t(m14) +
    unsettledflocc(m14);
    unsettledflocc(m14) = unsettledparticles(m14)/ 2.^(m14-1);
else if ds(m14)> 12
    settledparticles(m14)= 2.^(m14-1)*flocc_t(m14) +
    settledparticles(m14);

```

```

        c= sum(settledparticles);
        end
    end

    if ds(m14) >12
        flocs_t(m14) = 0;
    end

    for m18= 1: Nbmax
        part_reactor(m18,r)= settledparticles(m18);
    end

end

%end of layer loop
end

for m16 = 1: Nbmax
    particledistribution (m16)= unsettledparticles(m16) +
    settledparticles(m16);
    if log(particledistribution (m16))< 0;
        particledistribution (m16) =0;
        par = (particledistribution)';
        b= sum(particledistribution);
    end
end

end

%%

```

Appendix IX: Matlab Code for Jar test studies

```
%% Code to analyze turbulent flow properties

clear all
clear variables
clc

data = xlsread('New data','18rpml'_1');

%Instantaneous velocity data
U = data(1:600,3);
V = data(1:600,4);
W = data(1:600,5);

freq= 10; % Sampling frequency was 10Hz
dt= 1/freq;
m = length(U-1)';
time = (dt:dt:m/freq)';

% Mean values
Umean = sum(U*dt)/time(end);
Vmean = sum(V*dt)/time(end);
Wmean = sum(W*dt)/time(end);

% RMS Velocities of velocity fluctuations

u_p = U-Umean;
v_p = V-Vmean;
w_p = W-Wmean;

u_rms = (sum((u_p.^2).*dt)/time(end))^0.5;
v_rms = (sum((v_p.^2).*dt)/time(end))^0.5;
w_rms = (sum((w_p.^2).*dt)/time(end))^0.5;

% convective velocity
Uc = sqrt(Umean^2 + u_rms^2);

% Standard deviation
u_std=std(U);
v_std=std(V);
w_std=std(W);

% Reynolds stress tensor
TAU = [-mean(u_p.*u_p),-mean(u_p.*v_p),-mean(u_p.*w_p);-
mean(u_p.*v_p),-mean(v_p.*v_p),-mean(v_p.*w_p);-mean(u_p.*w_p),-
mean(w_p.*v_p),-mean(w_p.*w_p)];
```

```

% Total Kinetic Energy
TKE = 0.5*(sum ((u_p.^2).*dt)/time(end)+sum((v_p.^2).*dt)/time(end)+sum
((w_p.^2).*dt)/time(end));

% %Plotting the velocity time series
% figure('Name','Velocity Time Series','NumberTitle','off','Color',[1 1
1])
% hold on
% plot(time,U,'color',[0,0,0])
% plot(time,V,'color',[0.3,0.3,0.3])
% plot(time,W,'color',[0.6,0.6,0.6]);
% hold off
% xlabel('Time (sec)');
% ylabel('Velocity (cm/s)');
% title('Velocity Time Series Plot');

%Normalized autocorrelation to find the time scales

    for tau = 1:600                %varies until normalized autocor(r)
passes zero
        %sample length = 4000 points
        Rxx(tau)= mean(u_p(1:(length(U)-tau+1)).*u_p(tau:end));
%autocorrelation
        Ryy(tau)= mean(v_p(1:(length(U)-tau+1)).*v_p(tau:end));
        Rzz(tau) = mean(w_p(1:(length(U)-tau+1)).*w_p(tau:end));
        rx(tau)=Rxx(tau)/Rxx(1);
%normalized autocorrelation
        ry(tau)=Ryy(tau)/Ryy(1);
        rz(tau)=Rzz(tau)/Rzz(1);
    end

rx=rx';
% figure ('Name', 'Normalized autocorrelation', 'NumberTitle', 'off',
'Color',[1 1 1])
% hold on
% plot(rx,'color',[0,0,0]);
% % plot(ry,'color',[0.3,0.3,0.3]);
% % plot(rz,'color',[0.6,0.6,0.6]);
% hold off
% xlabel('tau (sec)');
% ylabel('r(tau)');
% title('Normalized autocorrelation function');

%% Integral time and length scale

int_timescale = trapz(rx(1:230)).*dt;           % secs
int_lengthscalescale = int_timescale*Uc;       % cm

%% Kolmogorov scale

nu = 1.12E-6*10000;                % kinematic viscosity (cm2/s)
eta = int_lengthscalescale*((nu^3/((TKE^0.5)^3)/(int_lengthscalescale^3))^0.25);
% cm

```

```

% eta_cm = eta*100
epsilon=(TKE^1.5)/int_lengthscales;
energy dissipation rate
eta2=(nu^3/epsilon)^0.25;
% eta2_cm = eta2*100

G = sqrt(epsilon/nu);

%% Taylor microscale
lambda=10^0.5*eta^(2/3)*int_lengthscales^(1/3);
% lambda_cm=lambda*100
lambda2=(10*nu*TKE/epsilon)^0.5;
% lambda2_cm=lambda2*100

```


VITA

Neha Mangesh Bhadbhade

Candidate for the Degree of

Doctor of Philosophy

Thesis: MODELING THE FLOCCULATION PROCESS FOR STORMWATER
SEDIMENT REDUCTION

Major Field: Biosystems and Agricultural Engineering

Biographical:

Personal Information: Daughter of Rupa and Mangesh Bhadbhade
Date of Birth: December 22nd, 1982
Country of Citizenship: India

Education:

Completed the requirements for the Doctor of Philosophy in Biosystems and
Agricultural Engineering at Oklahoma State University, Stillwater, Oklahoma in July,
2014.

Completed the requirements for the Master of Science in your Civil and Environmental
Engineering at Oklahoma State University, Stillwater, Oklahoma in December 2009.

Completed the requirements for the Bachelor of Engineering in Instrumentation and
Control at Pune University, Pune, India in August 2004.

Experience:

Research Assistant at Oklahoma State University at Biosystems and Agricultural
Engineering Department
Teaching Assistant at Oklahoma State University at Biosystems and Agricultural
Engineering Department
Engineering Intern for Kaw Indian Nation
Research Assistant at Oklahoma State University at Civil and Environmental
Engineering Department
Application Engineer at Manas Microsystems Pvt Ltd, Pune, India

Professional Memberships:

ASABE, Chi Epsilon